SCIENTIFIC COUNCIL DSc.03/31.03.2022.T/FM.10.04 ON AWARD OF A SCIENTIFIC DEGREE AT THE INSTITUTE OF FUNDAMENTAL AND APPLIED RESEARCH UNDER THE NATIONAL RESEARCH UNIVERSITY "TIIAME"

INSTITUTE OF FUNDAMENTAL AND APPLIED RESEARCH

Mazhar Iqbal

Studies of formation mechanisms and novel applications of micro/nanostructured materials processed by high repetition rate ultrafast femtosecond laser

01.04.02 – Theoretical Physics
(Physical and Mathematical Sciences)

PRESENTATION
on awarding the scientific degree of Doctor of Philosophy (PhD)
on the basis of published papers without
a dissertation

Tashkent – 2024

UDC 621.039.3

Taqdimnoma mundarijasi
Оглавление представлении
Content of thesis presentation

Studies of formation mechanisms and novel applications of micro/nanostructured materials processed by high repetition rate ultrafast femtosecond laser..... 4

Yuqori takrorlanish chastotasiga ega o'taqisqa femtosekund laseri yordamida ishlov berilgan mikro/nanostrukturali materiallarning shakllanish mexanizmlari va ularning yangi tadbiqlarini tadqiq qilish…….. 49

Исследования механизмов формирования и новых применений микро/наноструктурированных материалов, обработанных сверхбыстрым фемтосекундным лазером с высокой частотой повторения…….. 99

Elon qilingan ishlar ro'yhati
List of published works
Список опубликованных работ ……..... 113

The theme of the PhD research is registered by the Supreme Attestation Commission at the Ministry of Higher Education, Science and Innovations of the Republic of Uzbekistan under B.2024.2.PhD/FM1043.

The research work results have been carried out at the Institute of Fundamental and applied research under "TIIAME" National Research University.

Presentation of scientific research in three languages (Uzbek, English and Russian (only conclusions)) is posted on the websites of the Scientific Council (www.ifar.uz), National News Agency (www.uza.uz) and Information-educational portal "Ziyonet" (www.ziyonet.uz).

Scientific consultants:

Ganeev Rashid Ashirovich
Doctor of sciences in physics and mathematics, Professor,
Institute of Fundamental and Applied Research
"TIIAME" National Research University
Tashkent, Uzbekistan

Ali Sami Alnaser
Professor of Physics
American University of Sharjah,
Sharjah, United Arab Emirates

Presentation of the scientific research will be held on "___" _____ 2024 at ___ in the meeting of the Scientific Council No. **DSc.03/31.03.2022T/FM.10.04** at the Institute of Fundamental and Applied Research under the "TIIAME" National Research University (Address: 100000, Tashkent city, Qori Niyazov Street 39, Institute of Fundamental and Applied Research, Hall 312; tel.: 71 237-09-61.; e-mail: info@ifar.uz

The PhD presentation can be looked through at the Information Resource Center of the Institute of Fundamental and Applied Research under the "TIIAME" National Research University (registered under № ____). (Address: 100000, Tashkent city, 39 Qori Niyazov str., ph.: 71 237-09-62)

The presentation of the scientific research was distributed on "___" _____, 2024.

(Registry record № ___ dated "___"_____, 2024)

B.J. Ahmedov
Chairman of the Scientific Council
on Award of Scientific Degrees,
DSc, Professor

D.R. Rayimbayev
Scientific Secretary of Scientific Council
on Award of Scientific Degrees, DSc

ABSTRACT

Laser ablation method can be used in several material processing and analytical applications. Those applications include production of nanoparticles, micro-nano structuring, coloring of metals, controlling of wetting properties of surfaces, laser breakdown spectroscopy and pulse laser depositions. The research on the synthesis and characterization of metal and oxide nanoparticles using pulsed laser ablation technique is critical for understanding their properties and potential applications. A study of the laser assisted generation of Aluminum (Al) nanoparticles (NPs) in liquids and in vacuum was carried out. The ability of NPs to change the wettability and nonlinear optical properties of the surfaces, the suspensions and plasmas was demonstrated. By means of Molecular Dynamics combined with Two Temperature model, the formation process of aluminum NPs during the ablation of bulk targets was analyzed. The numerical simulations allowed identifying the main mechanisms of NPs formation in liquid media and the existence of the optimal laser irradiation parameters for producing Al NPs of the desired size and morphology. The low-order nonlinear optical properties of Al NPs produced during ablation of the bulk metal by nano-, pico-, and femtosecond (fs) pulses were determined. The coefficients of nonlinear refraction and absorption of Al NPs using 40 fs pulses at $\lambda = 400$ nm were measured to be $\sim 10^{-9}$ cm^2 W^{-1} and 10^{-7} cm W^{-1}, respectively. Al NPs allowed generation of 37th harmonic using 40 fs pulses propagating nearby to the ablating aluminum target. The formation of well-controlled nano/micrometer-sized structures on metallic surfaces enables the modification of their optical and wetting properties. The formation of such structures on the surface of biocompatible materials, in particular, can expand their applications in various areas of science and technology. A high-repetition rate fiber-based laser (150 KHz) with 37 fs ablating pulses with a central wavelength of 1030 nm was employed to form complex nanosized structures on the metal surfaces. A correlation was found between the optical properties of the laser-processed surfaces and their wettability properties. Oil-water separation using super-wetting and the selective permeability of membranes for oil or water has great ecological and economic significance. An environment-friendly, chemical free, and efficient approach was devised by using a high power, ultrafast femtosecond laser to nanostructure stainless steel and copper meshes to achieve desired variations of wetting properties. Laser scanning parameters, mesh pore size, and aging conditions were optimized to produce membranes exhibiting an extraordinary separation efficiency of 98% for the oil-water mixture.

INTRODUCTION

Relevance and necessity of the topic. Laser ablation and structuring have been studied extensively for many decades since the development of lasers in the 1960's. However, the interest of the researcher dramatically increased with the discovery of chirped-pulse amplification (CPA) technique and the discovery of high-fluence materials. The application of CPA regime produces short laser pulses nearly to few tens of a femtosecond. Although these pulses carry very low energies, the peak power exceeds terawatts and intensity of the range 10^{18} W/cm^2 or higher is possible. This corresponds to an electric field of 10^{11} V/cm. The fundamentals behind laser-matter interactions of such high peak power and short pulses are very complex and warrant understanding of various mechanisms, as the duration of the pulse is shorter than the time of the energy transfer between electron-ion pairs, the heat conduction time of the lattice, and hydrodynamics time of the sample.

The high peak intensities of ultrashort pulses lead to nonlinear processes and the strong electric field ionization and electron impact ionization take place. Depending on intensities, two mechanisms of ablation happen in the femtosecond regime which are coulomb's explosions and thermal vaporization. At low intensities, near the ablation threshold, coulomb explosions (soft ablation) are dominant whereas at high intensities the thermal vaporization (hard ablation) is dominant. In the coulomb explosion regime only a few nm materials per pulse is removed and in thermal vaporization an order of magnitude higher material per pulse is removed. Understanding the effects of plasma temperature and electron density is crucial in optimizing the products of the laser ablation of any target.

Laser ablation can be used in several material processing and analytical applications. Those applications include production of nanoparticles, micro-nano structuring, coloring of metals, controlling wetting properties of surfaces, laser breakdown spectroscopy and pulse laser depositions. The research on the synthesis and characterization of metal and oxide nanoparticles using pulsed laser ablation technique is crucial for understanding their properties and potential applications. By studying the factors that influence the properties of nanoparticles, such as laser parameters and surrounding media, researchers can optimize the synthesis process to tailor the properties of the nanoparticles for specific applications. The applications of nanoparticles in various fields, including medicine, optoelectronics, and energy sources, highlight their importance in advancing technology and improving existing systems. Understanding the formation mechanism of nanoparticles through numerical modeling can provide valuable insights into the underlying physics of the laser ablation process and help optimize the synthesis process for desired nanoparticle properties.

Furthermore, investigating the nonlinear optical properties of nanoparticles generated through laser ablation can lead to advancements in nonlinear optics applications, such as high-order harmonics generation. By studying the fundamental principles of these properties, researchers can explore new possibilities for utilizing nanoparticles in cutting-edge technologies. Femtosecond laser processing allows precise control over local nanosized structures on material surfaces to make them highly effective and multifunctional, particularly, in the coloring. Laser-induced coloring is environment-friendly as it eliminates the usage of any pigments or chemicals, while being quite flexible in achieving the desired results by optimizing laser irradiation parameters. The unique ability of high-power short laser pulses to modify almost all kinds of materials on the nanoscale poses great potential for various novel applications in optics, optoelectronics, microfluidics, color marking, and mechanics. Another application of laser-induced surface modification is the control of the wettability response of metallic surfaces, which is currently a topic of growing interest in the laser processing of materials. Surfaces can be modified with intense lasers to be water attracting (hydrophilic) or water repelling (hydrophobic). Such modified surfaces have many applications such as self-cleaning, corrosion prevention, drag reduction, anti-bacteria, anti-fogging, heat transfer, tribology, optical reflectance, and oil-water separation applications.

The development of femtosecond laser-structuring of metal meshes, two-dimensional (2D)- membranes, and three-dimensional (3D) adsorbent foams for oil-water separation represents a promising and environmentally friendly approach to addressing the challenges associated with traditional separation techniques. By leveraging the unique wettability responses of these materials, researchers can achieve high separation efficiency while minimizing harmful byproducts. Utilize of ultrashort laser structuring allows for precise control over the surface properties of the materials, enabling the creation of surfaces with tailored wetting behaviors. For example, superhydrophobic-superoleophilic surfaces repel water while selectively absorbing oil, facilitating efficient oil-water separation. Conversely, superhydrophilic-superoleophobic surfaces can selectively attract water while repelling oil, achieving a similar separation effect.

International context of the research. Many top universities and research centers around the globe are executing research in the field of the strong-field regime, particularly ionization, nanoparticle formation, nano-structuring for multifunctional surfaces, High Harmonic Generation (HHG) and application of coherent extreme ultraviolet (XUV) radiation to study ultrafast electron dynamics in atoms, molecules and materials with attosecond time scale. Among them are the group of Ultrafast Dynamics department at Max-Planck Institute for Multidisciplinary Sciences (Gettingen, Germany), the group of Laboratory for Laser Energetics (LLE) of

the University of Rochester (USA), the group of Nanostructures and Ultrafast X-Ray science at ETH-Zurich (Zurich, Switzerland), the group at MEPHI, Institute of Engineering Physics for Biomedicine (PhysBio), 115409 Moscow, Russia, the group at the Institute of Physics and Center for Interdisciplinary Nanostructure Science and Technology (CINSaT), University of Kassel, 34125 Kassel, Germany, the group of Nonlinear Optics at Changchun Institute of Optics, Physics and Fine Mechanics (Changchun, China), the group of Materials Science and Engineering Research Center at American University of Sharjah (Sharjah, UAE), the group of the Center of Nanotechnology at University of Munster (Munster, Germany), the group of Nonlinear Optics at the University of Tokyo (Tokyo, Japan), the group of the Laser Plasma Division at the Center of Advanced Technologies (Indore, India), the group at the National Institute of the Science (Montreal, Canada), HHG spectroscopy at Imperial College (London, England), HHG and EUV science group at the Advanced Research Center for Nanolithography (Amsterdam, Netherlands) and others.

Current state of the research on the topic.

Pulsed laser ablation is an ever-growing field. Among many other applications the formation of nanoparticles, preparation of multifunctional surfaces, laser induced breakdown spectroscopy and HHG are of high interest to the scientific community.

The formation of nanoparticles and micro-nano structures by laser ablation is superior to traditional methods as it involves no chemical, no human direct touch and is an eco-friendly method.

Connection of the research topic with the research activities of the institution. The majority of the results for Ph.D. research were obtained in the materials science and engineering research center at American University of Sharjah (UAE), while some results were obtained in collaboration with researchers from Uzbekistan, Germany, Latvia, Japan, and Russia.

The aim of the research work is to obtain theoretical and experimental knowledge on the formation mechanisms and novel applications of micro/nanostructured materials processed by high repetition rate ultrafast femtosecond lasers.

The tasks of the research are:

- Study the laser-assisted generation of Aluminum (Al) based nanoparticles (NPs) in liquids and in vacuum, and their ability to change the wettability and nonlinear optical properties of the surfaces, suspensions, and plasmas.
- Investigate the nonlinear absorption and refraction charactristics of NPs, as well as their various structural and linear optical properties for potential applications in optoelectronics, optical limiters, and photonics.

- Study the laser parameters and sample conditions that correspond to the formation of laser-induced periodic surface structures (LIPSS) and nanospikes on the surface of the metal targets.
- Investigate the wettability response of metal meshes, plane and curved surfaces of various materials processed by femtosecond laser pulses for oil-water separation.
- Study the application of nanoparticles enriched laser-induced plumes for HHG.

The object of the research is the laser-induced nano-micro structures on different materials surfaces, Al nanoparticles produced in air, vacuum and under water.

The subject of the research is wettability properties and optical characteristics of nano-micro structured surfaces of various materials, low- and high-order nonlinear optical properties of Al NPs, and spectral characteristics of generated high-order harmonics.

Methods of the research include both theoretical and experimental. Theoretical methods include simulation with analytical Molecular Dynamics (MD) and Two Temperature models (TTM) derived from diffusion differential equations. Experimental methods include forming nanoparticles in a vacuum and under water conditions by using high power, high repetition rate, short and ultrashort pulses. Structuring of Planes, curved surfaces of various materials and metal meshes by a femtosecond fiber laser. Quantitative measurements of wettability properties of surfaces by measuring contact angle and receding angle by using a drop shape analyzer.

The scientific novelty of the research

- MD-TTM numerical simulations were used to attain insight knowledge of optimal laser beam parameters for the formation of Al NP of desired size and morphology.
- Highest values in spectral region of 400 nm of the nonlinear absorption coefficients (β) and nonlinear refractive indices (γ) were observed *for the first time* in the case of the Al based NPs suspension, produced by ablation of aluminum using picosecond pulses. The values of β and γ of Al based NPs were $\sim 10^{-7}$ cm W^{-1} and 10^{-9} cm^2 W^{-1} respectively.
- We have established *for the first time* that the in-situ formation of Al NPs in vacuum followed with propagation of the driving pulses through the cloud of synthesized nanoparticles produces enhanced high harmonic yield compared to the aluminum atoms and ions. Al NPs allowed the generation of the high harmonics up to the 37th order by using 40 fs pulses.
- We have demonstrated *for the first time* that the deposition of the Al based NPs produced in water showed superhydrophilic properties and the NPs deposited in vacuum possessed superhydrophobic features.

- We showed *for the first time* that permanent and iridescent colors of the metals and metal alloys surfaces can be erased and re-colored by using a second stage femtosecond laser processing.
- A correlation between the spectral reflective properties of the laser-processed surfaces and their wettability properties was demonstrated *for the first time*.
- We established the potential use of AlNiCo alloy rods processed by using different fluencies of the ablating laser pulses, as a membrane for the oil–water separation applications *for the first time*.
- Through a systematic study on optimization of processing parameters like the thickness, pore size of the copper and stainless steel meshes, the laser scanning speed, and aging environments an efficiency of 98% was accomplished in separating oil-water mixtures *for the first time*.
- Expedited transition in wettability of femtosecond laser structured metals surfaces by aging in the low-pressure environment for self-cleaning applications was demonstrated.
- Complex periodic azimuthally and radially directed LIPSS fabricated by ultrafast laser on a large surface area of Tantalum (20mm) was presented *for the first time.* This is very important to improve the tendency for cell adhesion and proliferation when used as an implant.
- Copper Mesh and Foam Janus membranes manufactured by femtosecond laser with opposite wettability characteristics for efficient directional water transfer and fog collection applications were demonstrated.
- Laser structured zeolite-coated steel meshes exhibited enhanced superhydrophilic behavior and superior durability over an extended period for oil–water separation.

Practical results of the work. Results of the theoretical and experimental analysis were used during the technological improvements of nanoparticles generation and processing of micro-nano structuring surfaces of various material for novel applications at the materials science research facility at American University of Sharjah (UAE). Various codes for MD-TTM calculations and experimental data processing were developed and are now actively applied within the research groups at American University of Sharjah, (Sharjah, UAE), the laboratory of Nonlinear Optics at University of Latvia, (Riga, Latvia), Institute of Physics and Center for Interdisciplinary Nanostructure Science and Technology, University of Kassel, (Kassel, Germany), Faculty of Physics, Voronezh State University (Voronezh, Russia), and Tashkent Institute of Irrigation and Agricultural Mechanization Engineers (Tashkent, Uzbekistan).

The reliability of the research results is supported by the fact that they were obtained using modern calculations, simulations, and experimental techniques. The

reliability of the results is also based on the compatibility of obtained results with the experimental data. Moreover, to further underline the reliability of obtained results, all articles of the Ph.D. work were peer-reviewed by the experts in the field of, surface science, nanomaterials, nonlinear optics and published in the highly ranked journals attributed to the Q1 and Q2 quartiles.

Significance of research results. Theoretical and experimental results of the research on the formation mechanism of nanoparticles and processing of micro / nano structuring surfaces have many exotic applications. The nanoparticles produced by the laser method are green, non-toxic product hence favorable for early detection and treatment of cancer, energy, thin films, optoelectronic, signal enhancement Raman spectroscopy, and many more applications. The nanostructured surfaces are of high importance in producing the multifunctional surfaces of various materials like self-cleaning, corrosion prevention, drag reduction, anti-bacteria, anti-fogging, heat transfer, tribology, optical reflectance, and oil-water separation applications.

Implementation of the research results. The acquired results of the study were used in numerous scientific articles. Among them are "Ultrafast fiber laser-induced fabrication of superhydrophobic and self-cleaning metal surfaces," S.A. Khan, et.al. Appl. Surf. Sci. 542, 148560 (2021) (**75** Citations), "Expedited transition in the wettability response of metal meshes structured by femtosecond laser pulses for oil-water separation," S.A. Khan, et.al., Front. in Chem. 8, 768 (2020) (**20** citations), "The mechanism of laser-assisted generation of aluminum nanoparticles, their wettability and nonlinearity properties," M. Iqbal, et.al., Appl. Surf. Sci. 527, 146702 (2020) (**17** citations), "Superhydrophobic and superhydrophilic properties of laser-ablated plane and curved surfaces," G.S. Boltaev, et.al., Appl. Phys. A 126, 1-9 (2020) (**12** citations), "Near-field induced reaction yields from nanoparticle clusters," P. Rosenberger, et.al., ACS Photonics 7, 1885-1892 (2020) (**20** citations), "Anomalous formation of trihydrogen cations from water on nanoparticles," M.S. Alghabra, et.al., Nat. Commun. 12, 3839 (2021) (**15** citations), "Resonance enhancement of harmonics in the vicinity of 32 nm spectral range during propagation of femtosecond pulses through the molybdenum plasma," V.V. Kim, et.al., J. Phys. B: At. Mol. Opt. Phys. 53, 195401 (2020) (**14** citations), "Giant third-order nonlinear response of mixed perovskite nanocrystals," A.M. Abu Baker, et.al., Materials 15, 389 (2022) (**12** citations), "Enhanced XUV harmonics generation from diatomic gases using two orthogonally polarized laser fields," G.S. Boltaev, et.al., Sci. Rep..11, 5534 (2021) (**12** citations), "Application of 150 kHz laser for high-order harmonic generation in different plasmas," G.S. Boltaev, et.al., Photon. 7, 66 (2020) (**9** citations), "Simultaneous manipulation of the optical and wettability properties of metal surfaces using 150 kHz femtosecond fiber laser," M. Iqbal, et.al., Appl. Sci. 10, 6207 (2020) (**7** citations), etc.

Publication of the research results. The results of the Ph.D. research are presented in 30 peer-reviewed articles published in prestigious Q1/Q2 quartile scientific journals recommended by the Supreme Attestation Commission of the Republic of Uzbekistan for publication of the main scientific results of Ph.D. thesis and displayed in the *Web of Science* scientific database.

MAIN CONTENT OF THE WORK

The research results are presented in two parts. The first part of the presentation is devoted to the introduction on the formation mechanisms of nanoparticles and novel applica-tions [Appl. Surf. Sci. 527, 146702 (2020) and Appl. Surf. Sci. 542, 148560 (2021)]. The second part of the presentation focuses on the analysis of the formation mechanisms of nanostructures on materials surfaces and novel applications [Front. in Chem. 8, 768 (2020), J. Phys. D: Appl. Phys. 54, 185109 (2021), and Appl. Sci. 10, 6207 (2020)]. The findings presented here are published by Ph.D. candidate and his coauthors in 30 scientific articles from Q1/Q2 quartiles of scientific journals. The experimental data, theoretical calculations, and numerical simulations were developed and employed during the last 5 years of work in different institutions of the United Arab Emirates, Germany, Latvia, Russia, and of Uzbekistan.

Part 1. Formation mechanisms of nanoparticles and novel applications

The behavior of materials at the nanoscale differs significantly from their macroscopic counterparts due to quantum effects and an increased surface-to-volume ratio. This altered behavior often leads to unique properties and applications for nanomaterials. Aluminum nanoparticles (NPs) exhibit a variety of applications, including their ability to change the wettability and nonlinear optical properties of surfaces, suspensions, and plasmas. In this work [Appl. Surf. Sci. 527, 146702 (2020)], we present a theoretical and experimental study of the laser-assisted formation mechanisms of Al-based nanoparticles in liquids and in the vacuum.

Numerous factors, such as laser pulse duration, fluence, the type of surrounding media, temperature of the liquid, and characteristics of the irradiated targets, influence the properties of NPs. Additionally, the morphology and size of synthesized particles can cause variations in different macroscopic properties of NP-containing substrates and suspensions. We performed Molecular Dynamics (MD) numerical simulations to understand the formation process of aluminum NPs during the ablation of bulk targets. These simulations allowed us to identify the main mechanisms of NPs formation in liquid media and to determine the optimal laser irradiation parameters for producing Al NPs of the desired size and morphology.

The results of the simulations can be used for direct comparison with experimental measurements and also help us gain deeper insights into the fundamental physics of processes involved in laser-assisted generation of NPs. These simulations were performed using a combined atomistic-continuum model. The use of numerical simulations to study the mechanisms of nanoparticle formation in liquid media and to optimize laser irradiation parameters for producing aluminum nanoparticles is a powerful approach. By leveraging computational models, researchers can gain insights into the underlying physics of the laser-assisted generation of nanoparticles. The simulations allow for a detailed analysis of the interactions between the laser pulse, target material, and surrounding liquid environment, providing a comprehensive understanding of the nanoparticle synthesis process. By varying the simulation parameters, such as laser fluence, pulse duration, and target properties, researchers can identify the optimal conditions for producing aluminum nanoparticles with specific size and morphology.

The model addresses the kinetics of laser-induced non-equilibrium phase-transition processes at the atomic scale using the MD method [Science 280, 2085-2088 (1998)]. The processes of laser light absorption, electron heat conduction, and strong electron–phonon non-equilibrium, induced by a short laser pulse, are described with the Two-Temperature model (TTM) via the electron temperature. When used in a parallel version in a multi-processing regime, the combined MD-TTM model dynamics [Appl. Phys. A 111, 675–687 (2013)] can be applied in super large simulations on the scale directly attainable in experiments. The results of our simulations, therefore, can be directly considered during the interpretation of experimental data and for the generation of NPs with pre-designed properties. The model combines the MD approach, which describes atomic motion, with the diffusion differential equation for electrons entering the TTM model, accounting for the effect of free carriers as reported in [Phys. Rev. B, 68, 064114 (2003)].

In metals, when laser light interacts, it is absorbed by the conduction band electrons. The energy deposited is quickly equilibrated among the electrons, typically within femtoseconds, and then transferred more slowly to the atomic vibrations. This transfer process, governed by the strength of the electron-phonon coupling, can take from a fraction of a picosecond to several tens of picoseconds. Eventually, a thermal equilibrium is reached between the electrons and phonons, leading to heat flow from the surface region into the bulk of the irradiated target, described by common thermal diffusion. When the duration of the laser pulse is comparable to or less than the time needed for electron-phonon thermalization, laser irradiation creates a state of thermal nonequilibrium, where electrons and the lattice have different temperatures. At a continuum level, the evolution of the lattice and electron temperatures, T_l and T_e, respectively, can be described by the TTM. This model uses two coupled nonlinear

differential equations to represent this behavior, as explained in [Phys. Rev. B 68, 064114 (2003)].

$$C_e(T_e)\frac{\partial T_e}{\partial t} = \nabla[k_e(T_e)\nabla T_e] - G(T_e - T_l) + S(z,t) \quad (1)$$

$$C_l(T_l)\frac{\partial T_l}{\partial t} = \nabla[k_l(T_l)\nabla T_l] + G(T_e - T_l) \quad (2)$$

Where *C* and *K* are the heat capacities and thermal conductivities of the electron and lattice as denoted by the subscripts *e* and *l*, and *G* is the electron-phonon coupling constant. The source term *S(z,t)* describes the local energy deposition per unit area and unit time during the laser pulse duration.

The computational MD method is invaluable for gaining insights into the mechanisms of laser-metal interactions. However, the classical MD method is not directly suitable for simulating laser interactions with metals. This limitation arises because the electronic contribution to the thermal conductivity of a metal is dominant. In the conventional MD method, only the lattice contribution is considered, leading to a significant under-estimation of the total thermal conductivity. To address this issue, a combined TTM and MD model is often used. This combined approach allows for a more accurate representation of the processes involved in laser-metal interactions by accounting for both the lattice and electronic contributions to thermal conductivity.

In the combined method the MD method completely substitutes the TTM equation for the lattice temperature, Eq. (2). The diffusion equation for electron temperature T_e, Eq. (1), is solved by a finite difference method simultaneously with MD integration of the equations of motion of atoms and the electron temperature enters the coupling term which is responsible for the energy exchange between the electron and the lattice [Phys. Rev. B 68, 064114 (2003)];

$$C_e(T_e)\frac{\partial T_e}{\partial t} = \frac{\partial}{\partial z}\left[k_e(T_e)\frac{\partial}{\partial z}\,(T_e)\right] - G(T_e - T_l) + S(z,t) \text{ TTM}$$

$$m_i\frac{d^2\mathbf{r_i}}{dt^2} = \mathbf{F_i} + \eta\, m_i\mathbf{v_i} \qquad \text{MD} \quad (3)$$

where η is

$$\eta = \frac{1}{n}\sum_{k=1}^{n} GV_N(T_e - T_l)/\sum_i m_i(\mathbf{v_i})^2 \quad (4)$$

In Eq. 4, m_i and $\mathbf{r}_i$ are the mass and position of an atom *i*, and F_i is the force acting on atom *i* due to the interatomic interaction. An additional term, added to the ordinary MD equations of motion, accounts for the electron-phonon coupling. The step of the spatial discretization (Δt_{FD}) in the finite difference (FD) integration of Eq. (3) can be estimated based on the von Neumann stability criterion. The time steps in the two parts of the combined model are chosen so that one MD time step would correspond to an integer number of finite difference time steps, $\Delta t_{MD}=n\Delta t_{FD}$. In each finite difference discretization cell, the energy transferred between the electrons and the lattice due to

the electron-phonon coupling is accumulated for *n* steps of integration [Phys. Rev. B 68, 064114 (2003)],

$$\Delta E^{e-ph} = \sum_{k=i}^{n} \Delta t_{FD}\, G V_N (T_e - T_l) \quad (5)$$

The accumulated energy is then transferred to (or extracted from) the energy of the atomic motion in the corresponding part of the MD system by means of the coupling term added to the MD equations of motion, Eq. (4).

A Gaussian temporal profile is used in the simulations to describe the laser energy deposition [Phys. Rev. B 68, 064114 (2003)],

$$S(z,t) = I_o\,(1-R) L_p^{-1} \exp\left(-\frac{z}{Lp}\right) \exp\left[-(t-t_o)2/2\sigma^2\right. \quad (6)$$

Where I_o is the peak intensity, R is the reflectivity, L_p is optical absorption depth, and σ is the standard deviation of the Gaussian beam profile related to the pulse duration FWHM = $\sigma\sqrt{8\ln(2)}$. The laser fluence is related to peak intensity I_o,

$$F = \sqrt{\pi/4\ln(2)}\,\tau_L I_o \sim 1.0645\,\tau_L I_o \quad (7)$$

We performed modeling for short and long laser pulse ablation of aluminum target with same incident fluence of 10 J/cm^2. This allowed us to illustrate the pulse duration effect on the mechanism of NPs generation. To relate our simulation results to the experimental data, we chose two pulse durations of 0.3 ps and 50 ps that are correspondingly considered as short and long pulses as compared to the characteristic electron–phonon equilibration time for Al (~1.5 ps).

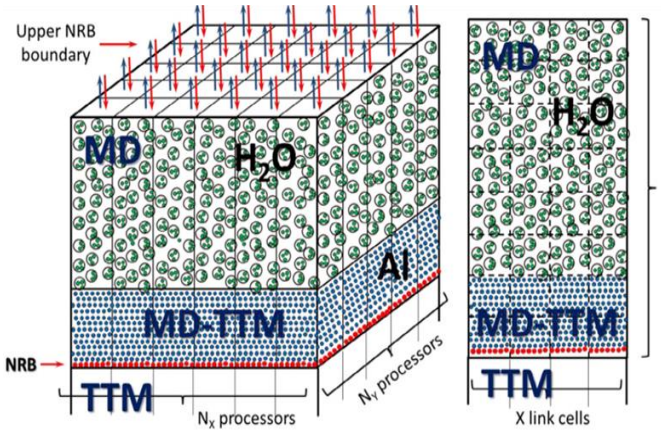

Fig.1. The total computational cell for simulations of laser generation of NPs under thick water layer is divided to sub-volumes N_x and N_y in X and Y directions for the processing by $N_x \times N_y$ processor cores correspondingly (left). Each separate core is divided to 3D mesh, where we solve the combined MD-TTM model, while the classical MD approach is applied for the water layer (2D view on the right) [Appl. Surf. Sci. 527, 146702 (2020)].

This approach enables the consideration of different regimes of target damage, followed by the NPs formation process, and covers the femtosecond (fs) and picosecond (ps) ranges of pulse durations used in the experimental part of this work. Similar to the experiment, the target is situated under spatial confinement by a thick water layer, where "thick" refers to a thickness large enough to prevent laser-induced pressure wave reflections from free surfaces during the NPs formation process. The total computational cell used in our simulations of aluminum NPs formation under spatial confinement due to water is schematically shown in Fig. 1.

Since the size of the laser spot in the experiment (0.3 mm) was much larger than the characteristic lateral size of the simulation cell (100 nm), the laser intensity across the cell's surface roughly remained uniform during the irradiation time. Moreover, the relatively slow processes of heat conduction in the lateral direction during the simulation time up to a few nanoseconds still allowed us to impose periodic boundary conditions (PBC) in the X and Y directions. The lateral size of the computational box was also large enough to fit the processes resulting in the formation of NPs with sizes in the range of approximately 10-100 nm, as measured experimentally. Thus, the aluminum-water MD supercell consists of approximately 300,000,000 atoms and has dimensions of $75 \times 100 \times 900$ nm^3 in the X, Y, and Z directions respectively, with thicknesses of 400 nm for the metal and 500 nm for the water layers, providing atomic resolution. To increase the computational efficiency of the simulation procedure, we applied the combined MD-TTM model for aluminum only within the 400 nm thickness below the surface. Here, we placed non-reflective boundary (NRB) conditions below, where we solved the TTM for aluminum only to account for the heat flux from the surface to a distance of up to approximately 50 μm beneath the surface [Comp. Mater. Sci 24, 421 (2002)]. The use of NRB conditions allowed for the absorption of laser-induced pressure waves generated near the surface due to rapid laser heating.

Similarly, to account for the presence of the liquid medium above, the NRB boundaries for water were placed at a distance of 500 nm above the metal-liquid interface. Thus, each processor core was devoted to solving the combined MD-TTM model for the metal part, the ordinary MD model for the water part, and the TTM model of the metal part below 400 nm from the surface (a 2D mesh is shown for a single processor in Fig. 1). To relate our simulation results to experimental data, we employed a realistic interatomic potential for aluminum. This potential accurately represents thermophysical properties of the material such as heat capacity, equilibrium melting temperature, thermal expansion coefficient, and volume of melting (greater than 95% accuracy).

The results of modeling the interaction between a 0.3 ps laser pulse and aluminum under water are depicted in Fig. 2 and generally align with the outcomes of NPs generation in water using an ultrashort laser pulse. In the latter scenario, the process of NP generation in liquid media is attributed to two main mechanisms: NP nucleation from the vapor phase at the top of the ablation plume and the formation of Rayleigh–Taylor instabilities across the liquid metal interface. These mechanisms are believed to be responsible for the formation of a bimodal NP size distribution, as discussed in [Nanoscale 10, 6900-6910 (2018)]. In our study, we enhanced these mechanisms with explanations that allow for the manipulation of NP size distribution by adjusting the

laser irradiation parameters. From the atomic snapshot in Fig. 2(a), it is evident that by the time of 175 ps, the irradiated target has undergone both the process of evaporation from its surface and the expansion process, leading to the formation of voids in the bulk of the material. This phenomenon is related to the onset of the spallation process.

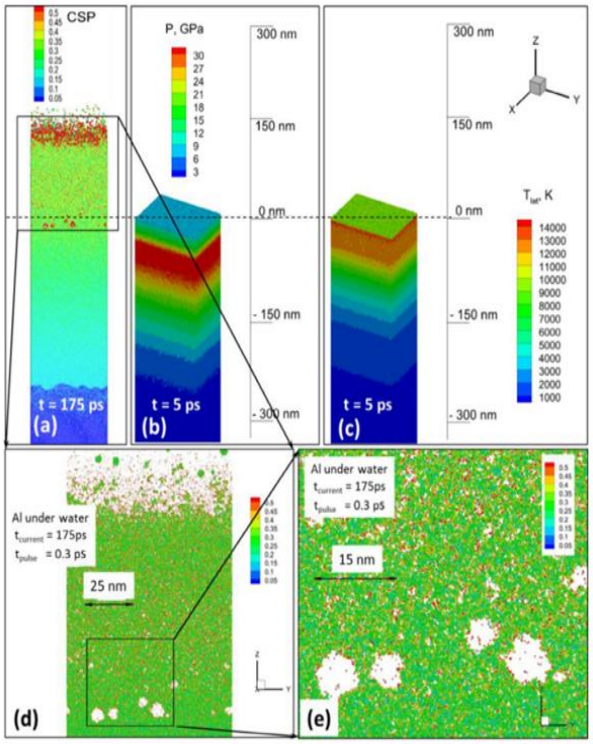

Fig.2. (a) The result of 0.3 ps laser-generation of Al NPs in water at the incident fluence of 10 J cm^{-2} is shown as atomic snapshots for the time of 175 ps and reveals the indication of subsurface voids growth. The atoms are colored by Central Symmetry Parameter (CSP) for identification of atomic local structure so that SCP values are: solid<0.08<defects<0.12<liquid<0.25<surface<0.50<vapor. Green liquid NPs are seen at the top of the plume with some contribution of red vapor atoms. The water atoms are not shown. (b) The pressure filed is shown for the moment of its maximum value of 36 GPa providing the conditions for involvement of the spallation mechanism into the process of ablation. (c) The lattice temperature field is shown for the moment of its maximum value of 11,000 K that provides conditions for the explosive boiling mechanism of the material ejection process. (d) The squared region in (a) is shown for a better observation of the forming NPs. (e) The framed region from (d) is zoomed for visual identification of the porosity forming inside the Al target [Appl. Surf.Sci. 527, 146702 (2020)].

There are two main channels of energy dissipation in the metallic target when exposed to a laser pulse: fast electron heat conduction and the process of electron–phonon energy exchange leading to lattice heating. The pulse duration of 0.3 ps is shorter than the electron–phonon relaxation time (~1.5 ps), so the heating rate is determined by the electron–phonon equilibration time. The high electronic temperature (~40,000 K) achieved during laser pulse absorption results in significant heating depth due to the strong function of electronic temperature on the electron heat conductivity. This heating rate exceeds the material's mechanical (acoustic) relaxation rate, leading to the accumulation of high internal stresses (up to 36 GPa) in the pre-surface area of the irradiated target, as shown in Fig. 2(b). These conditions, known as internal stress confinement, lead to their relaxation due to a strong unloading pressure wave propagating through the target. The mechanical relaxation leads to the formation of internal voids, as seen in Figs. 2(d) and (e), which coalesce, grow, and initiate the spallation process associated with the mechanical damage of the target [Appl. Phys. A 117, 2133 (2014)], resulting in the formation of a larger fraction of NPs due to the generation of Rayleigh–Taylor instabilities across the liquid metal interface. On the

other hand, the metal surface is overheated above the critical point (due to the large absorbed energy) to a maximum value of 11,000 K, as shown in Fig. 2(c), resulting in an ablation process governed by the explosive boiling mechanism. This leads to the formation of a smaller fraction of NPs due to the nucleation of the metal vaporized atoms. The connection between the spallation and phase explosion mechanisms of the ablation process, depending on the applied fluence, was discussed in more detail in [J. Chem. Phys. 113, 11892 (2009)].

A more interesting case for our work, which offers more advantages in the experimental part, was the generation of aluminum NPs under water using a long laser pulse. To simulate the interaction of a long pulse with an aluminum target, a pulse duration of 50 ps was chosen. Since this duration is much longer than the characteristic electron–phonon equilibration time for aluminum (~1.5 ps), the material's heating time is determined by the pulse duration. The results of modeling the NP formation in water due to a 50 ps laser pulse focused on the aluminum target are shown in Fig. 3. The sequence of atomic snapshots of the system is shown for times of 125, 250, and 500 ps from the beginning of the simulation, as depicted in Fig. 3(a).

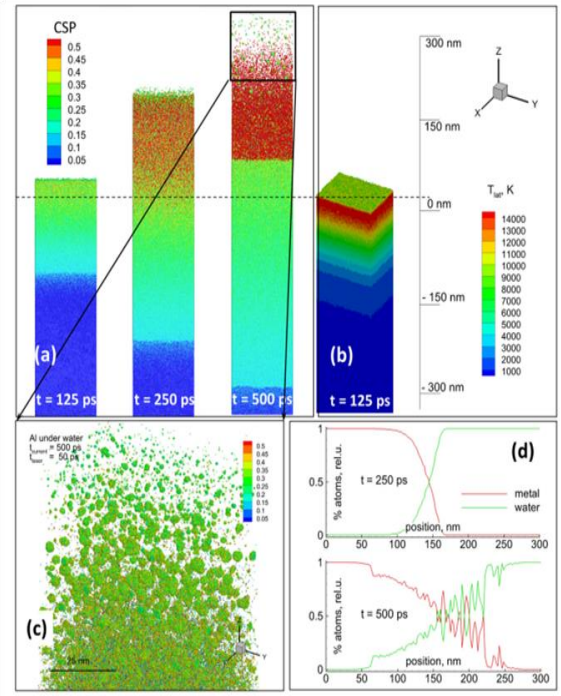

Fig.3. (a) The result of 50 ps laser pulse interaction with Al at the incident fluence of 10 J cm^{-2} is shown as the sequence of atomic snapshots for 125, 250, and 500 ps. The atoms are colored by Central Symmetry Parameter (CSP) for identification of atomic local structure: solid < 0.08 < defects < 0.12 < liquid < 0.25 < surface < 0.50 < vapor. Green NPs are seen at the top of the plume with significant contribution of red vapor atoms. The water atoms are blanked for a better visualization of the metallic part of the system. (b) The lattice temperature field is shown for the moment of its maximum value of 14,000 K at the time of 125 ps. (c) The rectangular region in (a) is zoomed for a more detailed observation of the forming NPs. (d) The relative density of metallic and water species at 250 ps and 500 ps reveals their mixing progress [Appl. Surf. Sci.527, 146702 (2020)].

In these simulations, the laser pulse reached its maximum intensity by 125 ps, and we considered a simulation time of 500 ps to be long enough to encompass the essential processes responsible for NP formation mechanisms. While the actual processes of NP formation can take much longer (a few nanoseconds), in this research, we were primarily interested in manipulating the established mechanisms of NP formation [J. Phys. Chem. C 121, 16549–16567 (2017)]. It should be noted that the conditions

determining the mechanism of NP formation are generally established by the time of electron–phonon equilibration or by the end of the pulse, whichever is longer. By this time, both channels of laser-deposited energy dissipation (electron heat conductivity and electron–phonon interaction) cease the most intensive energy transport, which essentially determines the subsequent evolution of the target and the NP formation process itself. The long laser pulse cannot induce strong electron–phonon nonequilibrium. The electronic temperature during the pulse remains roughly equal to the temperature of the lattice and is limited to around 15,000 K, where the energy dissipation channel through electron conductivity is much weaker than the electron–phonon interaction (lattice heating) channel. Consequently, the deposited heat cannot penetrate deep into the target (compared to the case of a short laser pulse) and roughly remains near the target's surface. This results in the establishment of a thermal confinement regime under conditions of gradual acoustic (mechanical) relaxation of the heated target, as reflected in Fig. 3(b), with a high temperature on the surface and a maximum internal pressure of 4 GPa, which is negligible compared to the previous case.

However, the long heating time results in the elevation of the lattice temperature above the critical point, up to 14,000 K, where the mechanism of the ablation process is governed by explosive boiling [J. Phys. Chem. C 113, 11892–11906 (2009)]. Since the irradiated target remains mechanically relaxed, the spallation mechanism of the ablation process is not involved here, and the incurred damage to the target is purely thermal. This can be seen in Fig. 3(a), where the mechanically relaxed melts, overheated to supercritical temperatures, resulted in the establishment of a smooth transition vapor–liquid mixture zone. The vaporized metal atoms undergo intensive cooling due to the water medium, which has both a significant heat capacity (comparable to that of metals) and high vaporization energy losses. Thus, the intensive process of nucleation of the metal NPs leads to their uniform generation in a visibly larger amount, as shown in Fig. 3(c). In contrast, for the case of a 0.3 ps laser pulse, the process involves moderate surface vaporization of metal atoms due to high absorbed fluence, essentially accompanied by the mechanical damage of the target due to the spallation mechanism of the material ejection process, followed by the growth of subsurface voids [Nanoscale 10, 6900-6910 (2018)]. The effect of a water layer on NP formation due to a laser pulse can be divided into several stages. First, the water medium, having an atomic density comparable to that of metal, causes significant mechanical resistance to the upward motion of the ablated material. Although acoustically relaxed, the presurface layer of molten metal still possesses a remaining non-zero pressure of 4 GPa by the time of 125 ps. As a result of this resistance, the size of the ablation plume is noticeably smaller compared to that in air or in vacuum. Second, the high heat capacity of water (comparable to that of metal) and its high

vaporization heat losses facilitate the intensive cooling of the vaporized metal atoms, resulting in the nucleation of NPs as early as 100 ps. The intensive evaporation process inside the ablation plume, however, prevents the liquid from penetrating deep into the ablated material, and its cooling mechanism is therefore governed by conventional heat conduction. This can be seen in Fig. 3(d), where the relative densities of metal and water particles are shown for 250 ps and 500 ps from the beginning of the simulation. The ablating material pushes the liquid away, and only an insignificant amount of vapor water atoms penetrates the top of the ablation plume at later times. This observation is consistent with similar analyses in [J. Colloid Interface Sci. 489, 3-17 (2020) and Phys. Chem. Chem. Phys. 22, 7077-7099 (2020)]. Moving from the top to the bottom of the ablation plume, one can identify that the small particles at the top are efficiently decelerated and cooled down by the water medium, limiting their growth and bringing their size close to the size of particles formed in the middle of the plume. This makes the NP generation mechanism in water very different from that in vacuum, where the ejected mixture of vapor and liquid droplets, once ejected, is not facilitated by intensive nucleation and formation processes anymore due to significant lift-off speed disperse as a function of the ejected clusters mass. As a result, the smaller droplets that are ejected and formed first have much higher upward velocities than those ejected later at lower temperatures and heavier masses [Appl. Phys. A 114, 11 (2014); Appl. Surf. Sci. 470, 1018 (2018)]. In contrast, during the NP formation process in liquids, the initial segregation of the newly formed NPs by size and speed is reversed due to the thermal and mechanical action of the water layer, and the lift-off velocity of nucleating NPs in liquid media is more than one order of magnitude slower than that in air or in vacuum [Nanomater. 10, 234 (2020)]. Thus, the effect of the liquid on the NP generation process results in a smoother size distribution of the final fraction compared to vacuum conditions. Such an effect from the liquid environment was also emphasized in recent theoretical works [Nanomater. 9, 767 (2019)] and holds for the range of femtosecond to nanosecond pulse durations. Moreover, the NP size distribution analysis, performed for both cases of short 0.3 ps and long 50 ps laser pulses, confirms our above discussions and reveals even more possibilities for the generation of NPs with a narrower size distribution. Figs. 4(a) and (b) show the atomistic view of a slice of the computational cell for the cases of short and long pulse durations. From these pictures, it is seen that the short pulse, resulting in stress confinement in the target (mechanical damage regime), facilitates the formation of a noticeably larger fraction of NPs with some input from vaporized metal atoms. Alternatively, the long pulse induces more pronounced thermal confinement (thermal damage regime), and the target, mechanically relaxed and gradually expanding, generates a much larger amount of

vaporized atoms under conditions of overcritical heating. The process of deceleration and cooling of this vapor due to the liquid environment facilitates the nucleation of noticeably smaller NPs with less size dispersion, as shown in Fig. 4(b). The simulations conducted cover a sufficiently long-time range to establish the main mechanisms responsible for the subsequent evolution of forming nanoparticles (NPs). This is evident from a more quantitative analysis of the NP size distribution, as shown in Figs. 4(c) and (d) for the short and long pulses in the rectangular areas in Figs. 4(a) and (b). In these regions, the NP formation process is no longer significantly affected by ablation products.

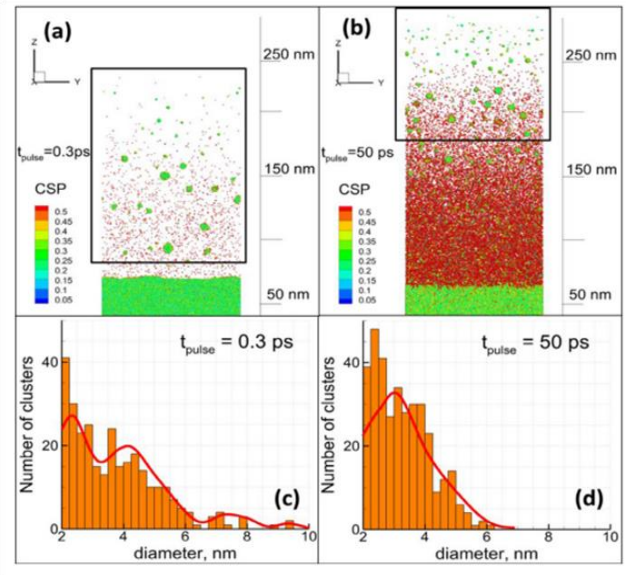

Fig. 4. The atomistic snapshots of the established NPs formation process is shown for the case of short 0.3 ps (a) and long 50 ps (b) pulses. The atoms are colored by CSP for visualization of the forming NPs whereas the water atoms are blanked. The NPs size distribution for the selected by black rectangles areas in (a) and (b) are correspondingly shown for the short 0.3 ps (c) and long 50 ps (d) pulses. The red curves imposed on the NPs distribution histograms are eye guyed [Appl. Surf. Sci. 527, 146702 (2020)].

The use of a large computational domain in our simulations enables the collection of sufficient statistical data and the construction of NP distribution histograms. It is observed that shorter pulses lead to a more dispersed distribution, revealing the formation of two or more fractions with different mean sizes. This observation aligns with recent theoretical findings on the formation mechanisms of bimodal size distribution during short laser pulse generation of NPs in liquids. Specifically, the smaller fraction forms due to the nucleation of vaporized metal atoms, while the larger fraction is a product of Rayleigh-Taylor instabilities across the metal-water interface, originating from the rapid advancement due to the mechanical relaxation of internal stresses (Fig. 4(c)). In contrast, longer pulses do not generate high compressive stresses but instead induce overcritical heating of the target surface, leading to the formation of a large amount of vapor, which then nucleates into a number of NPs of smaller size (Fig. 4(d)). Although the complete process of NP nucleation occurs over a much longer time scale, and the NP size distribution can later shift towards a larger diameter, it can be concluded from Fig. 4 that for longer pulses, the essential driving mechanism of particle formation is explosive boiling, resulting in the formation of smaller NPs. In this case, the ejection of the whole pre-surface layer, with its subsequent Rayleigh-Taylor instabilities and the formation of a larger NP fraction, is suppressed, as the rate

of heating does not exceed the rate of mechanical relaxation of the target. This result not only aligns with recent findings regarding the effect of pulse duration on NP generation in liquids by Shih et al. [Phys. Chem. Chem. Phys., 22, 7077 (2020)] but also suggests the possibility of manipulating the resulting NP size distribution through laser irradiation parameters (pulse duration and incident fluence). This manipulation could lead to a narrower distribution with a specific mean value, which is crucial for generating NPs for biomedical applications where a uniform size distribution of smaller NPs is often required [Sci. Rep. 9, 12890 (2019)]. The thermal confinement regime of NP generation or their production using long (100s of picoseconds and nanoseconds) laser pulses appears to be more preferable for industrial manufacturing. The number of NPs generated during the nucleation process from the metal vapor phase can be observed in Fig. 3(c). Their subsequent shape relaxation in the liquid phase will result in a spherical form, which is consistent with observations reported in [Nanoscale, 10, 6900 (2018)].

After the nucleation of the vapor phase and the completion of NP formation, the products of the ablation process NPs are propelled upward by the established hydrodynamic motion in the liquid medium. The process of NP solidification then occurs over the nanosecond range. Subsequently, suspended in the resulting colloidal liquid, the generated particles can continue to grow due to slow diffusion processes in water under relatively equilibrium conditions. This growth process takes a significantly longer time scale, during which the NP formation mechanism may exhibit a highly pronounced effect of crystal structure, surface chemistry, and oxidation. This effect can result in NPs with unusual shapes, as exemplified in Fig. 5(c).

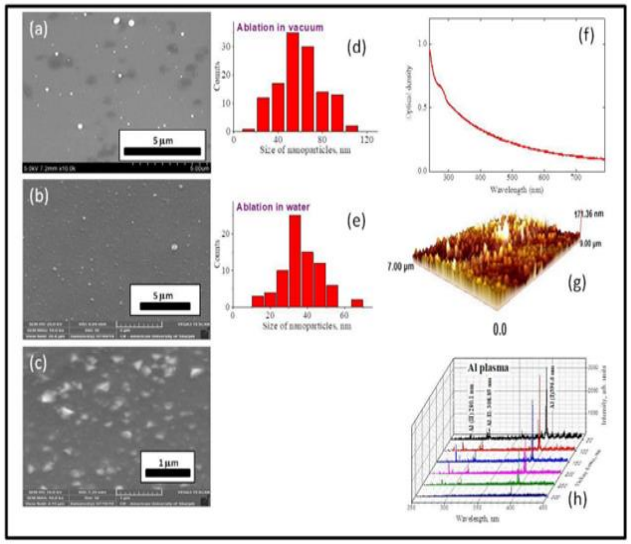

Fig.5. Structural and spectral properties of Al based NPs. (a-c) SEM images of the Al based NPs produced by ablation of target using 10 ns pulses in different environment: (a) vacuum, (b) water, and (c) water (after 30 days). The corresponding histograms of the NPs size distributions are shown in (d) and (e) in the case of ablation in vacuum and water, respectively. (f) Absorption spectrum of Al based NPs suspension. (g) Atomic force microscopy image of Al NPs layer deposited during ablation in vacuum. (h) Variation of plasma emission (250–450 nm). UV spectra of Al plasma were collected at different delays from the beginning of ablation by nanosecond pulses [Appl. Surf. Sci. 527, 146702 (2020)].

Aluminum-based NPs were produced by ablating a bulk aluminum target immersed in deionized water using laser pulses with a wavelength of 1064 nm, a pulse duration of 10 ns, and a repetition rate of 10 Hz at a pulse energy of 40 mJ (NL300, EKSPLA). The laser beam was focused using a F=100 mm focal length lens. Ablation of bulk Al in vacuum was also performed using the same laser, with the 10 ns pulses focused inside a vacuum chamber onto the surface of the aluminum target. The debris from the ablated material was deposited on nearby glass and silicon substrates, and the ablation process lasted for 30 minutes. Additionally, femtosecond pulses (300 fs, 1030 nm, 100 kHz, 0.5 mJ; AFS systems) were used to ablate the aluminum target in both water and vacuum.

The morphology of particles deposited during ablation by 10 ns pulses in vacuum and water was examined using a scanning electron microscope (SEM). The SEM images of Al-based NPs generated by nanosecond pulses in vacuum and water are depicted in Figs. 5(a)-(c), with NP sizes measured at 55 nm and 34 nm, respectively (Figs. 5(d) and 5(e)). A qualitative comparison of these two cases revealed a narrower size distribution when ablation occurred in water. This effect can be attributed to the thermal and mechanical action of the dense liquid environment (water), as suggested by the theoretical study. The process of NP formation can be influenced by either the spallation mechanism of material ejection (mechanical damage regime), the explosive boiling mechanism (thermal damage regime), or a combination of both, especially for sufficiently high values of absorbed laser energy (fluence).

Nonlinear Optical Properties: The motivation behind studying the nonlinear absorptive and refractive properties of NPs, along with their various optical characteristics, stems from their potential applications in optoelectronics, optical limiters, and photonics. However, previous studies have not addressed the impact of pulse duration during the ablation of Al targets on the coefficients of nonlinear absorption and nonlinear refraction of Al-based NPs. The search for small-sized materials with strong nonlinear refractive and absorptive properties led us to analyze NPs produced by nanosecond, picosecond, and femtosecond pulses. We examined the nonlinear optical properties of different Al-based NP suspensions prepared by ablating bulk aluminum in water with nanosecond, picosecond, and femtosecond pulses using the Z-scan scheme. The normalized transmittances of Al-based NP suspensions were analyzed using the standard fitting procedure to determine their nonlinear absorption coefficients (β) and nonlinear refractive indices (γ). The aluminum-based NPs were obtained by ablating Al bulk in water using pulses with different durations (5 ns, 200 ps, and 30 fs). The normalized transmittance T_{2PA} in the case of open-aperture (OA) scheme and two-photon absorption (2PA) can be written as follows:

$$T_{2PA}(z) = \frac{\ln(1+r)}{\mathrm{r}} \approx 1 - \frac{r}{2\sqrt{2}} \tag{8}$$

Here, $r=\beta I_0 L_{eff}/(1+(z/z_0)^2)$, $x=z/z_0$, $z_0=k(w_o)^2/2$ is the Rayleigh length, k is the wave number $k=2\pi/\lambda$, w_0 is the beam waist radius, I_0 is the peak intensity of input beam at focal plane, $L_{eff}=[1-exp(-\alpha_0 L)]/\alpha_0]$ is the effective length of the medium, α_0 is the linear absorption coefficient, and L is the sample thickness. In the case of closed aperture (CA) scheme, the transmittance can be presented as

$$T_{NRA}(z) = 1 + \frac{2(-\delta x^2+2x-3\delta)}{x^4+10x^2+9}\Delta\varphi_0 \quad (9)$$

Here $T_{NRA}(z)$ is the transmission of medium at the conditions of nonlinear refraction and absorption (NRA), $\delta = \beta/2k\gamma$ and $\Delta\varphi_0=k\gamma I_0 L_{eff}$ represents the nonlinear refraction-induced phase change. The nonlinear optical coefficients of 2PA and NRA of Al based

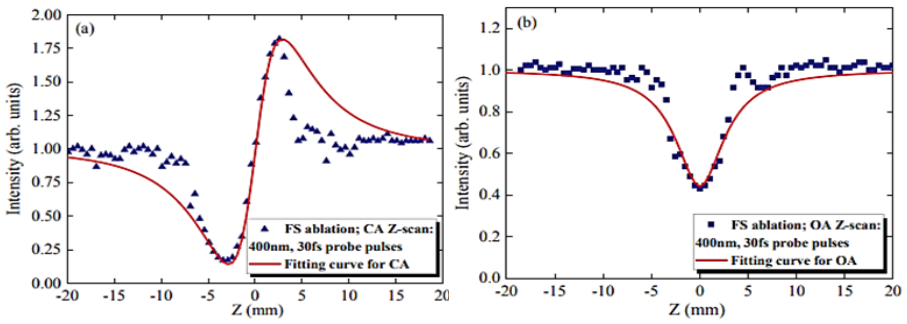

Fig.6. (a) CA and (b) OA Z-scans of suspensions measured using 400 nm, 30 fs pulses. The suspension was prepared by ablation of bulk aluminum in water using 30 fs pulses. Fitting curves (solid lines) correspond to Eqs. (7) and (8) [Appl. Surf. Sci. 527, 146702 (2020)].

NPs suspension were calculated using Eqs. (8,9). Fig. 6 shows the CA and OA Z-scans of samples using 400 nm, 30 fs pulses. Fitting of these curves allowed determining the nonlinear absorption coefficients and nonlinear refractive indices of three suspensions (generated by fs, ps, and ns pulses) using 400 nm, 30 fs pulses. The highest values of nonlinear optical parameters were observed in the case of the suspension produced by ablation of aluminum using picosecond pulses, while other two suspensions showed three (femtosecond ablation) and five (nanosecond ablation) times smaller γ and β. The γ and β of the NP suspension produced by picosecond pulses were measured to be ~ 10^{-13} cm^2 W^{-1} and 10^{-11} cm W^{-1}, respectively. Since the volume part of NPs in these suspensions was ~10^{-4}, the values of γ and β of Al based NPs were estimated as ~10^{-9} cm^2 W^{-1} and 10^{-7} cm W^{-1} correspondingly, which are among the highest values reported in this spectral region.

High Harmonic Generation (HHG): One of the goals of our study was to demonstrate high-order harmonic generation in laser plasmas produced on the surface of aluminum targets. Ablation of metals in vacuum under specific conditions can lead to the formation of laser-produced plasma (LPP) containing nanoparticles [Phys. Rev. B 71, 174405 (2005)]. Several requirements, such as the pulse duration of the heating radiation, the fluence of laser pulses, and the need for "optimal plasma" formation, must be maintained during the formation of nanoparticles. This is crucial for further

interaction with ultrashort pulses to generate strong high-order harmonics compared to the case of laser-atom interaction. The term "optimal plasma" refers to the conditions required for efficient HHG of ultrashort pulses. This involves maintaining a small number of free electrons in the plasma to suppress processes that lead to phase mismatch between the driving and harmonic waves, resulting in a decrease in harmonic conversion efficiency [Opt. Commun. 135, 251 (1997), Phys. Rev. A 83, 023832 (2012)].

The optimal delay between the beginning of ablation by heating pulses and the propagation of driving femtosecond pulses through the pre-formed plasma was a crucial parameter in these studies. This delay was determined to ensure that the maximum concentration of active species, such as NPs, coincided with the propagating laser pulse. The method used to determine the optimal delay involved analyzing the time-dependent spectrum of emission, in addition to direct experimental observation of harmonic yield. The studies conducted prior to the HHG experiments revealed that a delay in the range of 100 –150 ns from the start of ablation allowed the plasma to reach the region where the driving femtosecond beam propagated. This timing created optimal conditions for achieving the highest harmonic yield. A similar approach had previously been demonstrated in the case of gold plasma, indicating the importance of timing and spatial alignment in maximizing harmonic generation efficiency [J. Appl. Phys. 102, 073105 (2007)]. An additional motivation for our time-resolved studies of plasma emission was to determine the conditions of target ablation where only neutral (Al I) and singly ionized (Al II) particles are emitted in the near-ultraviolet (UV) range, as shown in Fig. 5(h).

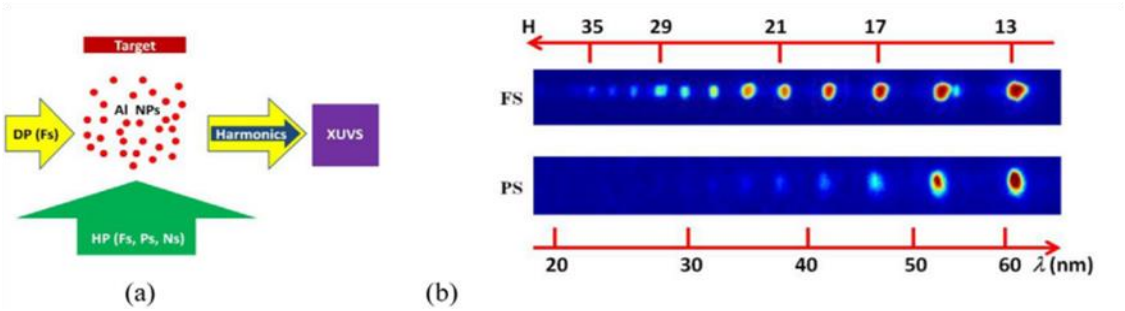

Fig. 7. (a) Scheme for HHG in Al LPP. DP (Fs): driving femtosecond pulse, HP (Fs, Ps): heating (either nanosecond, or picosecond, or femtosecond) pulse, Target: aluminum bulk target; Al NPs: aluminum nanoparticles-containing plasma, Harmonics: high-order harmonics from the driving pulse, XUVS: extreme ultraviolet spectrometer. (b) Harmonic spectra from femtosecond (upper panel) and picosecond (bottom panel) LPPs [Appl. Surf. Sci. 527, 146702 (2020)].

In our HHG experiments, we used a femtosecond laser with a wavelength of 800 nm and a pulse duration of 40 fs. The laser radiation propagated at a distance of approximately 200 μm above the target surface through the laser-produced plasma (LPP) containing aluminum nanoparticles, as illustrated in Fig. 7(a). The LPP was

generated by focusing 200 ps, 800 nm pulses of uncompressed radiation from the same laser onto the surface of an aluminum target using a 300-mm focal length cylindrical lens, resulting in the formation of a 5-mm long plasma plume. The harmonic emission was analyzed using an extreme ultraviolet (XUV) spectrometer consisting of a vertical slit, a gold-coated cylindrical mirror, a 1200 lines/mm flat-field grating, a microchannel plate, and a CCD camera. The harmonic spectrum shown in Fig. 7(b) demonstrates that the cutoff in the case of femtosecond-induced LPP (H35) is larger than in the case of picosecond-induced LPP (H25). Additionally, the yield of higher-order harmonics in the former case was larger than in the case of HHG in the LPP formed by picosecond pulses.

We applied the Lewenstein model of HHG [Phys. Rev. A 49, 2117 (1994)] to analyze the influence of neutrals and ions on the harmonic yield. The harmonics from the aluminum NPs plasma mainly originate from the neutral particles. It is noteworthy that increasing the intensity of the picosecond heating pulse above 3×10^{10} W/cm^2 led to a significant decrease in harmonic yield due to the appearance of a large number of free electrons. In addition, we conducted HHG in NP LPP using a two-color pump (TCP, 800 nm+400 nm) on the aluminum plasma. In our experiments, the conversion efficiency of second harmonic pulses (λ = 400 nm) was relatively low (~2% and ~4% with 0.2- and 0.4-mm thick beta barium borate (BBO) crystals, respectively). Due to the small group velocity dispersion in the former BBO crystal, the temporal overlap of the two driving pulses in the plasma area was sufficient for HHG in the longer-wavelength range of XUV. However, we observed the absence of the whole group of even harmonics, especially those corresponding to H=4(n+1). Specifically, the discrimination of H12, H16, and H20 was a distinctive feature in the case of TCP using a 0.4-mm thick BBO crystal, while in the case of applying a 0.2-mm thick BBO crystal, all those harmonics were nearly similar to other even harmonics, as well as comparable with the odd harmonics.

The findings from this study highlighted the importance of in-situ formation of aluminum nanoparticles in a vacuum environment for enhancing harmonic generation compared to using aluminum atoms and ions. The presence of aluminum nanoparticles facilitated the generation of high-order harmonics up to the 37th order when subjected to 40 fs pulses propagating near the ablating aluminum target. This research demonstrates the potential benefits of utilizing aluminum nanoparticles for enhancing harmonic yield in laser ablation processes.

Wettability: Wetting properties of materials surfaces play important role in different practical and fundamental applications and are characterized by their contact angle (CA), which is the angle between surface of the liquid and the outline of the contact

surface. Briefly, the contact angle of an ideally flat surface, depending on the surface free energy of the solid, liquid, and vapor interfaces, is described by Young's equation:

$$cos\,(\theta) = \frac{\gamma_{SV} - \gamma_{SL}}{\gamma_{LV}} \quad (10)$$

where θ is the water contact angle at the interface with solid (S), liquid (L), and vapor (V), while γ_{SV}, γ_{SL} and γ_{LV} are the interfacial surface tensions, respectively.

One can deduce, from Eq. (10) that the contact angle is a result of thermodynamic equilibrium of free energy at the solid, liquid, and vapor interface. However, this equation is not useful for the real surfaces, which show the roughness or chemical heterogeneity. In general, the roughness factor of surfaces should be considered during the evaluation of the surface wettability. For rough surfaces, the Young's equation reads as follows [Ind. Eng. Chem. 28, 988–994 (1936)],

$$cos\theta_w = \frac{r(\gamma_{SV} - \gamma_{SL})}{\gamma_{LV}} = r cos\theta \quad (11)$$

where r is the surface roughness factor that significantly improves the wettability response. According to this relation the increase of the roughness of the hydrophobic material leads to the growth of its hydrophobicity and vice versa. Equations 10 and 11 are commonly used to correlate the surface roughness with the contact angle of a liquid droplet on a solid surface. The water contact angles (WCA) of $<90^0$ are considered hydrophilic, whereas surfaces with WCA$>90^0$ are considered hydrophobic. The surfaces are called superhydrophobic when a contact angle becomes larger than 150^0. The development of superhydrophobic surfaces with different states has the far-reaching impact on the practical applications and will also be of much relevance for fundamental research [Adv. Mater. 19, 3423–3424 (2007)]. According to [Langmuir 26, 18621–18623 (2010)], the superhydrophilicity can be referred to those textured and /or structured materials (rough and/or porous) having a surface roughness factor (as defined from the equation (11) larger than one ($r > 1$).

The wetting contact angle for rough surface is given by equation:

$$cos\,\theta_c = f \times cos\theta_\gamma + f - 1 \quad (12)$$

where f is the ratio of the solid–liquid contact area of a water droplet. One can infer from this equation that WCA increases due to the roughness of the surfaces by decreasing the value of f (Fig. 8).

In the case of the modified surface of metal alloy the saturation process can play important role for changing the wetting contact angle after ablation due to the formation of the oxidation of metal surface. In our next work [Appl. Surf. Sci. 527, 146702 (2020)], we studied the wetting properties of the Al based NPs films prepared by self-assembly of NP layers deposited on the glass surfaces. The film preparation process involved creating suspensions of aluminum-based nanoparticles in water by using nanosecond and femtosecond pulse-induced ablation of bulk material. These

suspensions were then applied layer by layer onto cleaned glass slides using the drop-casting method. Each layer was dried thoroughly before the next layer was added.

The number of layers deposited influenced the color of the glass slides and altered their wetting properties. The wettability of the aluminum-based nanoparticle layers produced during the ablation process in a vacuum was also examined. Contact angle measurements were conducted on both the coated and uncoated glass surfaces using a Drop Shape Analyzer (DSA 100-E, Kruss). The formation of highly rough nanostructured films during the nanoparticle deposition in a vacuum environment resulted in the superhydrophobic nature of the aluminum nanoparticle coatings.

These nanostructures displayed low adhesion to water. Atomic Force Microscopy (hpAFM, Nanomagnetics) was utilized to analyze the surface topography of the nanoparticle-coated surface. The thickness of these coatings deposited under vacuum conditions was approximately 150-200 nm. By combining these techniques, valuable insights were gained into the surface properties and characteristics of the aluminum-based nanoparticle coatings, providing a better understanding of their wettability and structural attributes.

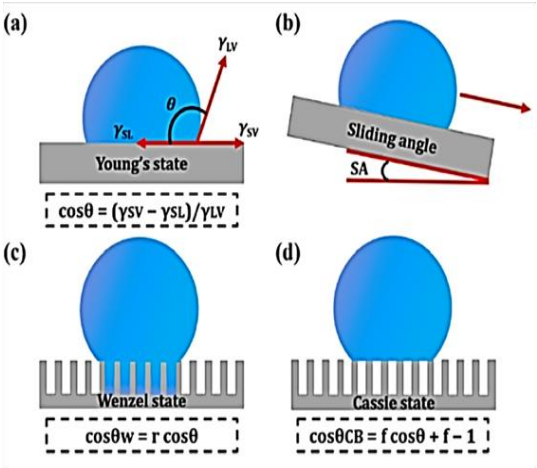

Fig. 8. Schematic of different wetting states of water for contact angle analysis. (a) Young state of water droplet on a flat surface; (b) sliding angle (SA) or roll-off angle definition; (c) Wenzel state, where water droplet penetrates the surface structures; (d) Cassie–Baxter state, where water rests on top of the microstructures and air gets trapped beneath it limiting penetration. Here 'r' and 'f' represents surface roughness and effective area fraction being in contact for Wenzel and Cassie- Baxter states, respectively [Ind. Eng. Chem.28, 988–994 (1936), Trans, Faraday, Soc. 40, 546 – 551 (1944)].

The findings from the contact angle measurements on the deposited surfaces, which appeared almost transparent, confirmed the superhydrophobic properties of the aluminum nanoparticles regardless of the coating thickness. Despite the non-uniformity of the coating, the contact angle remained consistent across different regions of the coated glass. The reported contact angle measurements in Figure 9 represent the average values obtained from various coated regions on the glass. The role of the medium in which the nanoparticles are synthesized is crucial. In a water environment, the formation of aluminum hydroxide ($Al(OH)_3$), aluminum oxide hydroxide (AlO(OH)), and aluminum oxide (Al_2O_3) can occur. It is essential to minimize oxidation during the laser ablation process in water or air, as oxidation can

significantly impact the formation, structure, and size distribution of the nanoparticles on a nanosecond time scale. The oxidation process can also influence the wettability properties of the synthesized nanoparticles. Special attention should be paid to controlling oxidation to ensure the desired characteristics and properties of the aluminum-based nanoparticles are preserved. Minimizing oxidation can help maintain the superhydrophobic nature of the coatings and prevent unwanted changes in their structure and performance.

Hence, the alternative explanation for the difference in wettability of surfaces coated with aluminum-based nanoparticles may be attributed to the presence or absence of hydroxides on the surface after deposition. During laser ablation in a liquid environment, the newly created surface undergoes a reaction with water, resulting in the formation of aluminum hydroxide ($Al(OH)_3$), which exhibits hydrophilic properties. In contrast, when ablating an aluminum surface under vacuum conditions,

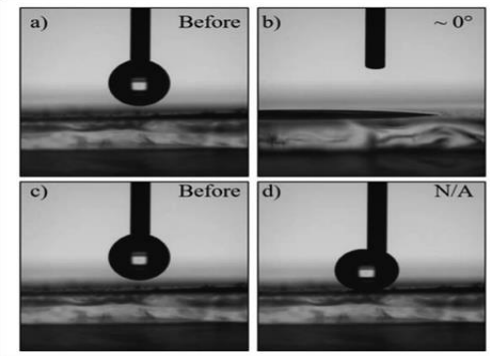

Fig. 9. Contact angle measurement of (a, b) Al based NPs suspension produced during ablation in water and deposited on the glass slides showing the superhydrophilic properties with a contact angle of nearly 0°. (c, d) Al NPs deposited on the glass slide by laser ablation in vacuum show an extremely superhydrophobic surface. During these measurements we were unable to place the water droplet on the surface [Appl. Surf. Sci. 527, 146702 (2020)].

primarily aluminum nanoparticles are deposited, as there is no interaction with oxygen and water components. In this scenario, variations in the wettability of substrates are predominantly influenced by changes in surface free energy. It is important to note that the wettability of solid substrates is determined by both their surface free energy and geometric structure.

In another paper [Appl. Surf. Sci. 542, 148560 (2021)] we investigated the variation of wetting properties of three different metals (aluminum, copper and galvanized steel) ablated by ultrafast fiber lasers (femtosecond and picosecond pulse durations). The role of pulse duration and scanning speed used in the laser-surface structuring was analyzed. Scanning electron microscopy, atomic force microscopy, and attenuated total reflection Fourier transform infrared spectroscopy (ATR-FTIR) were employed to characterize the roughness and chemistry of the laser-structured surfaces. The degree of hydrophobicity and self-cleaning characteristics of three laser-structured metals were compared when aged in different post-ablation environments. Freshly laser-treated samples of aluminum, copper, and galvanized steel demonstrated superhydrophilic wetting response when their contact angles were measured immediately after laser ablation. The superhydrophilic characteristics of these freshly laser-structured surfaces were found to evolved to hydrophobic state after 30 days of

ageing in ambient atmospheric conditions, while they took only 6 h to transform to superhydrophobic state when aged in low-pressure environment. Ultrafast laser-surface nano-structuring, coupled with vacuum ageing, proved to be an effective and rapid approach in achieving extreme superhydrophobic states in different metals, which makes it suitable for a wide range of self-cleaning applications.

The surface structuring was performed using the laser system (AFS-UFFL-300-2000-1030-300; Active Fiber Systems GmbH) at λ=1030 nm and repetition rate 50 kHz. The laser beam scanned over the samples by galvanometric scanner (FARO tech. Xtreme-20) equipped with F-Theta lens with *f* =160 mm. 40 femtoseconds (fs) and 1.0 picosecond (ps) laser pulses were used to structure the surface of aluminum, copper and galvanized steel at different scanning speeds (50-1250 mm/s in steps of 200 mm/s) by focusing the laser beam on the surface of the target. The laser beam was scanned over the sample in rectangular pattern by irradiating the sample in the horizontal direction (0◦) and then along the vertical direction (90◦), this was done to create grid patterns. The distance between two adjacent lines was 100 μm. The diameter of the focused spot on the surface was ~100 μm. Fixed laser fluence of 5 J/cm^2 was used for the ablation, which is higher than the ablation thresholds of aluminum, copper, and galvanized steel.

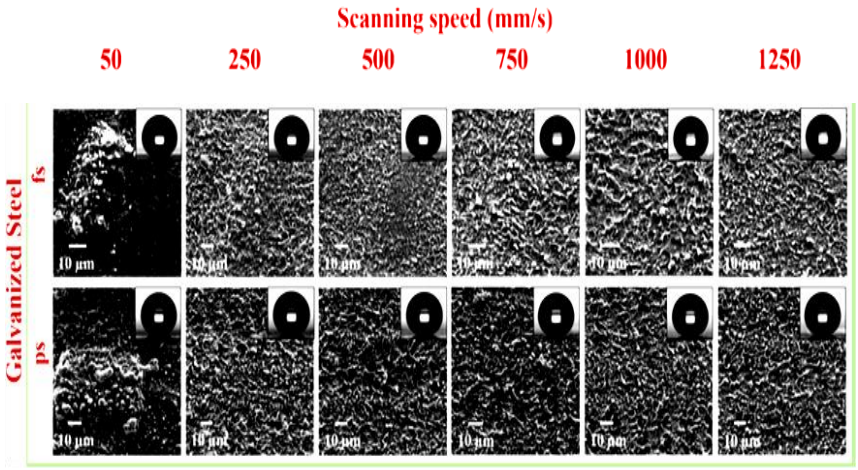

Fig. 10. SEMs of the ablated surfaces of galvanized steel stored in vacuum after irradiation with fs and ps laser at different scanning speeds. The insets show the water droplet shapes on the structured samples at different scanning speeds [Appl. Surf. Sci. 542, 148560 (2021)].

Prior to laser ablation, the surfaces of aluminum and copper sheets were smoothed by sequentially increasing the sand paper number (300#, 800#, 1000# and 1200#) and then polished by applying 1-μm diamond paste. Galvanized steel was used as received from the local supplier. The laser ablation enhances the surface roughness and creates different surface structures depending on the scanning speed and pulse duration. Fig. 10 shows a comparison of the structures produced by 40 fs and 1.0 ps laser pulses on the surfaces of studied metals at different scanning speeds ranging from 50 to 1250 mm/s. In the case of aluminum, highly random surface structures that significantly enhance the surface roughness were formed with both fs and ps lasers.

For copper and galvanized steel, laser-induced periodic surface structures (LIPSS) and hierarchical micro and nanoscale structures along the laser beam path were observed. LIPSSs were predominant at 250 and 500 mm/s scanning speeds, while uniform large-scale roughness with significantly less LIPSS and high coral reef-like structures were formed at higher scanning speeds (see the SEM images at scanning speeds of 750 mm/s and higher). The formation of elevated micro/nanostructures in the case of fs laser pulses, in comparison with ps pulses, is attributed to the shorter interaction time with the metal surface. The rough structures were formed in the case of both ps and fs laser structuring of all metals. Surface roughness improved the inherent wettability characteristic of the material. The observed sharp surface structures can facilitate lower adhesion with the surface improving the water repellent characteristic.

To demonstrate the transformation of the laser-structured surfaces from superhydrophilic to superhydrophobic state after ageing in vacuum, we measured the contact angle before and after aging. Fig. 11(a,b) shows the water contact angles of aluminum, copper and galvanized steel samples ablated by (a) fs and (b) ps lasers after aging in vacuum for ~6 h. As shown in those graphs, the plates structured by either ps or fs lasers showed superhydrophobic characteristics manifested by the high value of the contact angle in a broad range of scanning speeds.

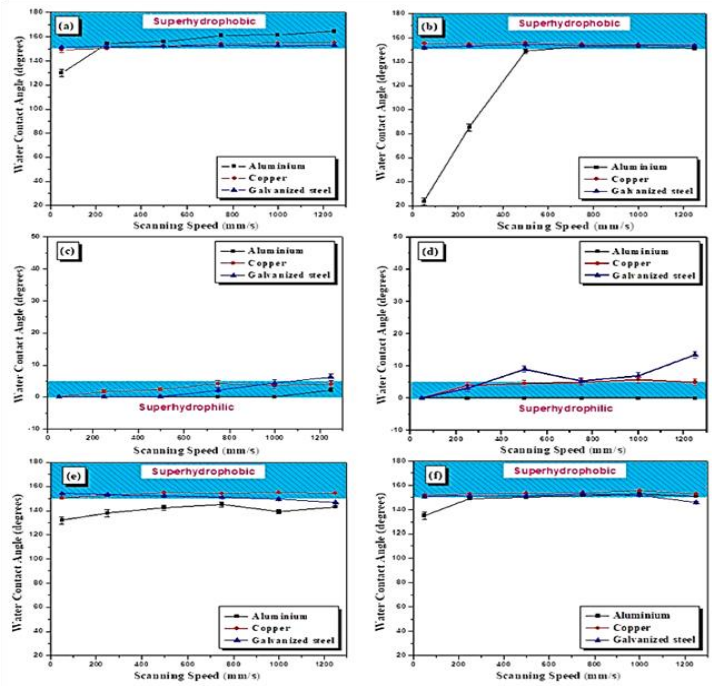

Fig.11. Water contact angles of aluminum, copper and galvanized steel samples ablated by fs laser ablation (a) after 6 h storage in vacuum, and (c) measured immediately after structuring in air. Similarly, samples ablated by ps laser ablation and stored in (b) vacuum and (d) air. The samples processed with (e) fs and (f) ps laser ablation and aged in air for 30 days showed superhydrophobic response. The contact angle an average value of the measurements performed at different spots on the laser-structured surface [Appl. Surf. Sci. 542, 148560 (2021)].

Meanwhile, Fig. 11(c,d) shows the contact angles of aluminum, copper and galvanized steel samples measured immediately after ablation by (c) fs and (d) ps laser pulses, respectively. All metals surfaces structured at different scanning speed, generally showed superhydrophilic response for both fs and ps right after the laser ablation, with measured contact angle way below 5◦ for aluminum and copper and less than 15◦ for galvanized steel. It is worth to mention that the unstructured polished

surfaces of aluminum, copper and galvanized steel showed water contact angles of 85.2◦, 78.8◦ and 86.0◦ respectively.

Among the three metals presented in our work, to the best of our knowledge, galvanized steel has not been explored before for wettability applications using ultrafast laser structuring followed by vacuum or air ageing. Galvanized steel is one of the most commonly used construction materials in roofing, rails, poles, etc. due to its relatively low cost and high corrosion resistance compared to other steel variants. Thus, the water repellent characteristic imparted on galvanized steel can provide a wide range of applications in self-cleaning. As shown in Fig. 11(a,b), galvanized steel has also demonstrated high contact angle after aging in vacuum following the fs and ps laser ablation. The contact angle after vacuum storage reached to a highest value of 153◦ and 154◦ for fs and ps laser ablation at scanning speeds of 500 mm/s and 750 mm/s, respectively. However, for the sample aged in air a contact angle of 151◦ was obtained. This study showed that vacuum-aged structured surface has better performance compared to the air-aged ones in the case of galvanized steel especially at higher scanning speeds of laser processing. In addition to the water repelling characteristics of the laser-structured surfaces stored in vacuum, we also investigated their self-cleaning behavior by measuring the sliding angle of these surfaces.

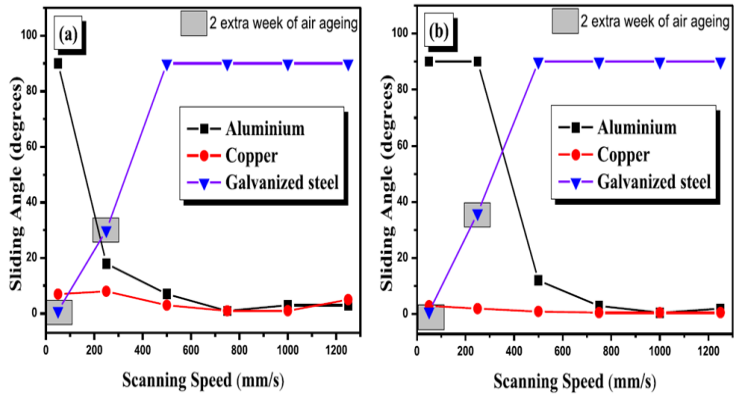

Fig. 12. Sliding angle measurements of the aluminum, copper, and galvanized steel treated by (a) fs and (b) ps pulses followed by vacuum storage. A roll-off angle of 90◦ showed that in certain speeds for aluminum and galvanized steel sliding angle could not be determined. Correspondingly, 90◦ is used as the highest value, which is an indication of high adhesion of water droplets to the surface [Appl. Surf. Sci. 542, 148560 (2021)].

Fig. 12 shows the sliding angle for the aluminum, copper, and galvanized steel sheets structured by fs and ps pulses after being aged in vacuum for 6 h. In the case of aluminum, the sliding angle of the fs and ps laser-structured surfaces decreased with the increase in the scanning speed. At lower scanning speed the water droplet remained adherent to the surface and did not roll off. On the other hand, copper showed self-cleaning water repellent behavior for all scanning speeds with small variation of 3◦ to ~0.5◦ at different scanning speeds. After aging in vacuum for 6 h, copper and aluminum samples demonstrated Cassie- Baxter wetting state at higher scanning speeds as they exhibited high contact angle as well as low roll off angle. Meanwhile, laser-structured galvanized steel, even after being aged in vacuum for 6 h, showed high roll off angle

of 90◦ and the droplet did not roll off due to the strong adhesion of water droplet with the laser-structured areas for all scanning speeds.

However, when the sliding angle was measured after storing the structured galvanized steel sample in air for additional two weeks, we found that its contact angle has increased to 150° and the roll off angle was significantly reduced, particularly, at low scanning speeds of 50 and 250 mm/s for fs and ps pulses treatment. Roll off angle of values ~0.5° and ~30° were achieved for those scanning speeds, respectively using fs pulses. Whereas for ps pulses, roll off angles of ~1° and ~36° were obtained at low scanning speeds of 50 and 250 mm/s. For high scanning speeds with both fs and ps laser ablation the roll off angle after vacuum aging and 2 extra weeks of aging, remained unchanged and the strong adhesion of water droplet was observed. Hence we conclude that galvanized steel requires more aging time, compared to aluminum and copper, in order to demonstrate transition to superhydrophobic wetting state and self-cleaning ability, and this only occurs at low scanning speeds. Low scanning speeds lead to deeper structures that would reach the deeper steel layer in galvanized steel, while at higher scanning speed the structures are mainly formed within the upper zinc layer. The ability of steel to adsorb carbon compounds is higher than the zinc layer, which is consistent with observing superhydrophobic and self-cleaning characteristics mainly at low scanning speeds.Fig. 13 shows the ATR-FTIR spectra for the laser-treated aluminum (Fig. 13(a)), copper (Fig. 13(b)), and galvanized steel (Fig. 13(c)) before and after vacuum storage. These samples were structured at scanning speed of 50 mm/s. It is seen that laser-treated samples are lacking the major IR modes in the regions 2800-3000 and 1100-1750 cm^{-1}. These regions are associated with the organic compounds attached to the surface. It was anticipated as the freshly structured metal surfaces were strongly hydrophilic with CA <5◦ due to hydroxylated layer formation.

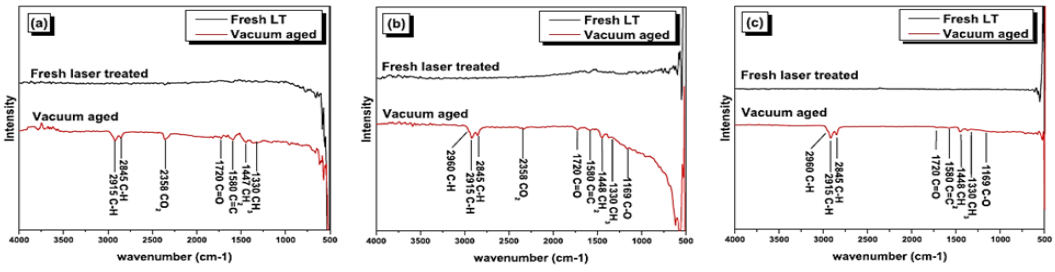

Fig. 13. ATR-FTIR analysis of the fs laser-structured (a) aluminum, (b) copper, and (c) galvanized steel before and after vacuum aging. The vacuum aged-samples showed the adsorption of the hydrocarbon [Appl. Surf. Sci. 542, 148560 (2021)].

The surface hydroxyl groups and the water adsorbed signatures are weak in their nature and hard to detect. In contrast, the ATR-FTIR spectra of the laser-structured metal surfaces that were aged in contaminated vacuum chamber showed IR modes associated with the adsorption of organic groups on the treated surfaces.

The bands that appeared at 2960, 2923, and 2858 cm^{-1} are assigned for symmetric and asymmetric C–H stretching modes for aliphatic $–CH_3$ and $–CH_2$-moieties. These bands are also associated with the υ_{CH3} bending mode that appears at 1370 cm^{-1} in the vacuum-aged metals. Further signatures appear at 1460 cm^{-1} that are assigned to the $\upsilon_{C=C}$ stretching modes. In addition, vacuum treated samples showed additional bands at 1720 and 1169 cm^{-1} that are assigned for C=O and C–O–C stretching modes, respectively. In summary, it was observed that very minute number of hydrocarbons is necessary for the wettability transformation and only the perfect combination of laser structuring and vacuum conditions will result in maximum water repellent and self-cleaning characteristics.

Part 2. Ultrafast femtosecond laser fabrication of multifunctional surfaces on different materials and their novel applications.

In this section we present our works [Front. in Chem. 8, 768 (2020), J. Phys. D: Appl. Phys. 54, 185109 (2021), and Appl. Sci.10, 6207 (2020)] on ultrafast femtosecond laser fabrication of multifunctional surfaces on different materials and their novel applications. The formation of well-controlled nano/micrometer-sized structures on metallic surfaces enables the modification of their optical and wetting properties. Forming such structures on the surface of biocompatible materials, in particular, can expand their applications in various areas of science and technology. Here in [J. Phys. D: Appl. Phys. 54, 185109 (2021)] we present results on covering tantalum (Ta), a biocompatible material, with complex nanosized structures comprising azimuthally- and radially-directed LIPSS by rotating the metallic sample with respect to the polarization direction of the irradiating laser pulses.

The interaction of material with ultrashort laser pulses induces periodic surface structures by confining the energy of the laser pulses on a very small micro/nanoscale spot of the targeted material surface. This initiates a chain of reactions that form a new surface topology. Drude model with Sipe efficacy theory explains that the low spatial frequency LIPSS (LSFL) formation process is initiated as result of the excitation of the surface plasmon polaritons (SPPs) of a rough surface after exceeding a critical carrier density level that creates a dense free-electron-plasma on the surface of the material [Appl. Surf. Sci. 257, 5420 (2011), IEEE J. Sel. Top. Quantum Electron. 23, 09–23 (2017)]. A subsequent thermal diffusion process and electron–phonon scattering occurs due to the temporal evolution of the electron and the lattice temperatures through the coupling parameter γ. The relationship of formed LIPSS structure period Λ_{LIPSS} with the incident beam wavelength λ, angle θ, and the surface plasmon

wavelength λ_{SP} was derived from a single-pulse laser experiment as [Opt. Express 19, 9035–43 (2011)]:

$$\Lambda_{LIPSS} = \frac{\lambda\, \lambda_{SP}}{\lambda \pm \lambda_{SP} \sin(\theta)} \tag{12}$$

$$\lambda_{SP} = \chi R \left[\frac{(\varepsilon_d + \tilde{\varepsilon_m})^{1/2}}{\epsilon_d \tilde{\varepsilon_m}}\right] \tag{13}$$

where $\tilde{\varepsilon}_m$, ε_d are the permittivity's of the metal and the surrounding dielectric medium. λ_{SP} is derived from the boundary conditions of the medium and targeted metal plasmon wave vector. The formation process can also be performed with multiple laser pulses which will accumulate more energy locally, increase the ripples' peak-to peak depth, and reduce the ripples' period. The increase of the accumulated fluence has a quadratic effect on the frequency of the collisions which triggers an increase in the real part of the dielectric constant of the metal, and as a result, the ripples reduce in period with the risk of completely disappearing at high fluence accumulation [Front. Phys. 10, 861098 (2022)].

However, as the pulse number increases, the accumulated fluence will increase and a periodic high-spatial-frequency LIPSS (HSFL) structure starts to appear due to the addition of the plasmonic excitation, which continues to take effect until reaching the ablation threshold where the heat accumulation would stop the formation of the HSFL. We used a fiber-based high-repetition rate femtosecond laser with a central wavelength of λ=1030 nm to cover the Ta's surface with radially and azimuthally directed LIPSS. The laser system generates 37 fs pulses with an energy of 30μJ/pulse at a 150 kHz repetition rate as shown in Fig.14. We estimated the peak fluence of the irradiating focused laser beam, with d=70 μm spot size on the target's surface to be F_P=0.8 J cm^{-2}. The peak fluence of laser beam F_P is calculated using the relation:

$$F_P = 4E/\pi d^2, \tag{14}$$

where E is the laser pulse energy. Fluence is one of the main parameters for the modification of surfaces by femtosecond laser pulses. During this study, we used a moderate fluence of the ablating beam. The high fluence of the ablating beam can either destroy the nano-ripple structures or deposit small-sized nanoparticles of the same target material on the ripples. By applying 0.8 J cm^{-2} fluence of ablating pulses, we observed nanoripples on the surfaces of Ta without any deposition of nanoparticles on the irradiated surface far from the central area of the sample.

The linearly-polarized laser beam was focused perpendicularly on the sample's surface, with the normal to the surface being along the incident light propagation. The width of the scanning line was equal to 70 μm, which corresponds to the spot size of the focused laser beam. After structuring the samples, their surface morphology was characterized using a scanning electron microscope (SEM, Tescan). The samples we

used were Ta sheets with the dimensions $30 \times 30 \times 0.5$ mm^3. The samples' surfaces were cleaned with ethanol before the laser ablation.

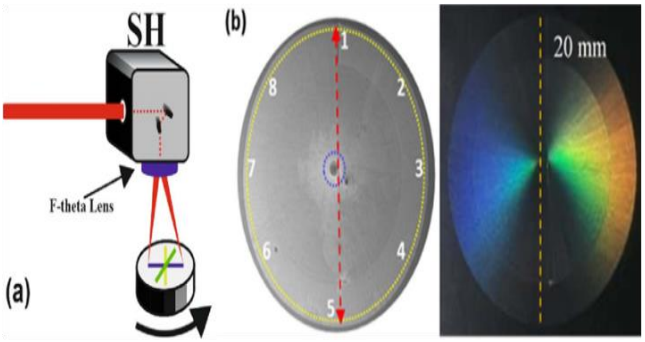

Fig. 14. (a) Experimental setup for the creation of radially and azimuthally oriented LIPSSs on the surface of Ta using 150 kHz repetition rate and 37 fs pulses. Faro scan head system (SH), which uses F-theta lens (FL = 160 mm) providing uniform fluence over the working area, was combined with the femtosecond laser source. (b) Far-field SEM image (left) and a colorful optical image (right) of the irradiated surface of Ta sample [J. Phy. D: App. Phy. 54, 185109 (2021)].

The upper panel in Figure 15 shows the SEM images and polarizations at the specific surface locations (marked with numbers and yellow dashed lines) of the first sample, where the polarization of the laser radiation was parallel to the scanning direction of irradiating pulses (red arrows). To switch the polarization direction of the ablating pulses from being parallel to perpendicular with respect to the scanning direction, we used a half-wave plate installed before the SH. The bottom panel of Figure 15 represents the SEM images of the surface locations of the second Ta sample, where the polarization of the ablating pulses was perpendicular to the scanning direction. In this case, we observed ripples that are directed radially relative to the center of the ablated area. Surface morphology measurements were performed on the marked areas shown in Figure 14(b).

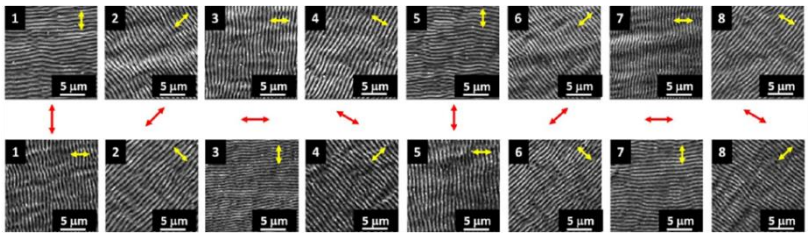

Fig.15. The SEM images of the marked locations corresponding to positions 1–8 in figure 14(b) on the outer circumference of the irradiated Ta disk, with different polarization orientations of the laser pulses [J. Phy. D: App. Phy. 54, 185109 (2021)].

We have presented results on covering Ta samples, for the first time, with azimuthally and radially directed LIPSS. We have demonstrated the advantage of combining the SH and the rotation stage in forming complex LIPSS on the metal's surface using high repetition rate (150 kHz) irradiating femtosecond laser. Rotating the target sample allowed for changing the polarization direction of the ablating pulses relative to the scanning direction. A 20 mm diameter disk of the ablated metallic surface was covered with parallel and perpendicularly directed ripples created by rotating the samples during the scanning process. Two different zones of LIPSS were formed on the surface. The first zone has HSFL with periodicity ($\Lambda_{HSFL} \approx 0.4 \pm 0.2 \mu m$) and the second one has

LSFL with periodicity ($\Lambda_{LSFL} \approx 1.5 \pm 0.1 \mu m$). Besides tuning the optical reflectance based on the laser-induced surface nanostructuring, the hydrophilic behavior of the complex LIPSS on the surface of Ta was demonstrated. We measured the wetting properties of the laser-treated Ta surface and found it to be hydrophilic with a WCA equal to $23^o \pm 5^o$. The formation of complex laser-induced periodic structures allows for controlling the wetting properties of the Ta and improves its tendency for cell adhesion and proliferation when used as implant. Our method can be easily extended to other metallic and dielectric materials where forming such complex structures on the surface expands the utilization of those materials in a wide range of applications.

In our work [Appl. Sci. 10, 6207 (2020)] we demonstrated how nanostructures (LIPSS) produced by ultra-short laser pulses can change the optical diffractive effects leading to the generation of angle-dependent colors on steel, copper, aluminum, and brass surfaces. We presented a simple process of re-coloring aluminum to prove the sustainability and reusability of the processed samples. We analyzed the wettability properties of such surfaces and demonstrated the relation between these properties and the lasting coloring of surfaces. We also demonstrated how a superhydrophobic aluminum surface can be developed by femtosecond laser processing when stored in vacuum for a number of hours after the laser treatment. Stainless steel, brass, aluminum, and copper plates were irradiated at different speeds by the scan head. Brass sample was 5 mm thick; the thickness of the other processed samples was ~2 mm. The surfaces of samples were cleaned with isopropanol before irradiation.

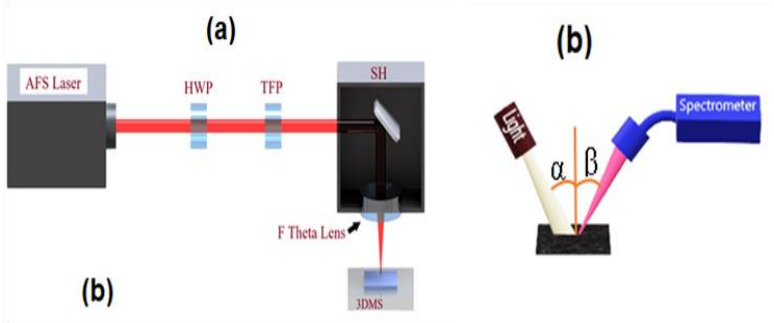

Fig. 16. (a) Experimental setup for metal surfaces treatment using a femtosecond laser at power 4.5 W, pulse duration 40 fs, central wavelength 1030 nm, and repetition rate 150 kHz coupled with a scan head (SH) containing an F-Theta objective lens [App. Sci. 10, 6207 (2020)].

A scanning electron microscope (SEM) was used to characterize the surfaces of different treated samples. The surface optical characteristics were analyzed using the experimental arrangement shown in Fig.16(b). The horizontally mounted sample was illuminated by an un-polarized light source with continuum spectrum in the visible spectral range, which was transformed to a parallel beam by two lenses and an aperture. In our study, the incident position angle (α) was fixed at 20^o. To inspect the colorizing effect of the treated area, the spectra of the scattered light from different angles (β) were measured by a fiber optics spectrometer (Flame, Ocean Optics). Color pallets of different metals are shown in Fig.17. Pallets (a–d) correspond to stainless steel, copper, aluminum, and brass samples, respectively. All samples were prepared at different scan

speeds to optimize LIPSS for the observation of different colors. The optimal scanning speeds for stainless steel, brass, aluminum, and copper were 350, 400, 500, and 450 mm/s, respectively. Pictures of the samples were taken in sunlight at fixed incident position ($\alpha = 20^o$). The angle of sample observation was changed from 0^o to 40^o when different colors were observed. The processing times for disks of 20 mm diameter of stainless steel, brass, aluminum, and copper were 15 s, 14 s, 11 s, and 12 s respectively. The measurements of the angle-dependent color reflectance from the surfaces were conducted using the setup shown in Fig.16(b). The broad-bandwidth emission from the tungsten lamp was directed on the laser-treated area of the sample and the diffracted light was measured using the fiber spectrometer at different angles with respect to the normal of the processed surface. The diffraction equation:

$$m\lambda = d\,(\sin\alpha + \sin\beta) \tag{15}$$

was used to determine the direction from which the different colors resulting from LIPSS were viewable. Here m is the diffraction order, λ is the wavelength, d is the LIPSS spacing, α is the angle of incident light, and β is the angle of diffracted light.

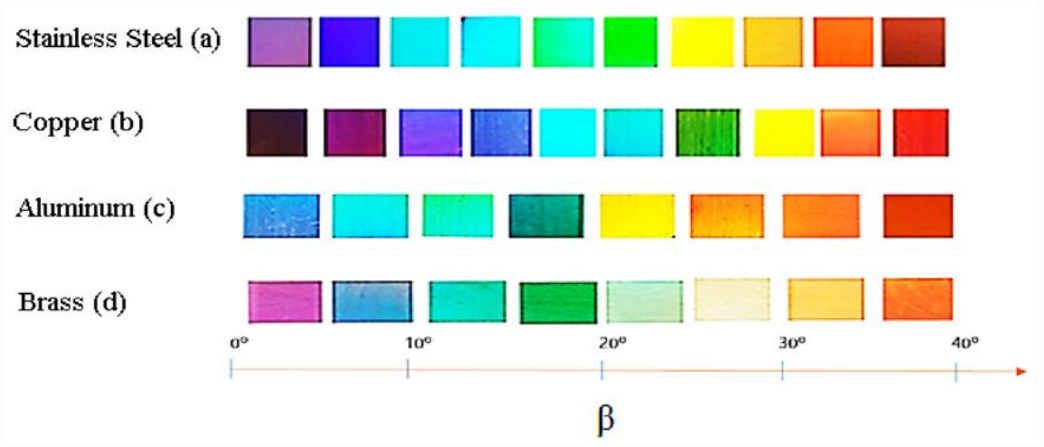

Fig.17. The color pallets are taken from processed (a) stainless steel, (b) copper, (c) aluminum, and (d) brass by digital camera at different viewing angles. The scanning speeds for stainless steel, copper, aluminum, and brass were 350, 400, 500, and 450 mm/s, respectively. The fluence of the laser beam was 1.0 J/cm^2. As β increased, colors shifted towards the longer wavelength region of the visible spectrum. The incident light angle was around 20 degrees. Scanning electron microscope (SEM, TESCAN Vega 3) images show that all angle-dependent colors were features of the periodic structures imprinted on the surface of each metal. The directions of all nanoripples were orthogonal to the polarization axis of the laser beam. The distance between nanoripples was measured by SEM and was found to be approximately 1 μm, which is very comparable to the wavelength of the used femtosecond laser [App. Sci. 10 (18), 6207 (2020)].

The spectral analysis of the treated aluminum, copper, and stainless-steel surfaces are shown in Figs.18(a)–(c). These graphs show a very consistent pattern for all metallic samples and hence serve as evidence of reflectance similarities due to the same LIPSS on different metallic surfaces. Meanwhile, in the case of non-treated surfaces

(Figs.18(d)–(f)), the reflectance spectra remain the same at different angles of observation, contrary to the case of treated surfaces (Figs.18(a)–(c)). Besides showing the ability to produce new colors on the pristine samples, below we demonstrate that the color on the surface of processed metals can be erased and re-colored by using the same laser radiation. As shown in Figure 19, a sample of aluminum was made dark golden (A) and then erased to restore it to almost its original color. The same sample was then colored to a whitish color (B), part of which was erased again, and colored to the black semi-circle (C). We demonstrated the appearance of permanent and angle-dependent colors using femtosecond laser surface structuring of aluminum, copper, steel, and brass through the formation of laser-induced periodic surface structures and non-periodic nano/microstructing. We showed that both these groups of colored species can be either erased or re-colored using an additional step of laser processing. The process of material surface restructuring was attributed to the SPP excitation and its interference with the incident laser irradiation. This interference resulted in the laser intensity redistribution across the surface and its periodic patterning. The scanning speed was found to be a key factor in determining the resulted optical properties of the generated structures.

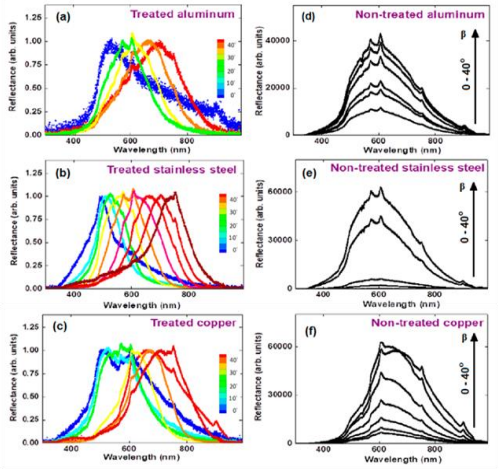

Fig.18. Reflectance spectra from the treated surfaces [(a) aluminum, (b) stainless steel, (c) copper] and non-treated surfaces [(d) aluminum, (e) stainless steel, (f) copper]. Different curves on each graph correspond to different angles of observation. One can see that, in the case of non-treated surfaces, the reflectance spectra remain the same at different angles of observation, contrary to the case of treated surfaces. The colors in (a–c) correspond to the colors viewable by eye at the corresponding angles. The angle (β) ranged from 0° to 40°, where 0° corresponds to the position of the spectrometer when it is perpendicular to the sample. As β increased, longer wavelengths were detected [App. Sci. 10, 6207 (2020)].

There is an optimal scanning speed at which the pre-modified surface structure can serve as feedback for each subsequent pulse, which enhances the accuracy of the produced LIPSS in a multi-pulse regime. The relation between the spectral reflective properties of different colored metals and the wettability of the processed metal surfaces was also studied. We demonstrated the possibility to simultaneously tailor the coloring as well as the wettability properties of metals by optimizing the set of laser parameters employed in the processing. Furthermore, vacuum storage of the laser-treated samples dramatically changed their wettability response from hydrophilic to superhydrophobic, lasting permanently even after leaving the vacuum-stored sample in an ambient atmosphere. Vacuum ageing allows the surface energy of the sample to

be changed via desorption of the oxide layer followed by adsorption of carbon species from the surrounding environment. Oil-water separation has great consequences for both the environment and the economy. We presented in [Front. Chem. 8,768 (2020)] the transformation in wettability response underwater, altering from being extremely attracted to water and repelling oil to being extremely attracted to oil and repelling water by utilizing ultrashort femtosecond laser to nanostructure stainless steel and copper meshes. Our method is eco-friendly, free of chemicals, and effective as it takes advantage of aging the processed samples in a high vacuum setting. We fine-tuned the laser beam scanning parameters, mesh pore size, and aging conditions to achieve exceptional separation efficiency of 98% for the mixture of oil and water for manufactured meshes.

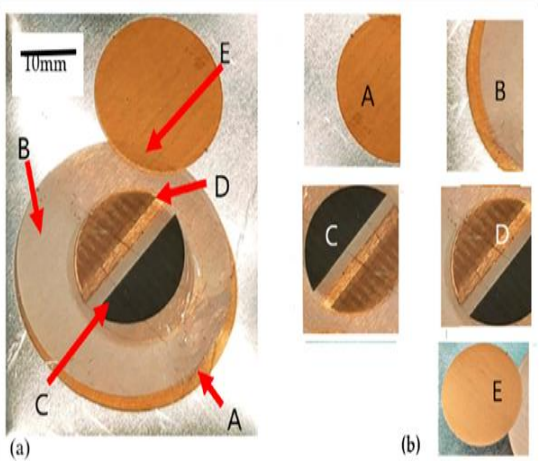

Fig.19. Demonstration of erasing the color from the treated sample and formation of new colors produced on the erased surface of aluminum. Panel (a): original sample; panel (b): explanation of panel (a): A, initially created dark golden disk. B, whitish color after erasing dark golden color, C, black semi-circle after erasing whitish color, D, light golden strip after erasing whitish color, and E, dark golden color painted on the whitish color. The scanning speeds for dark golden, white, black, and light golden were 70 mm/s, 1500 mm/s, 10 mm/s, 200 mm/s (two runs) respectively. The fluence of the laser beam was in the range 0.5–1.0 J/cm^2. Figure 5b represents the images of A, B, C, D and E parts, respectively [App. Sci. 10, 6207 (2020)].

Different meshes resulted in varying water and oil contact angles in relation to the scan speed at which the samples were scanned. Meshes made of stainless steel with a size of 150μm and copper meshes size of 100 μm have shown great performance for oil-water separation. Vacuum treatment led to a quick transition of wetting state from highly attracted to water to extremely water repellent, which is attributed to the fast adsorption of hydrocarbons onto laser-etched surfaces due to lack of any water molecules presence in the vacuum chamber. We created surface structures on stainless steel meshes at different scanning speeds. Stainless steel (SS) meshes (50, 100, 300, and 500) with different wire thicknesses and pore sizes were selected for LIPSS (see left column of Figure 20). In all panels, the orientation of the LIPSS was at right angle to the laser polarization. At higher scanning speed the depth of the periodic structures was noticeably less. SS meshes 50, 100, 300, and 500 have wire diameters of 200 μm, 100 μm, 30 μm and 25 μm and pore sizes of 400 μm, 150 μm, 50 μm 30 μm respectively. Based on the laser parameters, the structured surface can undergo

ablation through either spallation or phase explosion mechanisms [Appl. Surf. Sci. 255, 9724 (2009)]. Spallation involves the removal of large liquid or solid particles due to the relaxation of laser-induced stresses, while phase explosion, also known as explosive boiling, occurs when materials are removed due to the explosive decomposition of superheated regions on the target surface [J. Phys. Chem. C 113, 11892 (2009)].

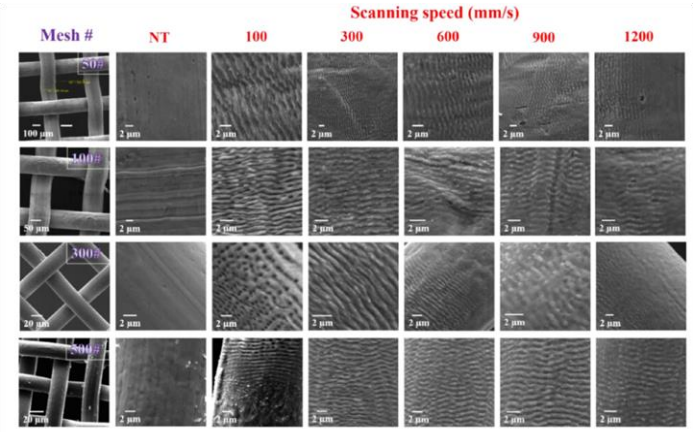

Fig. 20. SEM of SS meshes structured at different scanning speeds (100–1200 mm/s). Laser induced periodic surface structures (LIPSS) were observed at different scanning speeds for various mesh sizes with a period of ~1μm. NT is for non-treated surface [Front. Chem. 8, 768 (2020)].

At scanning speed of 100 mm/s for SS meshes 300 and 500, we observed the formation of micro-pores and the redeposition of micro-particles across the LIPSS. However, at scanning speeds of 300 and 600 mm/s, uniform LIPSS with a period of approximately 1 μm were formed on all mesh types. Compared to non-treated (NT) mesh surfaces, laser structured surfaces were full of LIPSS, significantly enhancing the surface roughness. We measured the contact angle of the laser-treated surfaces right after the ablation, the treated meshes exhibited a superhydrophilic charactiristics, as depicted in Fig. 21. This response is attributed to the formation of a metal oxides layer during the ablation process. The water contact angle for the freshly ablated metal meshes was ~0◦ and the water droplet permeated through the mesh in ~0.1ms, revealing superhydrophilic behaviour.

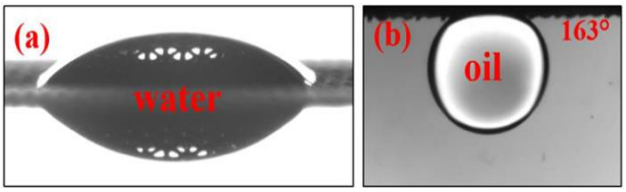

Fig. 21. Wettability of femtosecond laser structured mesh demonstrating (a) superhydrophilic behavior in air and (b) underwater-superoleophobic characteristics [Front. Chem. 8, 768 (2020)].

Those superhydrophilic meshes exhibited a superoleophobic behaviour under water, with oil contact angle (OCA) extending from 155 to 163° across all scanning speeds and metal mesh types. Following a 60-day exposure to the ambient air or a 4-hour aging period in vacuum, the laser treated meshes became superhydrophobic. Figures 22 shows the values of the contact angle for different SS laser treated meshes prepared at scanning speeds 100 mm/s - 1200 mm/s. The water and oil contact anlges were

measured by applying droplets of 5 µl volume of water and oil (n-hexane) on the treated regions of the meshes. Wetting characteristics of the samples aged in vacuum or air to the freshly treated surfaces were found significantly different. For SS 50, 100, and 300 meshes oil permeated, whereas for the SS 500 mesh, the oil contact angle was close to 0 degrees, and the oil did not permeate the mesh but rather spread evenly due to capillary action in LIPSS for both air aged and vacuum aged meshes. Laser treated meshes concurrently showed enhanced hydrophobic and oleophilic characteristics irrespective of aging environment. As the laser scanning speed increased, the oil permeability slightly decreased, while still exhibiting oleophilic characteristics. Copper meshes with pore sizes of 100, 500, and 800 µm and wire diameters of 50, 250, and 400 µm, respectively, were treated with a femtosecond laser and then exposed to air and vacuum conditions.

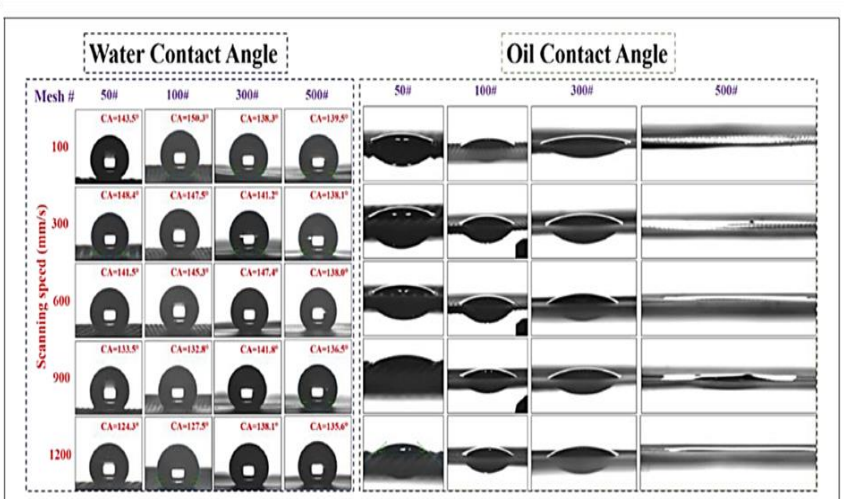

Fig. 22. Water contact angle and oil contact angle measurements of SS meshes (50#, 100#, 300#, and 500#) stored in vacuum for 4 h after structuring with a femtosecond laser at scan speeds of 100–1200 mm/s [Front. Chem. 8, 768 (2020)].

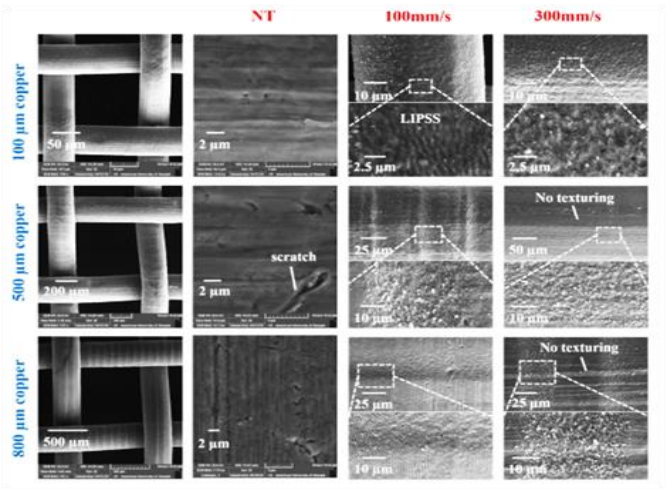

Fig. 23. SEM images of three copper meshes (100, 500, and 800µm pore sizes) structured by a femtosecond laser at scanning speeds of 100 and 300 mm/s. Laser treatment allowed the formation of LIPSS and rough surface structures. Some regions remained non-textured for meshes of 500 and 800µm pore sizes at scanning speeds of 300 mm/s. Note: NT stands for non-treated mesh [Front. Chem.8, 768 (2020)].

The laser treatment resulted in the formation of grayish-black laser-induced structures on the copper meshes, altering their surface appearance. Scanning the 100 µm copper mesh at a speed of 100 mm/s led to the creation of LIPSS covered with micro and nanoparticles, with an average ripple period of approximately 1 µm.

However, for the 500 and 800 μm copper meshes treated at a scanning speed of 300 mm/s, non-textured areas similar to the pristine copper mesh were observed. Furthermore, at a scanning speed of 300 mm/s, random nanostructures with protrusions were detected along the laser beam path. Water and oil contact angle measurements were conducted on the laser-structured copper meshes treated at two different scanning speeds and then subjected to vacuum aging for 4 hours and air aging for 60 days. The 100 μm copper mesh exhibited a strong superhydrophobic response at a scanning speed of 300 mm/s after vacuum storage, with a water contact angle of 153.2°. In comparison, air-aged samples under similar conditions achieved a water contact angle of 135.7°. This trend of higher water contact angles after vacuum storage was consistent for all copper meshes and scanning speeds.

The oil drops seep through the mesh, demonstrating a superoleophilic charactiristics. The laser-treated 500 and 800 μm copper meshes also exhibited hydrophobic behavior after air and vacuum aging. Copper mesh of 500 μm treated at scanning speeds of 100 and 300 mm/s showed contact angles of 145.2° and 141.1° respectively, after aging in high vacuum, whereas samples aged in air exhibited smaller water contact angles (134.2° and 132.7°, respectively).

The 800 μm mesh prepared at 100 mm/s showed water contact angle of 137.2° (aged in vaccum) and 126.8° (aged in air). Meanwhile, the oil contact angle of the samples exhibited high penetrability for oil, showing superoleophilic behaviour.

Fig. 24 shows the ATR-FTIR spectra for the laser structured stainless steel and copper metal surfaces before and after vacuum aging for samples prepared at scanning speeds of 100 mm/s.

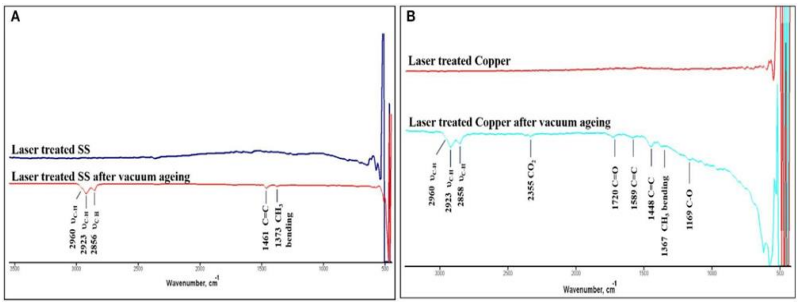

Fig. 24. ATR-FTIR spectra of the Laser treated (A) SS and (B) Copper before and after vacuum aging [Front. Chem.8, 768 (2020)].

The infrared (IR) spectroscopy results indicate that the laser-treated samples lack major IR modes in specific regions (2,800 –3,000 and 1,100–1,750 cm^{-1}), which are typically associated with hydrocarbon which are present on the surface. This observation is consistent with the strong hydrophilicity of the laser-treated samples immediately after structuring. However, the signatures of surface hydroxyl groups and adsorbed water are weak and difficult to detect by using ZnSe crystal. Whereas, in the case of attenuated total reflection (ATR) spectra for the laser-treated metal surfaces aged in vacuum, the IR modes associated with the adsorption of hydrocarbons were seen. Specific bands appeard at 2,960, 2,923, and 2,858 cm^{-1}, which are assigned to C-H

stretching modes for aliphatic -CH_3 and -CH_2- moieties. These bands are also linked with the u_{CH3} bending mode at 1,370 cm^{-1}. Futhermore, signatures appeared at 1,460 cm^{-1}, assigned to the $u_{C=C}$ stretching modes. Moreover, the vacuum-treated copper sample displayed additional bands at 1,720 and 1,169 cm^{-1}, which were assigned to C=O and C-O-C stretching modes, respectively. In summary, the storage of laser-treated metal surfaces in the vacuum chamber accelerates the adsorption of organic hydrocarbons on the surface, leading to the superhydrophobic behavior witnessed on the vacuum aged mesh surfaces.

We demonstrated that manufacturing superhydrophobic superoleophilic laser treated meshes when aged in high vacuum is highly effiecient method for oil-water separation applications. We also showed the materialization of wettability characteristics that beat those reported formerly using picosecond pulses, which also used air, vacuum, or carbon-rich atmospheres as storing surroundings [J. Laser Appl. 27, S29107 (2015)]. The highest water contact angle, using picosecond laser pulses, was reported to be 120°, while in our case of the vacuum aging of the copper meshes processed by 36 fs pulses, the contact angle value was obtained up to 153.5°, thus demonstrating the super hydrophobicity behavior of our samples. The higher value of water contact angle in our study can be ascribed to the formation of deeper periodic surface features with sharper edges of the nanoripples fabricated by femtosecond pulses. These structures exhibit stronger local fields near the sharp-edged nanoripples, which enables them to adsorb larger amounts of hydrocarbons from oily contaminants in vacuum pumps or on the walls of the vacuum chamber compared to structures formed by longer (picosecond) pulses.

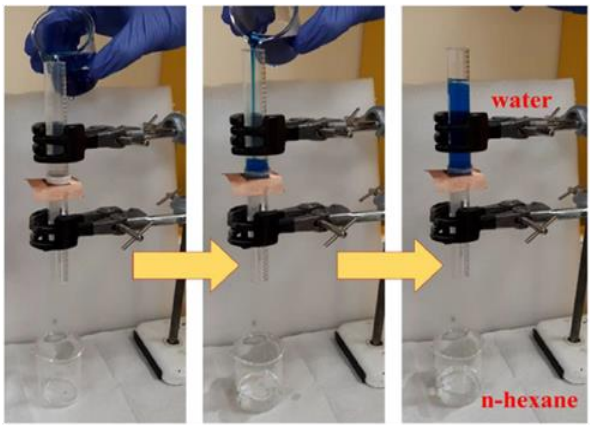

Fig. 25. Demonstration of oil-water separation using laser structured and vacuum-aged copper mesh prepared at a scanning speed of 300 mm/s. The water is dyed with methylene blue for better identification of the two liquids. Oil passes through, while water retains above the mesh that possesses a superhydrophobic-superoleophilic characteristic [Front. Chem.8, 768 (2020)].

The copper and stainless steel meshes produced in our study, which demonstrated superhydrophobicity and superoleophilicity after aging in vacuum and air, can be substantiated for separating oil-water mixtures by stopping water while permitting oil to permeate. Fig. 25 demonstrates the capability of the laser-structured copper mesh, aged in vacuum, for separating oil-water mixtures. The mesh was positioned so that

the laser-treated surface faced the mixture. The oil-water mixture, with water dyed methylene blue for identification, was poured onto the laser-structured mesh, which has high permeability for n-hexane (oil). Upon pouring the oil-water mixture onto the laser-structured surface of the copper mesh, the oil permeated through the mesh and was collected in the beaker under the tube, while water was blocked in the tube above the mesh (as seen in the right panel Fig. 25). The oil permeated the mesh in 15 seconds and was driven by gravitational force. The permeate flux (F) was 50 $Lm^{-2}h^{-1}$, and separation efficiency of 98%, with little or no water passing through the mesh.

Our systematic study on the pore size and thickness of the SS and copper meshes, laser scanning speed, and aging environments provided guidance for using femtosecond laser-structured meshes for oil-water separation with exceptional efficiency of 98% and higher. The wettability state transition from superhydrophilic underwater-superoleophobic to superhydrophobic–superoleophilic of metal meshes, fabricated by femtosecond laser was achieved through rapid, facile, chemical-free, echo friendly, and novel vacuum aging techniques, exhibiting a contact angle of 153.5^o and an oil contact angle of 0^o respectively.

In [Appl. Phys. A 126, 62 (2020)], we examined the hydrophobic and hydrophilic properties of the plane and curved surfaces of different materials ablated using 5 ns laser pulses in air. The difference in the contact angles between liquid and surface of the modified graphite and AlNiCo alloy rods using different fluencies of the ablating pulses are demonstrated. The wetting contact angle of ablated graphite rod was found to be 147°, i.e., the modified curved surfaces demonstrated the superhydrophobic properties. On the other hand, the superhydrophilic properties, with 7° wetting contact angle, were demonstrated in the case of ablated aluminum alloy. A schematic model was proposed for the application of the graphite rod as a membrane for the oil–water separation.

In another work [Front. Chem. 9, 792641 (2021)], we grew $NaAlSi_2O_6–H_2O$ zeolite on femtosecond laser-treated stainless steel (SS) substrates. We used SEM, EDX and XRD to analyze non-treated steel meshes, zeolite-coated meshes, and laser-structured meshes. Contact angle of non-treated steel meshes, zeolite-coated meshes, laser-structured meshes, and zeolite-coated laser-structured SS-100 meshes were measured for wettability characteristics. We observed enhanced superhydrophilic performance in coated and structured specimens, with the zeolite-coated laser-structured SS-100 meshes demonstrating a mean value of contact angle of 15° and superior reusability and durability over an extended period. Additionally, the zeolite-coated laser-structured SS-100 meshes were tested for oil–water separation and showed greater effectiveness for oil–water separation. In particular, the separation was driven by gravity in 18 seconds with a permeating water flux of 12,738 $L \cdot m^{-2} \cdot h^{-1}$ and separation efficiency of 95%. The functioning of the zeolite-coated laser-structured

SS100 meshes for oil–water separation was checked practically. We poured 20 ml of water–n-hexane mixture (1:1 by volume) on the SS mesh. The two liquids were distinguished by coloring water with methylene blue dye. The total water flux through the mesh and oil intrusion pressure was calculated by Eqs (16) and (17), respectively [J. Mem. Sci. 608, 118201 (2020)].

$$F = \frac{V}{A \times t} \tag{16}$$

where F is the permeation flux of water, V is the volume of the liquid permeated through the mesh area A (m^2), and t is the total time of separation.

$$P_{int} = 2\gamma_{l1/2}\frac{Cos\theta}{d} \tag{17}$$

P_{int} is the intrusion pressure (kPa), $c_{\ell 1/2}$ is the oil and water interfacial tension (mN/m), θ is the OCA (°), and d is the pore size of mesh (m). In these experiments, the mesh was placed such that the structured and coated surface faces the downward flowing flux.

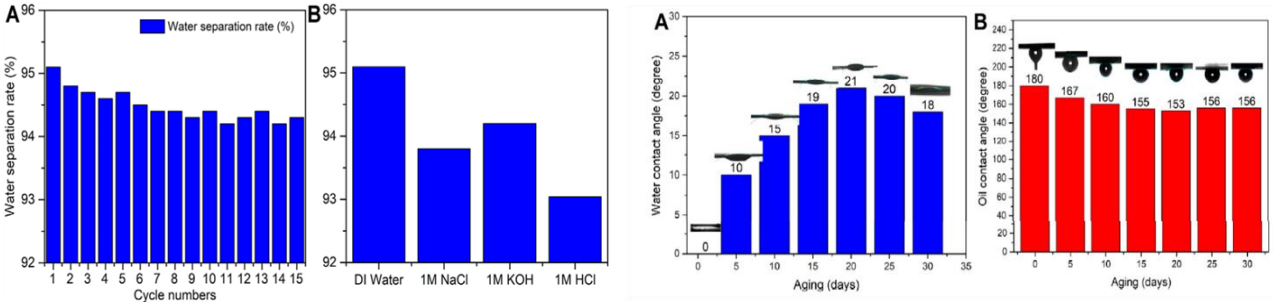

Fig. 26. Above shows the effect of aging time on the water contact angle (WCA) (A) and OCT (B) of the zeolite-coated laser-structured SS-100 meshes [Front. Chem. 9, 792641 (2021)].

The superhydrophilic surface property enabled water to pass through the mesh surface in a fraction of seconds, while oil was repelled and prevented from passing through. The oil-water separation mixture was driven by gravity and took only 18 seconds, with a permeating water flux of 12,738 $L \cdot m^{-2} \cdot h^{-1}$, resulting in a separation efficiency greater than 95% and an oil intrusion pressure of 1.2 kPa. Figure 26 shows the water separation efficiency for the zeolite-coated laser-structured SS-100 meshes after 15 cycles of operation, revealing an average efficiency of 94.4% in the last cycle. These results showed the durability and applicability of the zeolite-coated laser-structured SS-100 meshes for long term use. The demonstrated stability and reusability of these meshes make them highly attractive for oil-water separation use in industrial processes.

In our work [Langmuir 39, 1815−1825 (2023)], asymmetric wettability Janus membranes fabricated on copper foam and mesh were investigated in terms of directional water transport and fog collection. To obtain a wettability difference, one side of the membranes was treated by a femtosecond laser scanning process, which transformed it to a super- hydrophilic (SHL) state, while maintaining the untreated

surface hydrophobic (HB). The Janus structures allowed water to pass from the hydrophobic surface to the SHL side and did not allow its transport in the reverse direction. These anisotropic water penetration properties arose from a cross-sectional wettability gradient created in the foams and meshes by laser irradiation. The wettability gradient depended on the scanning speed of the laser treatment process. At a very low scanning speed, the membrane became completely hydrophilic (in the case of foam). Conversely, at a relatively high scanning speed, the thickness of the treated area was insufficient, as a result of which a drop of water adsorbed on the hydrophobic surface could not reach the hydrophilic part of the membrane.

The optimal scanning speed at which the membranes demonstrated the properties of a water diode was 50 mm/s. The effectiveness of water collection from frog by the hydrophobic/hydrophilic Janus mesh-based system was higher (3.9 g/cm^2 h) compared to that of the foam-based membrane (2.5 g/cm^2h). The efficiency of fog–water conversion decreased over time (to 0.5 g/cm^2 h in 2 weeks) due to the absorbance of organic contaminants, which degraded the superhydrophilicity of the treated surface. Coating the samples with TiO_2 protected them from degradation for at least 60 days, and restoring the samples' superhydrophilicity was achieved by simply exposing them to sunlight. We believe that these results can contribute to the further development of fog collection systems to overcome water scarcity problems, especially relevant in regions of deserts, coasts, and mountain ranges.

CONCLUSIONS

The main conclusions drawn from our studies are the following:

1. The numerical molecular dynamic simulations allowed insight knowledge of the main mechanisms of NPs formation in water and the existence of the optimal laser irradiation parameters for producing Al based NPs of desired size, shape and morphology.
2. Water environment resulted in a narrower and uniform size distribution of nanoparticles as compared to that in vacuum. Significant changes in sizes and shape of nanoparticles were observed after one month from ablation.
3. We have witnessed that the long laser pulses seem to be more efficient and technologically relevant from the point of manufacturing uniform nanoparticles of a possibly smaller size.
4. Glass surfaces deposited with Al-based NPs produced in water showed superhydrophilic properties and the ones with NPs deposited in vacuum possessed superhydrophobic features.
5. Highest values in the spectral region of 400 nm of the nonlinear absorption coefficients (β) and nonlinear refractive indices (γ) were observed in the case of the Al based NPs suspension produced by ablation of aluminium using picosecond

pulses. The values of nonlinear absorption coefficients (β) and nonlinear refractive indices (γ) of Al-based NPs were ~ 10^{-7} cm W^{-1} and 10^{-9} cm^2 W^{-1} respectively.

6. We have demonstrated that the in-situ formation of Al NPs in a vacuum followed by the propagation of the driving pulses through the cloud of synthesized nanoparticles resulted in enhanced harmonic yield compared with the application of aluminium atoms and ions. Al NPs allowed the generation of the high-order harmonics up to the 37th order using 40 fs pulses propagating nearby to the ablating aluminium target.
7. We showed that permanent and iridescent colors of the metals and metal alloy surfaces can be erased and re-colored by using a second stage of femtosecond laser processing.
8. We demonstrated the possibility of simultaneously tailoring the coloring as well as the wettability properties of metals by optimizing the set of laser parameters employed in the processing.
9. We observed that the laser-ablated carbon rod membranes are excellent candidates for the separation of water and oil mixture.
10. Ultrafast laser-surface nanostructuring, coupled with vacuum ageing, proved to be an effective and rapid approach in achieving extreme superhydrophobic states in different metals, which makes it suitable for a wide range of self-cleaning applications.
11. Stainless steel and copper mesh nanostructured with optimized laser scanning parameters, mesh pore size, and aging conditions to produce membranes, exhibited an efficiency of 98% for the oil-water separation.
12. Complex periodic azimuthally and radially directed LIPSS fabricated by ultrafast laser on a large surface area of Tantalum (20mm) were presented. This is proven to be very important for cell adhesion and proliferation when used as an implant.
13. Copper Mesh and Foam Janus membranes with opposite wettability characteristics can be manufactured by femtosecond laser and can be used for efficient directional water transfer and fog collection applications.
14. Laser-structured zeolite-coated steel meshes exhibited enhanced superhydrophilic behavior and superior durability over an extended period for oil–water separation

“TIQXMMI” MILLIY TADQIQOT UNIVERSITETI HUZURIDAGI FUNDAMENTAL VA AMALIY TADQIQOTLAR INSTITUTI HUZURIDAGI № DSc.03/31.03.2022.T/FM.10.04 RAQAMLI ILMIY KENGASH ASOSIDAGI BIR MARTALIK ILMIY KENGASH

“TIQXMMI” MILLIY TADQIQOT UNIVERSITETI

MAZHAR IQBAL

YUQORI TAKRORLANISH CHASTOTASIGA EGA O’TAQISQA FEMTOSEKUND LASERI YORDAMIDA ISHLOV BERILGAN MIKRO/NANOSTRUKTURALI MATERIALLARNING SHAKLLANISH MEXANIZMLARI VA ULARNING YANGI TADBIQLARINI TADQIQ QILISH

01.04.02 – Nazariy fizika.
(Fizika-matematika fanlari bo‘yicha)

dissertatsiya himoyasisiz chop etilgan maqolalar asosida falsafa doktori (PhD) ilmiy darajasini olish uchun
TAQDIMOTI

Toshkent-2024

Fizika-matematika fanlari bo‘yicha falsafa doktori (PhD) dissertatsiyasi mavzusi O‘zbe Respublikasi Oliy ta’lim, fan va innovatsiyalar vazirligi huzuridagi Oliy attestatsiya komissiy... B.2024.2.PhD/FM1043 raqam bilan ro‘yxatga olingan.

Dissertatsiya “Toshkent irrigatsiya va qishloq xo‘jaligini mexanizatsiyalash muhandislari instituti” Milliy tadqiqot universitetida bajarilgan.

Dissertatsiya avtoreferati uch tilda (ingliz, o‘zbek, rus (rezyume)) Ilmiy kengash veb-sahifasida (www.ifar.uz) va «Ziyonet» Axborot ta’lim portalida (www.ziyonet.uz) joylashtirilgan.

Ilmiy rahbarlar:

Ganeev Rashid Ashirovich
fizika-matematika fanlari doktori, professor,
“TIQXMMI” MTU Amaliy va Fundamental Tadqiqotlar Insituti, Toshkent O’zbekiston

Ali Sami Alnaser
Fizika fanlari Professori, Sharja shahridagi Amerika universiteti, Sharja, BAA

Dissertatsiya ishining taqdimoti “Toshkent irrigatsiya va qishloq xo‘jaligini mexanizatsiyalash muhandislari instituti” Milliy tadqiqot universiteti huzuridagi Fundamental va amaliy tadqiqotlar instituti huzuridagi **№DSc.03/31.03.2022.T/FM.10.04** raqamli Ilmiy kengashning 2024 yil «___»_____ soat____ dagi majlisida bo‘lib o‘tadi. (Manzil: 100000, Toshkent sh., Q. Niyoziy ko‘chasi-39, Fundamental va amaliy tadqiqotlar institute 108-katta majlislar zali; (+99871)237-09-61, fax (+99871) 237-48-67, e-mail: info@ifar.uz.

PhD dissertatsiyasi taqdimoti bilan “Toshkent irrigatsiya va qishloq xo‘jaligini mexanizatsiyalash muhandislari instituti” Milliy tadqiqot universiteti ning Axborot-resurs markazida tanishish mumkin (№_____ raqami bilan ro‘yxatga olingan). (Manzil: 100000, Toshkent sh., Q. Niyoziy ko‘chasi-39, Fundamental va amaliy tadqiqotlar instituti 108-katta majlislar zali; (+99871)237-09-61

Dissertatsiya ishining taqdimoti 2024 yil «____» _____kuni tarqatildi.

(2024 yil «____» _____ dagi _____ raqamli reestr bayonnomasi).

B. J. Ahmedov
Ilmiy darajalar beruvchi Ilmiy kengash raisi, O‘zRFA akademigi, fizika-matematika fanlari doktori, professor

D.R.Rayimbayev
Ilmiy darajalar beruvchi Ilmiy kengash ilmiy kotibi, DSc.

ABSTRAKT

Tdaurli materiallar sirtlarini lazer nurlanishi yordamida qayta ishlashda va bir qator amaliy tadbiqlarda lazer ablyasiyasi usulidan foydalanish mumkin. Ushbu amaliy tadbiqlar o’z ichiga nanozarrachalar sintez qilish, mikro-nano o’lchamli davriy tizimlarni hosil qilish, metallar sirtlarni organik bo’yoqlarsiz rangli shakl berish, qayta ishlangan yuzalarning fizikaviy va kimyoviy xususiyatlarini nazorat qilish, lazerli plazma spektroskopiyasi va yupqa qoplamalarni o’stirish singari tadbiqlarni oladi. Mazkur tadqiqot ishi dolzarbligi impulsli lazer nurlanishining materiallar sirtlari bilan o’zaro ta’siri natijasida metall va oksid nanozarrachalarni sintez qilish, ularning husisiyatlarini tushunishtirish va potentsial qo'llanilishini sohalarini aniqlash bilan bog’liqdir. Suyuqlik holatda va vacuum sharoitida alyuminiy nanozarrachalarini lazer nurlanishi yordamida hosil qilish bo'yicha tadqiqotlar olib borilgan. Bunda nanozarrachalarni bilan qoplangan sirtlarning namlash, ularning eritmalarining va nanozarrachalardan tarkib topgan plazma muhitlarining nochiziqli optik hususiyatlarining o’zgarishilari ko'rsatilgan. Ikki haroratli model bilan birlashtirilgan molekulyar dinamika usullari yordamida alyuminiy nanozarrachalarning lazer ablyasiyasi jarayonida hosil bo'lishi tahlil qilingan. Tadqiqotda olib borilgan raqamli simulyatsion usular suyuq muhitda nanozarrachalar hosil bo'lishining asosiy mexanizmlarini va kerakli o'lchamdagi va morfologiyadagi alyuminiy nanozarrachalarini olish uchun optimal lazer nurlanish parametrlarining mavjudligini aniqlashga imkon bergan. Davomiyliklari nano-, piko- va femtosekund bo’lgan lazer impulslari bilan qattiq alyuminiy metal namunani ablatsiya qilish jarayonida hosil bo'lgan nanozarrachalarning uchunchi-tartibli nochiziqli optik xususiyatlari aniqlangan. Bunda to’lqin uzunligi λ=400 nm va davomiylgi 40 fs lazer nurlanishi impulslari yordamida namunaning nochiziqli sinishi va yutilish koeffitsientlari mos ravishda ~ 10^{-9} sm^2 W^{-1} va 10^{-7} sm W^{-1} ga tengligi aniqlangan. Alyuminiy nanozarrachalaridan tarkib topgan nishoni sirtida uyg’otilgan lazer plazmasida davomiyligi 40 fs lazer nurlanishining yuqori tartibli 37-harmonkasigacha bo’lgan kogerent nurlanishi manbai o’lchangan. Tadqiqotda metallar sirtlarida lazer nurlnanishi ta’siri ostida o’lchamlarini boshqarish mumkin bo’lgan nano/mikro o’lchamli tuzilmalarning shakllanishi, va ularning optik va namlash xususiyatlarini boshqarish imkonini beruvchi omillar aniqlangan. Mazkur nano/mikro o’lchamli tuzilmalarning biomoslashuvchan materiallar yuzasida shakllanishi, xususan, ularning fan va texnikaning turli sohalarida qo'llanilishini kengaytirishi mumkin. Metall yuzalarda murakkab nano-o'lchamli tuzilmalarni hosil qilishda to'lqin uzunligi 1030 nm va davomiyligi 37 fs bo’lgan yuqori takrorlanish chastotasiga ega lazer nurlanishlaridan foydalanish imkoniyatlari ko’rsatilgan. Lazer bilan ishlov berilgan

sirtlarning optik xususiyatlari va ularning namlanish xususiyatlari o'rtasida korrelyatsiya aniqlangan. Yog’ va suv eritmalarini ajratish uchun yuqori namlash xususiyatlariga ega membranalarni lazer nurlanishi yordamida tayyorlash ekologik va iqtisodiy ahamiyatga ega ekanligi ko’rsatilgan. Yuqori quvvatli, o'ta tezkor femtosekundli lazer yordamida zanglamaydigan po'lat va mis to'rlarni sirtlarida xosil qilingan nanostrukturalarga ega namunalar yuqori namlash xusisiyatlariga ega ekanliklari aniqlandi va ularning atrof-muhitga zarar etkazmaydigan, kimyoviy moddalarsiz va samarali namunalari sifatida qollash mumkinligi tasdiqlangan. Yog '-suv aralashmasini yuqori 98% samaradorlik bilan ajratish imkonini beruvchi membranalarni ishlab chiqarish uchun lazerli skanerlash parametrlari, to'r g'ovaklarining o'lchami va namunalarning emirilishga chiqamlilik sharoitlari optimallashtirilgan.

KIRISH

Mavzuning dolzarbligi va zaruriyati. 1960-yillarda lazerlar paydo bo‘lganidan beri lazer ablayatsiyasi va lazer yordamida strukturalash ko‘p o‘n yillar davomida keng o‘rganilgan. Biroq, chirplangan impulslarni kuchaytirish (ChIK) texnikasi va yuqori energiya zichligiga ega materiallarning kashf etilishi bilan tadqiqotchlarning qiziqishi keskin oshdi. ChIK rejimini qo‘llash deyarli bir necha o‘n femtosekundgacha bo‘lgan qisqa lazer impulslarini hosil qiladi. Ushbu impulslar juda past energiyaga ega bo‘lsada, eng yuqori quvvati teravattdan oshadi va 10^{18} W/sm^2 yoki undan yuqori diapazondagi intensivlikni tashkil qilishi ham mumkin. Bu 10^{11} V/sm elektr maydoniga to‘g‘ri keladi. Bunday yuqori pik quvvati va qisqa impulslarning lazer-materiya o‘zaro ta’sirining asoslari juda murakkab va turli mexanizmlarni tushunishni kafolatlaydi, chunki impulsning davomiyligi elektron-ion energiyasini uzatish vaqtidan, panjaraning issiqlik o‘tkazuvchanligi vaqtidan va namunaning gidrodinamika vaqtidan ancha qisqaroq.

Ultraqisqa impulslarning yuqori maxsimal intensivligi nochiziqli jarayonlarga olib keladi va kuchli elektr maydon ionlanishi va elektron ta’sir ionlanishi sodir bo‘ladi. Intensivlikka qarab, femtosekund rejimida ablyatsiyaning ikkita mexanizmi sodir bo‘ladi, ular kulon portlashlari va termal bug‘lanishdir. Past intensivlikda, ablyatsiya ostonasiga yaqin joyda, kulon portlashlari (yumshoq ablyatsiya) ustunlik qiladi, yuqori intensivlikda esa termal bug‘lanish (qattiq ablyatsiya) ustunlik qiladi. Kulon portlash rejimida impuls uchun faqat bir necha nm materiallar chiqariladi va termal bug‘lanishda impuls uchun kattaroq kattalikdagi material chiqariladi. Plazma harorati va elektron zichligi ta’sirini tushunish har qanday nishonning lazerli ablyatsiya mahsulotlarini optimallashtirishda juda muhimdir.

Lazer ablyatsiyasi bir nechta materiallarni qayta ishlash va analitik tatbiqlarda qo‘llanilishi mumkin. Ushbu tatbiqlar orasida nanozarrachalar hosil qilish, mikro-nano tuzilma, metallarni bo‘yash, yuzalarning namlash xususiyatlarini nazorat qilish, lazerli parchalanish spektroskopiyasi va impulsli lazer changlatishlari kiradi. Impulsli lazer ablyatsiyasi turli metall va oksid nanozarrachalarini (NZ) sintez qilishda keng qo‘llaniladi. Biroq, lazer impulsining davomiyligi, energiya oqimi, atrofdagi muhit turi, suyuqlik harorati va nurlantirilgan nishonlarning xususiyatlari kabi ko‘plab omillar NZ xususiyatlariga ta’sir qiladi. Nanozarrachalar tibbiyot sohasida saratonni erta aniqlash va davolashni yaxshilash, optik sensorlar, optoelektronika, yupqa plyonkalar va energiya manbalarida qo‘llashda o‘z o‘rnini topadi. Sintezlangan nanozarrachalarning morfologiyasi va hajmi NZ o‘z ichiga olgan substratlar va suspenziyalarning turli makroskopik xususiyatlarining o‘zgarishiga olib kelishi mumkin. Shuning uchun NZ ning hosil bo‘lish mexanizmi nishonni hajmiy

ablyatsiyaning turli rejimlarida o‘rganilishi kerak. Shu maqsadda suyuq muhitda (suvda) alyuminiy nishonining turli nurlanish parametrlarida lazerli ablyatsiya jarayonini raqamli modellashtirish amalga oshirildi. Simulyatsiya natijalari bir tomondan ularni tajriba o‘lchovlar bilan to‘g‘ridan-to‘g‘ri taqqoslash uchun ishlatilishi mumkin, biroq boshqa tomondan lazer yordamida NZ hosil bo‘lishi bilan bog‘liq jarayonlarning asosiy fizikasi haqida chuqurroq ma’lumot olishga yordam beradi. NZ ning past va yuqori tartibli nochiziqli optik xususiyatlarini o‘rganish kichik o‘lchamli agregatlarni nochiziqli optikaning turli sohalarida qo‘llashning amaliy va fundamental tamoyillariga asoslanadi. Metall yuzalarni lazer yordamida olib tashlash jarayonida hosil bo‘ladigan bu agregatlar ekstremal ultrabinafsha diapazonida yuqori tartibli garmonikalarni hosil qilish uchun samarali vosita bo‘lib xizmat qiladi.

Femtosekundli lazer bilan ishlov berish material yuzasida lokal nano o‘lchamdagi tuzilmalarni aniq nazorat qilish imkonini beradi, bu ularni juda samarali va ko‘p funksiyali qiladi, ayniqsa rang berishda. Lazer yordamida bo‘yash atrof-muhit uchun xavfsiz hisoblanadi, chunki u har qanday pigmentlar yoki kimyoviy moddalardan foydalanishni yo‘q qiladi, shu bilan birga lazer nurlanish parametrlarini optimallashtirish orqali kerakli natijalarga erishishda juda moslashuvchan. Yuqori quvvatli qisqa lazer impulslarining noyob qobiliyati deyarli barcha turdagi materiallarni nano-miqyosda modifikatsiya qilishi optika, optoelektronika, mikrofluidika, rangli naqshlash va mexanikada turli xil yangi tatbiqlar uchun katta imkoniyatlar yaratadi. Lazerli sirt modifikatsiyasining yana bir qo‘llanilishi metall yuzalarning namlanish reaktsiyasini nazorat qilishdir, bu hozirda materiallarni lazer bilan qayta ishlashga qiziqish ortib borayotgan mavzudir. Sirtlarni intensiv lazerlar yordamida suvni tortuvchi (gidrofil) yoki suvni qaytaruvchi (gidrofobik) qilib o‘zgartirish mumkin. Bunday o‘zgartirilgan sirtlar o‘z-o‘zini tozalash, korroziyani oldini olish, qarshilikni kamaytirish, bakteriyalarga qarshi, tumanga qarshi, issiqlik uzatish, tribologiya, optik aks ettirish va neft-suvni ajratish kabi ko‘plab tatbiqlarga ega.

Moy-suvni ajratish katta ekologik va iqtisodiy ahamiyatga ega. Yondirish, yog‘sizlantirish va kimyoviy dispersiya kabi an’anaviy moyni ajratish usullari qisman samarali, ammo ular ajralish effektivligini yomonlashtiradigan zararli qo‘shimcha mahsulotlarni ishlab chiqaradi. Femtosekundli lazer yordamida strukturalangan metall to‘rlar, 2D membranalar yoki 3D adsorbent ko‘piklarning ho‘llash javobi ekologik toza va yuqori ajratish samaradorligi xususiyatlariga ega. Moy va suv fazalari uchun selektiv o'tkazuvchanlikka ega bo‘lgan membranalarni suv ostida namlash hodisasida o‘zini supergidrofobik-superoleofil yoki supergidrofil-superoleofobik tutishi orqali olish mumkin.

Tadqiqotning xalqaro konteksti. Dunyo bo‘ylab ko‘plab nufuzli universitetlar va tadqiqot markazlari kuchli maydon rejimi, xususan, ionizatsiya, nanozarrachalar

shakllanishi, ko‘p funksiyali sirtlarni nanostrukturalash, YuTG va atomlar, molekulalar va materiallarda elektronlarning o‘ta tez dinamikasini attosekund vaqt shkalasida o‘rganish uchun kogerent ulrtabinafsha nurlanishlarni (XUV) qo‘llash sohasida tadqiqotlar olib bormoqda. Ular orasida Maks-Plank ko‘p tarmoqli fanlar institutining Ultrafast Dynamics bo‘limi (Gettingen, Germaniya), Rochester universiteti lazer energetikasi laboratoriyasi (LLE) guruhi (AQSh), Nanostrukturalar va Ultrafast X-Ray Science guruhi ETH-Zurich (Tsyurix, Shveytsariya), MEPHI dagi Biotibbiyot muhandislik fizikasi instituti guruhi (PhysBio), 115409 Moskva, Rossiya, Fizika instituti va fanlararo nanostruktura fanlari va texnologiyalari markazidagi guruh (CINSaT), Kassel universitetidagi guruh, 34125 Kassel, Germaniya, Changchun optika, fizika va nozik mexanika institutining nochiziqli optika guruhi (Changchun, Xitoy), Sharja Amerika universiteti (Sharja, BAA) Materialshumoslik va muhandislik tadqiqot markazi guruhi, Nanotexnologiyalar markazi guruhi, Munster universiteti (Munster, Germaniya), Tokio universiteti (Tokio, Yaponiya) qoshidagi nochiziqli optika guruhi, Ilg‘or texnologiyalar markazi (Indore, Hindiston) qoshidagi lazer plazmasi bo‘limi guruhi, Milliy Fan instituti guruhi (Monreal, Kanada), Imperial kollejida YuTG spektroskopiyasi (London, Angliya), Nanolitografiya ilg’or tadqiqot markazida YuTG va EUB ilmiy guruhi (Amsterdam, Niderlandiya) va boshqalar.

Mavzu bo‘yicha tadqiqotning hozirgi holati.

Impulsli lazer ablyatsiyasi doimiy ravishda o‘sib borayotgan sohadir. Boshqa ko‘plab tatbiqlar qatorida nanozarrachalarni shakllantirish, ko‘p funksiyali sirtlarni tayyorlash, lazerli parchalanish spektroskopiyasi va YuTG ilmiy hamjamiyat uchun katta qiziqish uyg’otadi.

Nanozarrachalar va mikro-nano tuzilmalarni lazer ablyatsiyasi bilan shakllantirish an’anaviy usullardan ustundir, chunki u hech qanday kimyoviy, insonning bevosita teginishini o‘z ichiga olmaydi va ekologik toza usuldir.

Tadqiqot mavzusini muassasaning ilmiy-tadqiqot faoliyati bilan bog‘liqligi. PhD taqdimnomasidagi asosiy tadqiqotlar Sharjadagi Amerika universitetining (BAA) Materialshunoslik va Muhandislik tadqiqot markazida olingan va boshqa bir qator natijalar O’zbekiston, Latviya, Germaniya, Yaponiya va Rossiyaning turli universitetlari bilan hamkorlikda olingan.

Tadqiqot ishining maqsadi yuqori takrorlanish tezligi ultra tez femtosekundli lazerlar tomonidan qayta ishlangan mikro/nanostrukturali materiallarning shakllanish mexanizmlari va yangi tatbiqlari bo‘yicha nazariy va tajriba bilimlarni olishdir.

Tadqiqotning vazifalari quyidagilardan iborat:

- Suyuqlik va vakuumda alyuminiy (Al) asosidagi nanozarrachalarning (NZ) lazer yordamida hosil bo‘lishini hamda ularning sirtlar, suspenziyalar va

plazmalarining ho‘llanishi va nochiziqli optik xususiyatlarini o‘zgartirish qobiliyatini o‘rganish.

- Optoelektronika, optik cheklovchilar va fotonikada potentsial qo‘llanilishi uchun NZlarning nochiziqli yutish va sinish xususiyatlarini, shuningdek ularning turli optik xususiyatlarini tadqiq qilish.
- Metall nishonlar yuzasida lazer yordamida hosil qilingan davriy sirt tuzilmalari (LIPSS) va nanospayklar shakllanishiga mos keladigan lazer parametrlari va namunaga qo‘yiladigan shartlarni o‘rganish.
- Moy-suvni ajratish uchun femtosekund lazer impulslari bilan qayta ishlangan turli xil materiallarning metall to‘rlar, tekislik va egri sirtlarning namlanish reaktsiyasini tadqiq qilish.
- YuTGni olish uchun lazer yordamida hosil qilingan nanozarrachalar bilan boyitilgan fakelning qo‘llanilishini o‘rganish.

Tadqiqotning ob'ekti - turli xil materiallar yuzasida lazer yordamida yaratilgan nano-mikro tuzilmalar, havoda, vakuumda va suv ostida hosil qilingan Al nanozarralari.

Tadqiqotning predmeti - turli materiallarning nano-mikro tuzilmali sirtlarining namlanish xususiyatlari va optik xususiyatlari, Al NZ ning nochiziqli optik xususiyatlari va hosil bo‘lgan yuqori tartibli garmonikalarning spektral xususiyatlari.

Tadqiqotning usullari ham nazariy, ham tajriba usullarni o‘z ichiga oladi. Nazariy usullar analitik molekulyar dinamika (MD) va diffuziya differentsial tenglamalarida olingan ikkita harorat modeli (TTM) bilan simulyatsiyani o‘z ichiga oladi. Nanozarrachalarni vakuumda va suv sharoitida yuqori quvvat, yuqori takrorlash tezligi, qisqa va ultra qisqa impulslar yordamida hosil qilishning tajriba usullari. Turli materiallar va metall to‘rlarni tekisliklar, egri sirtlarini femtosekundli tolali lazer yordamida strukturalash. Tomchi shakli analizatori yordamida kontakt burchagi va chekinish burchaklarini o‘lchash orqali sirtlarning namlanish xususiyatlarini miqdoriy o‘lchash.

Tadqiqotning ilmiy yangiligi

- MD-TTM raqamli simulyatsiyalari kerakli o‘lchamdagi va morfologiyadagi alyuminiy (Al) nanozarrachalarini (NZ) hosil qilish uchun lazer nurlanishining optimal parametrlari haqida tushunchaga ega bo‘lish uchun ishlatilgan.
- 400 nm spektral sohada nochiziqli yutilish koeffitsientlari (β) va nochiziqli sindirish ko‘rsatkichlarining (γ) yuqori qiymatlari birinchi marta pikosekundli impulslar yordamida alyuminiyni ablyatsiya qilish natijasida hosil bo‘lgan Al asosidagi NZ suspenziyasida kuzatildi. Al asosidagi NZlarning (β) va (γ) parametrlarining qiymatlari mos ravishda ~ 10^{-7} sm W^{-1} va 10^{-9} sm^2 W^{-1}.

- Biz birinchi marta vakuumda Al NZ ning in-situ shakllanishi, sintez qilingan nanozarrachalar buluti orqali harakatlantiruvchi impulslarning tarqalishi alyuminiy atomlari va ionlari bilan solishtirganda yuqori garmonik rentabellikni keltirib chiqarishini aniqladik. Al NZ lar 40 fs impulslar yordamida 37-tartibga qadar yuqori garmonikalarni hosil qilishga imkon berdi.
- Biz birinchi marta suvda hosil bo‘lgan Al asosidagi NZlarning cho‘kishi supergidrofil xususiyatga ega ekanligini va vakuumda to‘plangan NZlarning supergidrofobik xususiyatlarga ega ekanligini ko‘rsatdik.
- Biz birinchi marta metallar va metall qotishmalari yuzalarining doimiy va yorqin ranglarini ikkinchi bosqichli femtosekundli lazerli ishlov berish yordamida o‘chirish va qayta bo‘yash mumkinligini ko‘rsatdik.
- Lazer bilan ishlov berilgan sirtlarning spektral aks ettiruvchi xususiyatlari va ularning namlanish xususiyatlari o‘rtasidagi bog‘liqlik birinchi marta ko‘rsatildi.
- Biz birinchi marta neft va suvni ajratish tatbiqlari uchun membrana sifatida ablyatsiya lazer impulslarining turli xil oqimlari yordamida qayta ishlangan AlNiCo qotishma novdalaridan potentsial foydalanishni o‘rnatdik.
- Mis va zanglamaydigan po‘lat to‘rlarining qalinligi, g‘ovak o‘lchami, lazerni skanerlash tezligi va eskirish muhiti kabi qayta ishlash parametrlarini optimallashtirish bo‘yicha tizimli tadqiqotlar natijasida birinchi marta moy-suv aralashmalarini ajratishda 98% samaradorlikka erishildi.
- O‘z-o‘zini tozalash tadbiqlari uchun past bosimli muhitda eskirish orqali femtosekundli lazerli strukturali metallar yuzalarining namlanishining tezlashtirilgan o‘tishi ko‘rsatildi.
- Tantalning katta yuzasida (20 mm) ultratez lazer yordamida ishlab chiqarilgan murakkab davriy azimutal va radial yo‘naltirilgan davriy strukturalarni hosil qilish mumkinligi birinchi marta taqdim etildi. Bu implant sifatida foydalanilganda hujayra yopishish va proliferatsiya tendentsiyasini yaxshilash uchun juda muhimdir.
- Samarali yo‘nalishli suv o‘tkazish va tumanni yig‘ish tatbiqlari uchun qarama-qarshi namlanish xususiyatlariga ega femtosekundli lazer tomonidan ishlab chiqarilgan mis to‘r va ko‘pikli Janus membranalari namoyish etildi.
- Zeolit bilan qoplangan po‘latdan yasalgan lazer yordamida hosil qilingan tuzilmali to‘rlar yaxshilangan supergidrofil hodisasi va moy-suvni ajratish uchun uzoq vaqt davomida yuqori chidamlilikni namoyish etdi.

Tadqiqot ishning amaliy natijalari. Nazariy va tajriba tahlil natijalaridan Sharja Amerika universiteti (BAA) qoshidagi materialshunoslik tadqiqot markazida nanozarrachalar hosil qilish va turli materiallarning mikro-nano strukturaviy sirtlarini

qayta ishlash texnologiyasini takomillashtirishda foydalanildi. MD-TTM hisob-kitoblari va ma'lumotlarni tajriba qayta ishlash uchun turli kodlar ishlab chiqilgan va hozirda Sharja Amerika universiteti (Sharjah, BAA), Latviya universiteti (Riga, Latviya) qoshidagi nochiziqli optika laboratoriyasida, Fizika instituti va tadqiqot markazining Fanlararo nanostruktura fanlari va texnologiyasi tadqiqot guruhlarida, (CINsaT), Kassel universitetida, (Kassel, Germaniya), Voronej davlat universiteti, Fizika fakultetida (Voronej, Rossiya) va Toshkent irrigatsiya va qishloq xo'jaligini mexanizatsiyalash muhandislari institutida (Toshkent, O'zbekiston) faol qo'llanilmoqda.

Tadqiqot natijalarining ishonchliligi ular zamonaviy hisob-kitoblar, simulyatsiyalar va tajriba usullardan foydalangan holda olinganligi bilan tasdiqlanadi. Natijalarning ishonchliligi, shuningdek, olingan natijalarning tajriba ma'lumotlarga mos kelishiga asoslanadi. Bundan tashqari, olingan natijalarning ishonchliligini yanada ta'kidlash uchun tadqiqotchining barcha maqolalari sirtiy jarayonlar, nanomateriallar, nochiziqli optika sohasidagi mutaxassislar tomonidan ko'rib chiqilgan va Q1 va Q2 kvartillariga tegishli bo'lgan yuqori reytingli jurnallarda nashr etilgan.

Tadqiqot natijalarining ilmiy ahamiyati. Nanozarrachalarning hosil bo'lish mexanizmi va mikro/nano strukturaviy sirtlarni qayta ishlash bo'yicha tadqiqotning nazariy va tajriba natijalari ko'plab ekzotik tatbiqlarga ega. Lazer usuli bilan ishlab chiqarilgan nanozarralar yashil, toksik bo'lmagan mahsulotdir, shuning uchun saratonni erta aniqlash va davolash, energetika, yupqa plyonkalar, optoelektronika, Raman spektroskopiyasi signalini kuchaytirish va boshqa ko'plab ilovalar uchun qulay. Nanostrukturali sirtlar o'z-o'zini tozalash, korroziyani oldini olish, qarshilikni kamaytirish, bakteriyalarga qarshi, tumanga qarshi, issiqlik o'tkazuvchanligi, tribologiya, optik aks ettirish, moy-suvni ajratish kabi turli xil materiallarning ko'p funksiyali sirtlarini ishlab chiqarishda katta ahamiyatga ega.

Tadqiqot natijalarining joriy qilinishi.

Tadqiqot natijalari ko'plab ilmiy maqolalarda qo'llanilgan. Ular orasida "Ultrafast fiber laser-induced fabrication of superhydrophobic and self-cleaning metal surfaces," S.A. Khan, et.al. Appl. Surf. Sci. 542, 148560 (2021) (**75 ta** iqtibos), "Expedited transition in the wettability response of metal meshes structured by femtosecond laser pulses for oil-water separation," S.A. Khan, va b., Front. in Chem. 8, 768 (2020) (**20 ta** iqtibos), "The mechanism of laser-assisted generation of aluminum nanoparticles, their wettability and nonlinearity properties," M. Iqbal, va b., Appl. Surf. Sci. 527, 146702 (2020) (**17 ta** iqtibos), "Superhydrophobic and superhydrophilic properties of laser-ablated plane and curved surfaces," G.S. Boltaev, va b., Appl. Phys. A 126, 1-9 (2020) (**12 ta** iqtibos), "Near-field induced reaction yields from nanoparticle clusters," P. Rosenberger, va b., ACS Photonics 7, 1885-1892 (2020) (**20 ta** iqtibos), "Anomalous formation of trihydrogen cations from water on nanoparticles," M.S. Alghabra, va b.,

Nat. Commun. 12, 3839 (2021) (**15 ta** iqtibos), "Resonance enhancement of harmonics in the vicinity of 32 nm spectral range during propagation of femtosecond pulses through the molybdenum plasma," V.V. Kim, va b., J. Phys. B: At. Mol. Opt. Phys. 53, 195401 (2020) (**14 ta** iqtibos), "Giant third-order nonlinear response of mixed perovskite nanocrystals," A.M. Abu Baker, va b., Materials 15, 389 (2022) (**12 ta** iqtibos), "Enhanced XUV harmonics generation from diatomic gases using two orthogonally polarized laser fields," G.S. Boltaev, va b., Sci. Rep..11, 5534 (2021) (**12 ta** iqtibos), "Application of 150 kHz laser for high-order harmonic generation in different plasmas," G.S. Boltaev, va b., Photon. 7, 66 (2020) (**9 ta** iqtibos), "Simultaneous manipulation of the optical and wettability properties of metal surfaces using 150 kHz femtosecond fiber laser," M. Iqbal, va b., Appl. Sci. 10, 6207 (2020) (**7 ta** iqtibos), va boshqalar.

Tadqiqot natijalarining nashr etilganligi. PhD dissertatsiyasining ilmiy tadqiqot ishlari natijalari O'zbekiston Respublikasi Oliy attestatsiya komissiyasi tomonidan falsafa fanlari doktorlik (PhD) ilmiy darajasining asosiy ilmiy natijalarini nashr etish uchun tavsiya etilgan nufuzli taqrizlanuvchi Q1/Q2 kvartillardagi ilmiy jurnallarda chop etilgan 30 ta ilmiy maqolalarda taqdim etilgan va Web of Science ilmiy ma'lumotlar bazasida ko'rsatilgan.

ISHNING ASOSIY MAZMUNI

Taqdimnomada belgilangan vazifalar bo'yicha olib borilgan tadqiqotlar asosida olingan ilmiy natijalar quyidagi ikki bo'limda keltirilgan. Taqdimnonaming **birinchi bo'limda** nanozarrachalaming hosil bo'lish mexanizmlari va ularning turli sohalarda qo'llanilishiga doir natijalar ko'rib chiqilgan [Appl. Surf. Sci. 527, 146702 (2020), Appl. Surf. Sci. 542, 148560 (2021)]. Taqdimnonaning **ikkinchi bo'limi** o'z ichiga materiallar yuzalarida nanostrukturalarning shakllanish mexanizmlarini tahlil qilishga va ularning turli sohalarda qo'llanilishiga bo'yicha olingan ilmiy natijalarni oladi [Fron. Chem. 8, 768 (2020); J. Phys. D: Appl. 54, 185109 (2021), Appl. Sci. 10 (18), 6207 (2020)]. Mazkur taqdimnomada keltirilgan ilmiy natijalar PhD darajasiga nomzodi va uning hammualliflari tomonidan nufuzli Q1/Q2 kvartillariga ega ilmiy jurnallarda 30 ta ilmiy maqolalar ko'rinishida chop etilgan. Tajribada olingan ma'lumotlar, nazariy hisob-kitoblar va raqamli simulyatsiya usullari so'nggi 5 yil davomida Birlashgan Arab Amirliklari, Germaniya, Latviya, Rossiya va O'zbekistonning turli ilmiy muassasalarida ishlab chiqilgan va qo'llanilgan.

I-Bo'lim. Nanozarrachalarning hosil bo'lish mexanizmlari va yangi ilovalar
Materiallaming nano o'lchamdagi ishlashi ularning makroskopik harakatlaridan butunlay farq qiladi. Impulsli lazer ablyatsiyasi turli metall va oksid nanozarrachalarini

(NZ) sintez qilishda keng qo'llaniladi. Shu munosabat bilan alyuminiy NZ turli xil ilovalarni ko'rsatadi. Ushbu bo'limda [Appl. Surf. Sci. 527, 146702 (2020)] suyuqlik-larda va vakuumda Al-asosli nanozarrachalarning lazer yordamida hosil bo'lish mexanizmlarini nazariy va tajriba o'rganishni va ularning sirtlarning namlanuvchanligi va nochiziqli optik xususiyatlarini o'zgartirish qobiliyatini taqdim etilgan. Lazer nurlanishi impulsining davomiyligi, oqim tezligi, atrofdagi muhit turi, suyuqlik harorati va nurlangan nishonlarning xususiyatlari kabi ko'plab omillar NZlarning xususiyatlariga ta'sir qiladi. Shuningdek, sintezlangan zarrachalarning morfologiyasi va hajmi NZ o'z ichiga olgan substratlar va suspenziyalarning turli makroskopik xususiyatlarining o'zgarishiga olib kelishi mumkin. Ommaviy nishonlarni ablatsiya qilish paytida alyuminiy NZ larning hosil bo'lish jarayonini tushunish uchun biz molekulyar dinamikaning raqamli simulyatsiyasini amalga oshirdik. Raqamli simulyatsiyalar suyuq muhitda NZ hosil bo'lishining asosiy mexanizmlarini va kerakli o'lchamdagi va morfologiyadagi Al NZlarni olish uchun optimal lazer nurlanish parametrlarining mavjudligini aniqlashga imkon berdi.

Simulyatsiya natijalari bir tomondan ularni tajriba o'lchovlar bilan to'g'ridan-to'g'ri taqqoslash uchun ishlatilishi mumkin, biroq boshqa tomondan lazer yordamida NZ hosil bo'lishi bilan bog'liq jarayonlarning asosiy fizikasi haqida chuqurroq ma'lumot olishga yordam beradi. Ushbu simulyatsiyalar birlashtirilgan atomistik-uzluksiz modeldan foydalangan holda amalga oshiriladi. Model molekulyar dinamika (MD) usuli [Science 280, 2085 (1998)] yordamida atom o’lchamlarida lazer nurlanishi bilan uygotilgan muvozanatsiz fazaga o'tish jarayonlarining kinetikasini ko'rib chiqilgan, shu bilan birga lazer nurining yutilishi, elektron issiqlik o'tkazuvchanligi va kuchli elektron jarayonlari - Qisqa lazer nurlanishi ta’siri bilan induktsiya qilingan fonon nomutanosibligi elektron harorati orqali ikki harorat modeli (TTM) bilan tavsiflanadi.

Birlashtirilgan MD-TTM modeli dinamikasi [Appl. Phys. A 111, 675–687 (2013)] eksperimentda bevosita erishish mumkin bo'lgan o'lchovdagi o'ta katta simulyatsiyalarda qo'llanilishi mumkin. Shunday qilib, bizning simulyatsiyamiz natijalari tajriba ma'lumotlarni sharhlashda va oldindan ishlab chiqilgan xususiyatlarga ega NZlarni yaratishda bevosita hisobga olinishi mumkin. Model atom harakatini tavsiflovchi MD yondashuvini TTM modeliga kiruvchi elektronlar uchun diffuziya diffuziya tenglamasi bilan birlashtiradi [Phys. Rev. B 68, 064114 (2003)].

Metalllarda lazer nuri energiyasi o'tkazuvchanlik zonasida joylashgan elektronlari tomonidan yutiladi. To'plangan energiya tez, qisqa vaqt femtosekund (10^{-18}s) davomida elektronlar o'rtasida muvozanatlanadi va atom tebranishlariga uzatiladi. Oxirgi jarayon elektron-fonon birikmasining ta’siri bilan boshqariladi va soniyaning pikosekund (10^{-12}s) qismidan bir necha o'nlab pikosekund (10^{-12}s) gacha davom etishi mumkin. Nihoyat, elektronlar va fononlar o'rtasida termal muvozanat o'rnatiladi va sirt

hududidan nurlangan nishonning asosiy qismiga issiqlik oqimi umumiy termal diffuziya sifatida tavsiflanishi mumkin. Lazer pulsining davomiyligi elektron-fononni issiqlik bilan solishtirish uchun zarur bo'lgan vaqtga teng bo'lsa yoki undan kamroq bo'lsa, lazer nurlanishi natijasida termal nomutanosiblik holati yaratiladi, elektronlar va panjara har xil haroratga ega. Kontinuum darajasida panjara va elektron temperaturalarining vaqt evolyutsiyasi T_l va T_e ni ikkita bog‘langan nochiziqli differensial tenglamalar yordamida ikki temperaturali TTM modeli orqali tasvirlash mumkin [Phy. Rev. B 68, 064114 (2003)],

$$C_e(T_e)\frac{\partial T_e}{\partial t} = \nabla[k_e(T_e)\nabla T_e] - G(T_e - T_l) + S(z,t) \quad (1)$$

$$C_l(T_l)\frac{\partial T_l}{\partial t} = \nabla[k_l(T_l)\nabla T_l] + G(T_e - T_l) \quad (2)$$

Bu erda *C* va *K* - elektron va panjaraning issiqlik sig'imlari va issiqlik o'tkazuvchanliklari *e* va *l* pastki belgilar bilan belgilanadi va *G* - elektron-fonon bog'lanish doimiysi. Manba atamasi *S(z,t)* lazer impulsining davomiyligi davomida maydon birligi va birlik vaqtiga lokal energiya to'planishini tavsiflash uchun ishlatiladi.

Hisoblash molekulyar dinamikasi MD usuli lazer-metall o'zaro ta'sir mexanizmlari haqida tushuncha beradi. Biroq, klassik MD usuli lazerning metallar bilan o'zaro ta'sirini simulyatsiya qilish uchun bevosita qo'llanilmaydi. Metallning issiqlik o'tkazuvchanligiga elektron hissasi dominant bo'lganligi sababli, faqat panjara hissasi mavjud bo'lgan an'anaviy MD usuli umumiy issiqlik o'tkazuvchanligini sezilarli darajada kam baholaydi. Biroq, birlashtirilgan TTM va MD modeli jarayonlarga eng yaxshi javob beradi.

Kombinatsiyalangan usulda MD usuli panjara harorati uchun TTM tenglamasini to'liq almashtiradi (2-tenglama). Elektron temperaturasi uchun diffuziya tenglamasi T_e, (1-tenglama), atomlar harakati tenglamalarini MD integratsiyasi bilan bir vaqtda chekli farq usuli bilan yechiladi va elektron harorati elektron va panjara o'rtasidagi energiya almashinuvi uchun kerakli bo'lgan boglanish davrini o’z ichiga oladi [Phys. Rev. B 064114 (2003)];

$$C_e(T_e)\frac{\partial T_e}{\partial t} = \frac{\partial}{\partial z}\left[k_e(T_e)\frac{\partial}{\partial z}\,(T_e)\right] - G(T_e - T_l) + S(z,t) \text{ TTM}$$

$$m_i\frac{d^2\mathbf{r_i}}{dt^2} = \mathbf{F_i} + \eta\, m_i\mathbf{v_i} \qquad \text{MD} \quad (3)$$

where η is

$$\eta = \frac{1}{n}\sum_{k=1}^{n} GV_N(T_e - T_l)/\sum_i m_i(\mathbf{v_i})^2 \quad (4)$$

4- tenglamada m_i va r_i i atomning massasi va holati, $\boldsymbol{F_i}$ esa atomlararo ta’sir tufayli *i* atomiga ta’sir etuvchi kuchdir. Oddiy MD harakat tenglamalariga qo'shilgan qo'shimcha atama elektron-fonon birikmasini hisobga oladi. Tenglamaning chekli farqli (FD) integrasiyasida fazoviy diskretlanish (Δt_{FD}) bosqichi. (3) fon Neyman

barqarorlik mezoniga asoslanib baholanishi mumkin. Birlashtirilgan modelning ikkinchi qismidagi vaqt oraliqlari shunday tanlanadiki, bir MD vaqt qadami $\Delta t_{MD}=n\Delta t_{FD}$ chekli farqli vaqt qadamlarining butun soniga mos keladi. Har bir chekli farqli diskretlanish katakchasida elektron-fonon birikmasi tufayli elektronlar va panjara o'rtasida o'tkaziladigan energiya n integratsiya bosqichlari uchun umimiy summa korinishida keltirilishi mumkin [Phys. Rev. B 68, 064114 (2003)],

$$\Delta E^{e-ph} = \sum_{k=i}^{n} \Delta t_{FD}\, G V_N (T_e - T_l) \quad (5)$$

Keyin to‘plangan energiya MD harakat tenglamalariga qo‘shilgan bog‘lanish termini yordamida MD tizimining tegishli qismidagi atom harakati energiyasiga o‘tkaziladi (yoki undan olinadi), 4-tenglama. Lazer energiyasini yaqsimoyini tavsiflash uchun olib borilgan hisoblashlarda quyidagi Gauss profilidan foydalanildi [Phys. Rev. B 68, 064114 (2003)],

$$S(z,t) = I_o\,(1-R) L_p^{-1} \exp\left(-\frac{z}{Lp}\right) \exp\left[-(t-t_o)2/2\sigma^2\right. \quad (6)$$

Bu erda I_o - eng yuqori intensivlik, R - aks qaytaruvchanlik, L_p - optik yutilish chuqurligi va s - impuls davomiyligi FWHM = $\sigma\sqrt{8\ln(2)}$ bilan bog'liq Gauss nurlari profilining standart og'ishi. Lazer nurining energiya oqimi eng yuqori intensivligi I_o bilan bog'liq,

$$F = \sqrt{\pi/4\ln(2)}\,\tau_L I_o \sim 1.0645\,\tau_L I_o \quad (7)$$

Biz 10 J/sm^2 bir xil energiya oqimi bilan alyuminiy nishonini qisqa va uzoq lazer

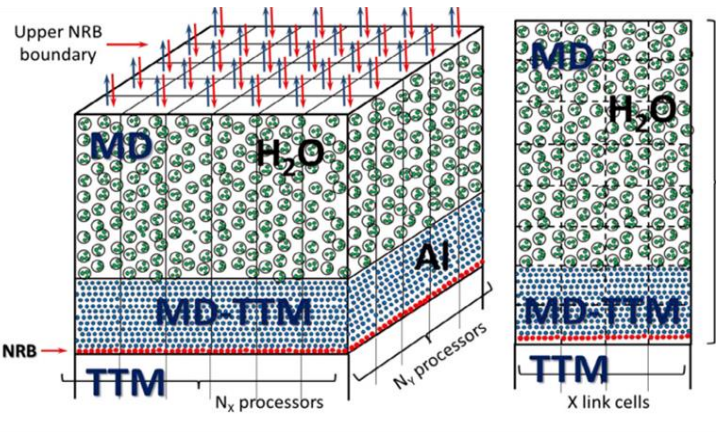

1-rasm. Qalin suv qatlami ostida NZ ni lazer hosil qilish simulyatsiyasi uchun umumiy hisoblash yacheykasi mos ravishda $N_x \times N_y$ protsessor yadrolari bilan ishlov berish uchun X va Y yo'nalishlari bo'yicha N_x va N_y kichik hajmlariga bo'linadi (chapda). Har bir alohida yadro 3D to‘rga bo‘lingan, bu yerda biz birlashtirilgan MD-TTM modelini hal qilamiz, suv qatlami uchun esa klassik MD yondashuvi qo‘llaniladi (o‘ngdagi 2D ko‘rinishi) [Appl. Surf. Sci. 527, 146702 (2020)].

impulsli ablyatsiyasini modellashtirishni amalga oshirildi. Bu bizga impulsning NZ hosil bo'lish mexanizmiga ta'sirini ko'rsatishga imkon berdi. Simulyatsiya natijalarini tajribada olingan malumotlar bilan bog'lash uchun biz Al uchun xarakterli elektron-fonon muvozanat vaqtiga (~ 1,5 ps) nisbatan kichik va katta davomiyliklardagi lazer impulslari (0,3 ps va 50 ps) tanlab olindi.

Bunday yondashuv NZ hosil bo'lish jarayoni bilan nishonda nurlanish yutilishing turli rejimlarini ko'rib chiqishga imkon beradi va mos ravishda ushbu ishning tajriba qismida qo'llaniladigan lazer impulslari davomiyligining fs va ps diapazonlarini

qamrab oladi. Bundan tashqari, tajribada bo'lgani kabi, nishon fazoviy chegarada qalin suv qatlami tomonidan joylashgan bo'lib, bu erda "qalin" atamasi lazer ta'siri ostida bo'lgan bosim to'lqinining NZ paytida erkin yuzalardan aks etishini oldini olish uchun etarlicha katta qalinlik ma'nosida ishlatiladi. shakllantirish jarayoni. Suv ta'sirida fazoviy chegarada Al NZ hosil bo'lishi bo'yicha bizning simulyatsiyalarimizda foydalanilgan umumiy hisoblash katakchasi sxematik tarzda 1-rasmda ko'rsatilgan.

Tajribadagi lazer nuqtasining o'lchami (0,3 mm) simulyatsiya xujayrasining xarakterli lateral o'lchamidan (100 nm) ancha katta bo'lganligi sababli, nurlanish vaqtida hujayra yuzasi bo'ylab lazer intensivligi taxminan bir xil bo'lib qoladi. Bundan tashqari, simulyatsiya vaqtida bir necha ns gacha bo'lgan lateral yo'nalishda issiqlik o'tkazuvchanligining nisbatan sekin jarayonlari bizga X va Y yo'nalishlarida davriy chegara shartlarini (PBC) o'rnatishga imkon berdi. Hisoblash qutisining lateral o'lchami tajriba o'lchovlariga ko'ra, o'lchamlari ~10-100 nm oralig'ida bo'lgan NZ hosil bo'lishiga olib keladigan jarayonlarga mos keladigan darajada katta edi. Shunday qilib, alyuminiy-suv MD super hujayrasi ~300 000 000 atomdan iborat bo'lib, X, Y va Z yo'nalishlarida mos ravishda 75×100×900 nm^3 o'lchamlarga ega, qalinligi metall uchun 400 nm va suv qatlamlari uchun 500 nm. atom rezolyutsiyasi. Simulyatsiya protsedurasining hisoblash samaradorligini oshirish uchun biz Al uchun birlashtirilgan MD-TTM modelini faqat sirt ostidagi 400 nm qalinlikda qo'lladik, bu erda biz aks etmaydigan chegara (NRB) shartlarini joylashtirdik uning ostida biz Al uchun TTM ni faqat sirtdan sirt ostidan ~50 mkm gacha bo'lgan masofaga issiqlik oqimini hisobga olish uchun hal qildik [Comp. Mater. Sci 24, 2002, 421]. NRB shartlaridan foydalanish tez lazerli isitish tufayli yuzaga yaqin joyda hosil bo'lgan lazer ta'siridan kelib chiqqan bosim to'lqinlarini o'zlashtirishga imkon berdi.

Xuddi shunday, yuqorida suyuq muhit mavjudligini hisobga olish uchun suv uchun NRB chegaralari metall-suyuqlik interfeysidan 500 nm masofada joylashgan. Shunday qilib, har bir protsessor yadrosi metall qism uchun birlashtirilgan MD-TTM modelini, suv qismi uchun oddiy MD modeli va sirtdan 400 nm dan past bo'lgan metall qismning TTM modelini (bitta protsessor uchun 2D to'r ko'rsatilgan) echishga bag'ishlangan. 1-rasm). Simulyatsiya natijalarini tajriba ma'lumotlar bilan bog'lash imkoniyatiga ega bo'lish uchun biz simulyatsiyalarimizda alyuminiy uchun real atomlararo potentsialdan foydalandik, bu potentsial bilan materialning issiqlik sig'imi, muvozanat erish harorati, termal kengayish koeffitsienti va hajmi kabi termofizik xususiyatlari mavjud. erishi yuqori aniqlikda (95% dan ortiq) ifodalanadi.

Suv ichiga joylashtirilgan alyuminiy namunasining davomiyligi 0,3 ps bo’lgan lazer impulslari bilan o'zaro ta'sirini modellashtirish natijalari 2-rasmda ko'rsatilgan va umuman olganda, ultraqisqa lazer impulsi tufayli suvda NZ hosil bo'lishi natijalari

bilan o'zaro bog'liq bo'lib, suyuqlikda NZ hosil bo'lish jarayoni sodir bo'ladi. media ikkita boshqaruv mexanizmiga bog'liq ekanligi aniqlandi: ablyatsiya plyusining yuqori qismidagi bug 'fazasidan NZ yadrolari va suyuq metall interfeysida Reyleigh-Teylor beqarorliklarining shakllanishi. Ushbu ikkita mexanizm bimodal NZ o'lchamlari taqsimotini shakllantirish uchun javobgar hisoblanadi [Nanoscale, 2018, 10, 6900-6910]. Bizning ishimizda biz yuqorida aytib o'tilgan mexanizmlami lazer nurlanish parametrlari bilan manipulyatsiya orqali NZ o'lchamlarini taqsimlashni boshqarish imkoniyatini ta'minlaydigan tushuntirishlar bilan to'ldirdik.

2(a)-rasmdagi atom suratidan biz 175 ps ga kelib nurlangan nishon uning yuzasidan bug‘lanish jarayoniga ham, kengayish jarayoniga ham o‘tganini ko‘rishimiz mumkin, bu esa uning katta qismida bo‘shliqlar hosil bo‘lishiga olib keladi.

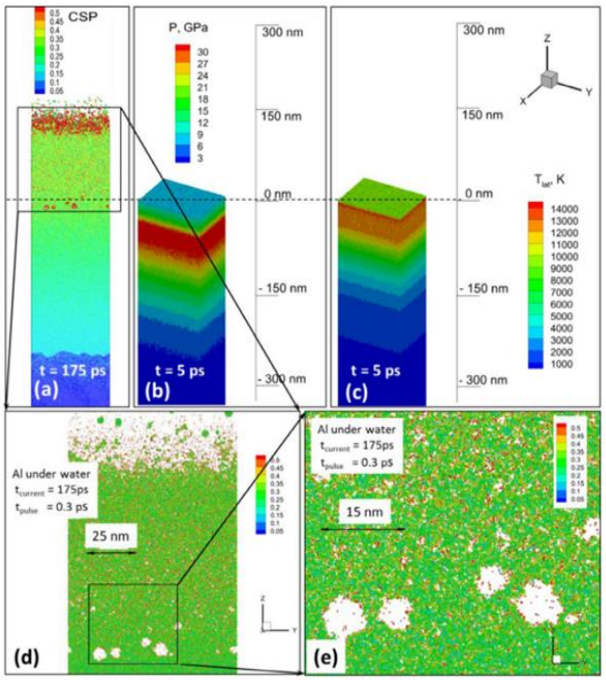

2-rasm. (a) Energiya zichligi 10 $J \cdot sm^{-2}$ va davomiyligi 0,3 ps lazer nurlanishi yordamida Al NZ hosil bo'lishi jarayonini 175 ps vaqtiy interval bilan atomlar harakatlari tasviri ko'rsatilgan. SCP qiymatlari: qattiq <0,08<nuqsonlar<0,12<suyuqlik <0,25<sirt <0,50<bug' bo'lishi uchun atomlarning lokal tuzilishini aniqlash uchun atomlar Markaziy simmetriya parametri (CSP) bilan ranglanadi. Yashil suyuqlik NZlari qizil bug' atomlarining ba'zi hissasi bilan shleyfning yuqori qismida ko'rinadi. Suv atomlari ko'rsatilmagan. (b) etkazilgan bosim uning maksimal qiymati 36 GPa momenti uchun ko'rsatiladi, bunda spallatsiya mexanizmini ablyatsiya jarayoniga jalb qilish uchun shart-sharoitlar mavjud. (c) panjara harorati maydoni uning maksimal qiymati 11000 K momenti uchun ko'rsatilgan, bu materialni chiqarish jarayonining portlovchi qaynash mexanizmi uchun sharoitlarni ta'minlaydi. (d) hosil qiluvchi NZlarni yaxshiroq kuzatish uchun (a) dagi kvadrat mintaqa ko'rsatilgan. (e) (d) dan hoshiyalangan hudud Al nishoni ichida hosil bo'ladigan g'ovaklikni vizual aniqlash uchun kattalashtiriladi [Appl. Surf. Sci. 527, 146702 (2020)].

Material, bu spallatsiya jarayonining boshlanishi bilan bog'liq. Metall nishonda energiya tarqalishining (lazer zarbasi bilan yotqizilgan) asosan ikkita asosiy kanali mavjud: tez elektron issiqlik o'tkazish jarayoni va panjara isitishiga olib keladigan elektron-fonon energiya almashinuvi jarayoni. Impulsning davomiyligi 0,3 ps bo'lganligi sababli, bu elektronlar va fononlarning relaksatsiya vaqtidan (~1,5 ps) qisqaroq, isitish tezligi elektronlar va fononlar o'rtasidagi muvozanatga erishish vaqti bilan belgilanadi.

Lazer impulsining yutilishi jarayonida erishilgan yuqori elektron harorati (~ 40 000 K) tufayli elektronning haroratiga juda bog'liq bo'lgan elektron issiqlik o'tkazuvchanligi kanali sezilarli darajada isitish chuqurligiga olib keladi. Shu bilan birga, bu isitish tezligi mexanik materialning (akustik) bo'shashish tezligidan oshib ketadi va yuqori ichki stresslar (36 GPa gacha) nurlangan nishonning sirt maydonida to'planadi, 2-rasm (b). Bunday sharoitlar ichki stress chegarasi deb ataladi va nishon bo'ylab tarqaladigan kuchli tushirish bosimi to'lqini tufayli ularning bo'shashishiga olib keladi. Shuning uchun mexanik bo'shashish ichki bo'shliqlarning shakllanishiga olib keladi, 2-rasm (d) va (e), ular birlashadi, o'sadi va nishonning mexanik shikastlanishi bilan bog'liq bo'lgan spallatsiya jarayonining boshlanishiga olib keladi [Appl. Phys. A. A 117, 2133 (2014)] va suyuq metall interfeysi bo'ylab Rayleigh-Teylor beqarorlik-larining paydo bo'lishi tufayli NZ ning katta qismi shakllanishi.

Boshqa tomondan, kritik nuqtadan yuqorida (katta miqdorda yutilgan energiya tufayli) yuqori haroratlarga erishgan metal yuzasi (11000 K maksimal qiymatga), 2-rasm (c), keyingi hosil bo'lishi bilan portlovchi qaynash mexanizmi tomonidan boshqariladigan ablyatsiya jarayoniga olib keladi. Metall bug'langan atomlarning yadrolanishi tufayli NZlarning kichikroq qismi. Qo'llaniladigan oqimga qarab, ablyatsiya jarayonining spallatsiya va fazali portlash mexanizmi o'rtasidagi bog'liqlik [J. Chem. Phys. 113, 11892 (2009)]. Bizning ishimiz uchun tajriba qismda ko'proq afzalliklarga ega bo'lgan qiziqarli holat uzoq lazer zarbasi tufayli suv ostida Al NZ avlodi bo'ldi. Al nishoni bilan uzoq pulsli o'zaro ta'sirni taqlid qilish uchun 50 ps pulsning davomiyligi tanlangan. Al uchun xarakterli elektron-fonon muvozanat vaqtidan ancha uzoqroq bo'lganligi sababli (~ 1,5 ps), materialning isitish vaqti impuls davomiyligi bilan belgilanadi. Al nishoniga yo'naltirilgan 50 ps lazer zarbasi tufayli suvda NZ hosil bo'lishini modellashtirish natijalari 3-rasmda ko'rsatilgan. Tizimning atomik suratlari ketma-ketligi simulyatsiya boshlanishidan 125, 250 va 500 ps vaqtlari uchun ko'rsatilgan, 3(a)-rasm. Ushbu simulyatsiyalarda puls 125 ps ga qadar maksimal intensivlikka erishdi va biz 500 ps simulyatsiya vaqtini NZ shakllanishi uchun mas'ul bo'lgan mexanizmlarni o'rnatadigan muhim jarayonlarni qamrab olish uchun etarlicha uzoq deb hisobladik. NZ hosil bo'lish jarayonlarining o'zi ancha uzoqroq (bir necha ns) bo'lishi mumkin bo'lsa-da, biz ushbu tadqiqotda asosan NZ shakllanishining o'rnatilgan mexanizmlari bilan manipulyatsiya qilish usullarini qidirdik [J. Phys. Chem. C, 121, 30, 16549–16567 (2017)]. E'tibor bering, bu erda, oldingi holatda bo'lgani kabi, NZ hosil bo'lish mexanizmi uchun javobgar bo'lgan shartlar asosan elektron-fonon muvozanati vaqtiga yoki impulsning oxiriga qarab belgilanadi. Bu vaqtga kelib, lazerning har ikkala kanali energiyaning tarqalishi (elektron issiqlik o'tkazuvchanligi va elektron-fonon o'zaro ta'siri tufayli) nishonning keyingi evolyutsiyasini va NZ hosil

bo'lish jarayonining o'zini belgilaydigan eng intensiv energiya tashishni to'xtatadi. Uzoq lazer impulsi kuchli elektron-fonon nomutanosibligini keltirib chiqara olmaydi. Impuls ta’siri paytida elektron harorat taxminan panjara haroratiga teng bo'lib qoladi va elektron o'tkazuvchanlik orqali energiya tarqalish kanali elektron-fonon o'zaro ta'sir (panjara isitish) kanalidan ancha zaif bo'lganda, 15000 K chegarasida qoladi.

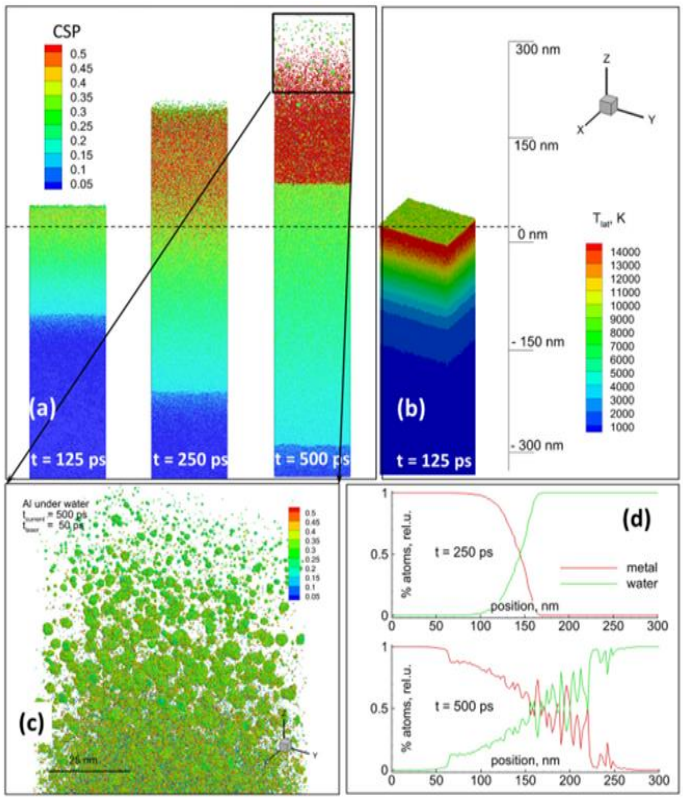

3-rasm. (a) 10 J sm-2 lik oqim oqimida Al bilan 50 ps lazer zarbasining o'zaro ta'siri natijasi 125, 250 va 500 ps uchun atomik suratlar ketma-ketligi sifatida ko'rsatilgan. Atomlarning mahalliy tuzilishini aniqlash uchun atomlar Markaziy simmetriya parametri (CSP) bilan ranglanadi: qattiq<0,08<nuqsonlar<0,12< suyuqlik<0,25< sirt<0,50<bug'. Yashil NZlar qizil bug 'atomlarining muhim hissasi bilan shleyfning yuqori qismida ko'rinadi. Tizimning metall qismini yaxshiroq ko'rish uchun suv atomlari bo'sh bo'ladi. (b) Panjara harorati maydoni 125 ps vaqtida uning maksimal qiymati 14000 K momenti uchun ko'rsatilgan. (c) (a) dagi to'rtburchaklar mintaqa hosil qiluvchi NZlarni batafsilroq kuzatish uchun kattalashtiriladi. (d) 250 ps va 500 ps da metall va suv turlarining nisbiy zichligi ularning aralashish jarayonini ochib beradi [Appl. Surf. Sci. 527, 146702 (2020)].

Shuning uchun to'plangan issiqlik nishonning chuqur qismiga kira olmaydi (qisqa lazer zarbasi bilan solishtirganda) va taxminan nishon yuzasiga yaqin joyda qoladi. Bu qizdirilgan nishonning asta-sekin akustik (mexanik) bo'shashishi sharoitida termal cheklash rejimini o'rnatishga olib keladi, bu 3(b)-rasmda maksimal 4GPa ichki bosim (ko'rsatilmagan) bilan sirtning yuqori harorati sifatida aks ettirilgan. Shunga qaramay, uzoq isitish vaqti ablyatsiya jarayonining mexanizmi portlovchi qaynash bilan boshqarilsa, panjara haroratining kritik nuqtadan 14000 K gacha ko'tarilishiga olib keladi [J. Phys. Chem. C 113, 11892–11906 (2009)]. Nurlangan nishon mexanik ravishda bo'shashganligi sababli, ablyatsiya jarayonining spallatsiya mexanizmi bu yerda ishtirok etmaydi va nishonning yetkazilgan zarari sof termal xususiyatga ega. Buni 3(a)-rasmda ko'rish mumkin, bu erda mexanik bo'shashgan eritmalar o'ta kritik haroratgacha qizib ketganda bug '-suyuqlik aralashmasining silliq o'tish zonasi paydo bo'ladi. Bug'langan metall atomlari sezilarli issiqlik sig'imi (metallar bilan taqqoslanadigan) va yuqori bug'lanish energiya yo'qotishlariga ega bo'lgan suv muhiti tufayli intensiv sovutish jarayoniga o'tadi. Shunday qilib, metall NZlarning yadrolanishining intensiv jarayoni ularning hajmini sezilarli darajada kattaroq

miqdorda bir xil hosil bo'lishiga olib keladi, Fig.3(c). Aksincha, lazer zarbasi 0,3 ps bo'lgan taqdirda, yuqori yutilgan oqim tufayli metall atomlarining o'rtacha sirt bug'lanishi jarayoni, asosan, materialni chiqarish jarayonining spallatsiya mexanizmi tufayli nishonning mexanik shikastlanishi, keyin esa er osti qatlami bilan birga keladi. bo'shliqlar o'sishi, 1.2-rasm (a). Bu chiqarilgan klasterlarning katta qismining paydo bo'lishiga olib kelishi mumkin [Nanoscale 10, 6900-6910 (2018)].

Suv qatlamining lazer zarbasi tufayli NZ hosil bo'lishiga ta'siri bir necha bosqichlarga bo'linadi. Birinchidan, metall zichligi bilan taqqoslanadigan atom zichligiga ega bo'lgan suv muhiti ablyatsiyalangan materialning yuqoriga qarab harakatlanishiga sezilarli mexanik qarshilik ko'rsatadi va akustik bo'shashgan bo'lsa-da, eritilgan metallning sirt qatlami hali ham nol bo'lmagan bosimga ega. 125 ps vaqtida 4 GPa. Bunday qarshilik natijasida ablyatsiya plyusining o'lchami havodagi yoki vakuumdagiga qaraganda sezilarli darajada kichikroq bo'ladi. Ikkinchidan, suvning yuqori issiqlik sig'imi (metallning issiqlik sig'imi bilan solishtirish mumkin) va uning yuqori bug'lanish issiqlik yo'qotishlari bug'langan metall atomlarining intensiv sovishini osonlashtiradi, bu esa 100 ps ga yaqin NZlarning yadrolanishiga olib keladi, 3-(c) rasm). Ablyatsion plyus ichidagi intensiv bug'lanish jarayoni suyuqlikning ablatsiya qilingan materialning chuqur qismlariga kirib borishini oldini oladi va shuning uchun uning sovutish mexanizmi an'anaviy issiqlik o'tkazuvchanligi mexanizmi bilan boshqariladi. Buni simulyatsiya boshidan 250 ps va 500 ps uchun metall va suv zarralarining nisbiy zichligi ko'rsatilgan. Ablyatsion material suyuqlikni itarib yuboradi va keyinroq bug 'suvining arzimas miqdori yuqori qismiga kirib boradi. Xuddi shu narsa 0,3 ps impuls uchun ham olinadi va [J. Colloid. Inter. Sci. 489, 3-17 (2020), Phys. Chem. Chem. Phys. 22, 7077-7099 (2020)]. Ablatsiya plyusining yuqori qismidan pastga qarab harakatlanayotganda, yuqoridagi kichik zarralar suv muhiti tomonidan samarali ravishda sekinlashishi va sovutilishini aniqlash mumkin, bu ularning o'sishini cheklaydi va ularning hajmini o'rtada hosil bo'lgan zarrachalar hajmiga yaqinlashtiradi. shleyfning. Bu suvda NZ hosil bo'lish mexanizmini vakuumdagidan juda farq qiladi, bunda bug 'va suyuqlik tomchilarining o'chirilgan aralashmasi, bir marta chiqarilgandan so'ng, ko'tarilish tezligining sezilarli darajada tarqalishi tufayli intensiv yadrolanish va hosil bo'lish jarayonlariga yordam bermaydi. chiqarilgan klasterlar massasi. Natijada, birinchi bo'lib chiqadigan va hosil bo'lgan kichikroq tomchilar pastroq haroratda keyinroq chiqarilgan va kattaroq massaga ega bo'lganlarga qaraganda ancha yuqori yuqori tezlikka ega [Appl. Phys. A 114, 11 (2014), Appl. Surf. Sci. 470, 1018 (2018)]. Aksincha, suyuqliklarda NZ hosil bo'lish jarayonida yangi hosil bo'lgan NZlarning hajmi va tezligi bo'yicha dastlabki ajratilishi suv qatlamining termal va mexanik ta'siri tufayli qaytariladi va suyuq muhitda yadro

hosil qiluvchi NZlarning ko'tarilish tezligi. havodagi yoki vakuumdagidan sekinroq kattalikdagi birdan ortiq tartib [Nanomater. 10, 234 (2020)]. Shunday qilib, suyuqlikning NZ hosil bo'lish jarayoniga ta'siri vakuum sharoitlari bilan solishtirganda yakuniy fraktsiyaning o'lchamlarini yanada yumshoqroq taqsimlashga olib keladi. Suyuq muhitning bunday ta'siri so'nggi nazariy ishlarda ham ta'kidlangan [Nanomater. 9, 767 (2019)] va fs - ns impuls davomiyligi uchun amal qiladi.

Bundan tashqari, qisqa 0,3 ps va uzun 50 ps lazer impulslarining ikkala holatlari uchun NZ o'lchamlarini taqsimlash tahlili yuqoridagi muhokamalarimizni tasdiqlaydi va afzalroq torroq o'lchamdagi NZlarni yaratish bo'yicha ko'proq imkoniyatlarni ochib beradi. 4(a) va (b)-rasmda qisqa va uzoq impuls davomiyligi holatlari uchun hisoblash katakchasining atomistik ko'rinishi ko'rsatilgan. Ushbu rasmlardan ko'rinib turibdiki, nishondagi stressni ushlab turish sharoitlariga (mexanik shikastlanish rejimi) olib keladigan qisqa puls bug'langan metall atomlarining bir oz kirishi bilan NZ ning sezilarli darajada katta qismini shakllantirishga yordam beradi, 2-rasm. 4(a). Shu bilan bir qatorda, uzoq impuls issiqlik chegarasini yanada aniqroq (termik shikastlanish rejimi) keltirib chiqaradi va nishon mexanik ravishda bo'shashadi va asta-sekin kengayadi, haddan tashqari kritik isitish sharoitida ko'proq bug'langan atomlarni hosil qiladi. Suyuq muhit tufayli bu bug'ning sekinlashishi va sovishi jarayoni sezilarli darajada kichikroq yadro hosil bo'lishini osonlashtiradi.

Amalga oshirilgan simulyatsiyalar NZ shakllanishining keyingi evolyutsiyasi uchun mas'ul bo'lgan asosiy mexanizmlarni yaratish uchun etarlicha uzoq vaqt oralig'ini qamrab olishga imkon beradi. Buni NZ o'lchamlari taqsimotining ko'proq miqdoriy tahlilidan ko'rish mumkin, shakl. 4(c) va (d), shakldagi to'rtburchaklar sohalarida qisqa va uzun impulslar uchun. 4 (a) va (b), bu erda NZ hosil bo'lish jarayoni endi ablyatsiya mahsulotlari tomonidan intensiv ta'sir qilmaydi. Simulyatsiyalarimizda qo'llaniladigan katta hisoblash sohasi etarli statistik ma'lumotlarni to'plash va NZ tarqatish gistogrammalarini yaratish imkonini beradi. Ko'rish mumkinki, qisqaroq impuls ko'proq dispers taqsimotga olib keladi va har xil o'rtacha kattalikdagi ikki yoki undan ortiq fraktsiyalarning shakllanishini aniqlaydi. Ushbu kuzatish suyuqliklarda NZ ning qisqa lazerli impuls hosil qilish jarayonida bimodal o'lchamlarni taqsimlashning shakllanish mexanizmlari bo'yicha so'nggi nazariy topilmalarga mos keladi. Ya'ni, kichik fraktsiya bug'langan metall atomlarining yadrolanishi natijasida hosil bo'ladi, katta qismi esa ichki kuchlanishlarning mexanik bo'shashishidan kelib chiqadigan tez o'sishi tufayli metall-suv interfeysi bo'ylab Reyleigh-Teylor beqarorliklari mahsulotidir, 4-(c) rasm). Shu bilan bir qatorda, davomiylig etarlicha katta bo’lgan lazer impulslari yuqori bosim kuchlanishlarini yaratmaydi, lekin taglik sirtning haddan tashqari kritik isishi va katta miqdordagi bug' hosil bo'lishiga olib keladi, keyinchalik u kichikroq o'lchamdagi NZlar soniga o'tadi (4-(d) rasm). NZ yadrolarining to'liq hosil bo'lishi jarayoni ancha uzoqroq vaqt oralig'ini o'z ichiga olsa ham va NZ o'lchamlarini

taqsimlash keyinchalik kattaroq diametrga o'tkazilishi mumkin bo'lsa-da, 4-rasmdan xulosa qilish mumkinki, uzoqroq impulslar uchun, isitish tezligi tufayli

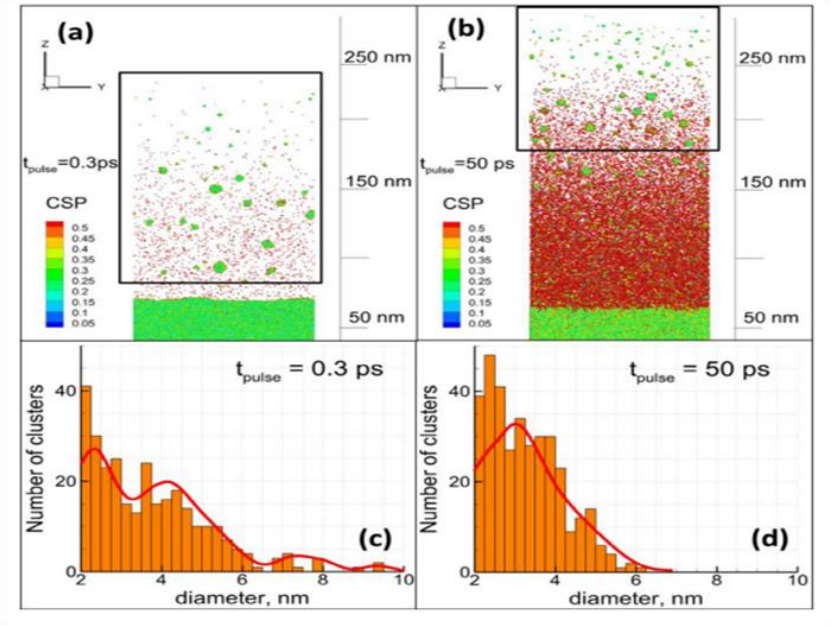

4-rasm. Qisqa 0,3 ps (a) va uzun 50 ps (b) impulslar uchun belgilangan NZ hosil bo'lish jarayonining atomistik suratlari ko'rsatilgan. Atomlar hosil bo'lgan NZlarni ko'rish uchun CSP tomonidan ranglangan, suv atomlari esa bo'sh. (a) va (b) dagi qora to'rtburchaklar tomonidan tanlangan maydonlar uchun NZ o'lchamlari taqsimoti mos ravishda qisqa 0,3 ps (c) va uzun 50 ps (d) impulslar uchun ko'rsatilgan. NZ taqsimoti gistogrammalariga o'rnatilgan qizil egri chiziqlar ko'z bilan ifodalanadi [Appl. Surf. Sci. 527, 146702 (2020)].

Taglikning mexanik bo'shashish tezligidan oshmagan holda, zarrachalar hosil bo'lishining asosiy harakatlantiruvchi mexanizmi portlovchi qaynashdir, bu esa kichikroq NZ hosil bo'lishiga olib keladi, shu bilan birga, butun sirt qatlamining chiqishi va Reyleigh-Teylorning keyingi beqarorligi va hosil bo'lishi bilan birga. kattaroq NZ fraktsiyasi bostiriladi. Bu natija, shuningdek, Shih va boshq. [Phys. Chem. Chem. Phys., 22, 7077 (2020)], shuningdek, lazer nurlanish parametrlari (impuls davomiyligi va hodisa oqimi) orqali hosil bo'lgan NZ o'lchamlarini taqsimlash bilan manipulyatsiya qilish va uning torroq taqsimlanishi va o'ziga xos o'rtacha ko'rsatkichlarga erishish mumkinligi haqida xulosa chiqarishga imkon beradi. Ikkinchisi, ehtimol kichikroq NZlarning bir xil o'lchamdagi taqsimoti tez-tez talab qilinadigan bo'lsa, biotibbiyot uchun NZlarni yaratishda juda muhimdir [Sci. Rep. 9, 12890 (2019)]. Ko'rinishidan, NZ hosil bo'lishining termal chegaralash rejimi yoki ularning uzoq (100 ps va ns) lazer zarbasi tufayli ishlab chiqarilishi sanoat ishlab chiqarishi nuqtai nazaridan afzalroqdir. Metall bug 'fazasidan yadrolanish jarayonida hosil bo'lgan NZlar sonini 3(c)-rasmda ko'rish mumkin. Ularning keyingi shakli bo'shashishi (suyuq fazada) dan sharsimon bo'lishiga olib keladi, bu ham [Nanoscale, 2018,10, 6900] da xabar qilingan kuzatishlarga mos keladi. Oxir-oqibat, bug 'fazasining yadrolanishi tufayli NZ hosil bo'lish jarayoni tugagach, suyuq muhitda o'rnatilgan gidrodinamik harakat tufayli ablyatsiya jarayonining mahsulotlari (NZ) yuqoriga suriladi va NZ ning qotib qolish jarayoni sodir bo'ladi. nanosekundlar oralig'i. Nihoyat, olingan kolloid suyuqlikda to'xtatilgan holda hosil bo'lgan zarralar ancha muvozanatli sharoitlarda suvda sekin tarqalish jarayoni tufayli o'sishda davom etishi

mumkin. Bu jarayon ancha kattaroq vaqtni oladi, bunda NZ hosil bo‘lish mexanizmi kristall strukturasi, sirt kimyosi va oksidlanishning aniq ta’siri bilan bog‘liq bo‘lishi mumkin. Masalan c) rasm. Al-asosli NZlar to'lqin uzunligi 1064 nm, impuls davomiyligi 10 ns va energiyasi 40 mJ (NL300, EXPLA) bo’lgan va chastotasi 10 Hz lazer impulsalri yordamida deionizatsiyalangan suvga botirilgan alyuminiy blokining ablyatsiyasi orqali sintez qilindi. Lazer nurlari fokus uzunligi 100 mm bo'lgan linzalar tomonidan yo'naltirilgan. Vakuumda katta miqdordagi Al ning ablatsiyasi xuddi shu lazer yordamida amalga oshirildi. 10 ns impulslar alyuminiy nishoni yuzasidagi vakuum kamerasiga qaratilgan. Yopilgan materialning qoldiqlari yaqin atrofdagi shisha va kremniy substratlarga to'plangan. Ablatsiya 30 daqiqa davom etdi. Shuningdek, biz alyuminiy nishonni suv va vakuumda yo'q qilish uchun femtosekund impulslaridan (300 fs, 1030 nm, 100 kHz, 0,5 mJ; AFS) foydalanilgan.

Vakuum va suvda 10 ns impulslar bilan ablyatsiya paytida cho'kilgan zarrachalarning morfologiyasi skanerlash elektron mikroskop (SEM) yordamida tahlil qilindi.

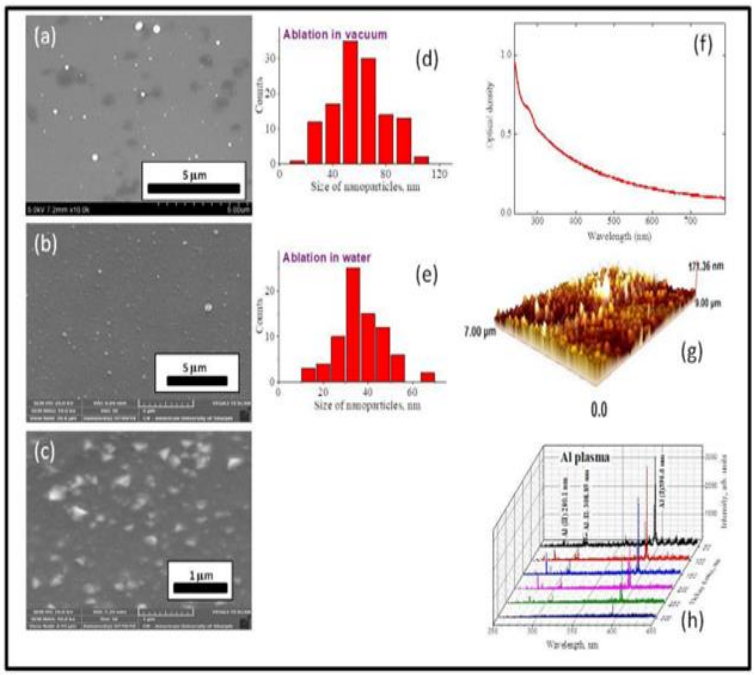

5-rasm. Al asosidagi NZ larning strukturaviy va spektral xossalari. (a-c) turli muhitda 10 ns impulslar yordamida nishonni ablatsiya qilish natijasida olingan Al asosidagi NZlarning SEM tasvirlari: (a) vakuum, (b) suv va (c) suv (30 kundan keyin). NZ o'lchamlari taqsimotining tegishli gistogrammalari mos ravishda vakuum va suvda ablyatsiya holatida (d) va (e) da ko'rsatilgan. (f) Al asosidagi NZ suspenziyasining yutilish spektri. (g) vakuumda ablyatsiya paytida yotqizilgan Al NZlar qatlamining atom kuchi mikroskopi tasviri. (h) Plazma emissiyasining o'zgarishi (250-450 nm). Al plazmasining UV spektrlari ablyatsiya boshlanishidan boshlab nanosoniyali impulslar bilan turli kechikishlarda to'plangan [Appl. Surf. Sci. 527, 146702 (2020)].

Vakuum va suvda nanosoniyali impulslar tomonidan ishlab chiqarilgan Al asosidagi NZlarning SEM tasvirlari 2-rasmda ko'rsatilgan. 5(a)-(c). NZ o'lchamlari mos ravishda 55 va 34 nm ekanligi aniqlandi, shakl 5(d) va 5(e). Suvning NZ hajmining taqsimlanishiga ta'sirini sifat jihatidan bog'lash uchun biz ushbu ikki holatni solishtirdik va suvda ablyatsiya holatida o'lcham taqsimoti torroq ekanligini aniqladik. Yuqoridagi nazariy tadqiqotlarga asoslanib, zich suyuqlik muhitining (suv) termal va mexanik ta'siri tufayli NZ o'lchamlari taqsimoti ham toraygan. NZ hosil bo'lish jarayoniga materialni chiqarib yuborishning spallatsiya mexanizmi (mexanik shikastlanish rejimi) yoki portlovchi qaynatish mexanizmi (termik shikastlanish rejimi)

yoki yutilgan lazer energiyasining (oqimning) etarlicha yuqori qiymati uchun ularning aralashmasi ta'sir qilishi mumkin.

Nochiziqli optik xossalar: NZlarning nochiziqli yutish va sindirish xususiyatlarini, shuningdek ularning turli xil optik xususiyatlarini o'rganish motivatsiyasi ularning optoelektronika, optik cheklovchilar va fotonikada potentsial qo'llanilishiga asoslanadi. Shu bilan birga, ushbu turlarning oldingi tadqiqotlarida Al-nishonning ablatsiyasi paytida zarba davomiyligining Al-ga asoslangan NZlarning nochiziqli yutilish va nochiziqli sinishi koeffitsientlaridagi rolini tahlil qilish haqida xabar berilmagan. Kuchli nochiziqli sinishi va yutish xususiyatlariga ega bo'lgan kichik o'lchamdagi materiallarni qidirish bizni nanosekund, pikosoniya va femtosekund impulslari tomonidan ishlab chiqarilgan NZni tahlil qilishga undadi. Biz Z-skanerlash sxemasidan foydalangan holda nanosekund, pikosoniya va femtosekundli impulslar bilan suvdagi quyma alyuminiyning ablyatsiyasi paytida tayyorlangan turli xil Al-asosli NZ suspenziyalarining nochiziqli optik xususiyatlarini tahlil qildik. Al asosidagi NZ suspenziyalarining normallashtirilgan o'tkazuvchanliklari ularning nochiziqli yutilish koeffitsientlarini (b) va nochiziqli sinishi ko'rsatkichlarini (g) aniqlash uchun standart o'rnatish protsedurasi yordamida tahlil qilindi. Alyuminiy asosidagi NZlar turli muddatlarga (5 ns, 200 ps va 30 fs) ega bo'lgan impulslar yordamida suvdagi Al massasini ablatsiya qilish orqali olingan.

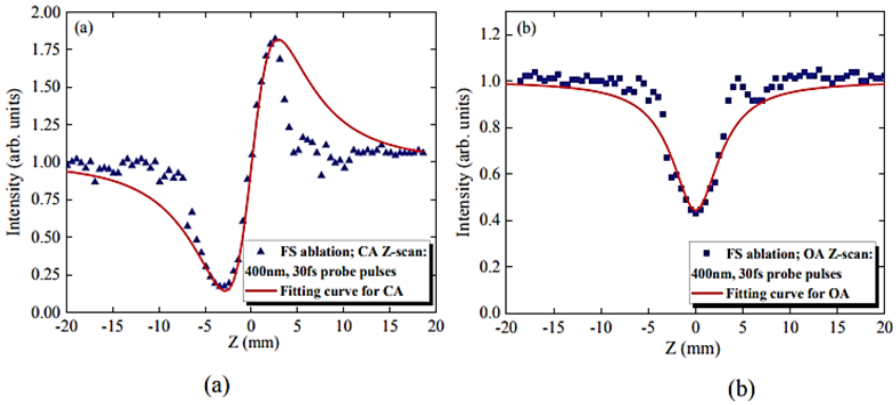

6-rasm. (a) CA va (b) 400 nm, 30 fs impulslar yordamida o'lchangan suspenziyalarning OA Z-skanerlari. Suspenziya 30 fs impulslar yordamida quyma alyuminiyni suvda ablatsiya qilish orqali tayyorlangan. Fitting egri chiziqlari (qattiq chiziqlar) tenglamalarga mos keladi. (7) va (8) [Appl. Surf. Sci. 527, 146702 (2020)].

Ochiq apertura (OA) sxemasi va ikki foton yutilish (2PA) holatida normallashtirilgan o'tkazuvchanlik T_{2PA} quyidagicha yozilishi mumkin:

$$T_{2PA}(z) = \frac{\ln(1+r)}{r} \approx 1 - \frac{r}{2\sqrt{2}} \qquad (7)$$

Bu yerda, $r=\beta I_0 L_{eff}/(1+(z/z_0)2)$, $x=z/z_0$, $z_0=k(w_0)^2/2$ - Reley uzunligi, k - to‘lqin soni $k=2\pi/\lambda$, w_0 nurning bel radiusi, I_0 tushayotgan nurning fokus masofadagi maksimum intensivligi, $L_{eff}=[1-exp(-\alpha_0 L)]/\alpha_0$] muhitning effektiv uzunligi, α_0 chiziqli yutilish koeffisienti, va L namunaning qalinligi. Yopiq apertura (YA) sxemasida, o‘tkazuvchanlik quyidagi ko‘rinishni oladi:

$$T_{NRA}(z) = 1 + \frac{2(-\delta x^2 + 2x - 3\delta)}{x^4 + 10x^2 + 9}\Delta\varphi_0 \quad (8)$$

Bu yerda $T_{NRA}(z)$ - nochiziqli sinishi va yutilish (NRA) sharoitida muhitning uzatilishi, $\delta=\beta/2k\gamma$ va $\Delta\varphi_0=k\gamma I_0 L_{eff}$ nochiziqli sinishi induktsiyasi bilan bog'liq bo'lgan faza o'zgarishini ifodalaydi. Al asosidagi NZ suspenziyasining 2PA va NRA ning nochiziqli optik koeffitsientlari 7- va 8-tenglamalar yordamida hisoblangan. 6-rasmda 400 nm, 30 fs impulslar yordamida namunalarning YA va OA Z-skanerlari ko'rsatilgan. Ushbu egri chiziqlarni o'rnatish 400 nm, 30 fs impulslar yordamida uchta suspenziyaning (fs, ps va ns impulslari bilan hosil qilingan) nochiziqli yutilish koeffitsientlarini va nochiziqli sinishi ko'rsatkichlarini aniqlash imkonini berdi. Nochiziqli optik parametrlarning eng yuqori qiymatlari pikosekundli impulslar yordamida alyuminiyni ablatsiya qilish orqali ishlab chiqarilgan suspenziyada kuzatildi, qolgan ikkita suspenziya uch (femtosekund ablyatsiyasi) va besh (nanosoniyali ablyatsiya) γ va β marta kichikroq ekanligini ko'rsatdi. Pikosekundli impulslar tomonidan ishlab chiqarilgan NZ suspenziyasining γ va β qiymati mos ravishda ~ 10^{-13} sm^2 W^{-1} va 10^{-11} sm W^{-1} bo'lib o'lchandi. Ushbu suspenziyalardagi NZlarning hajm qismi ~ 10^{-4} bo'lganligi sababli, Al asosidagi NZlarning γ va β qiymatlari mos ravishda ~ 10^{-9} sm^2 W^{-1} va 10^{-7} sm W^{-1} deb baholandi, ular orasida ushbu spektr mintaqasida qayd etilgan eng yuqori qiymatlar.

Yuqori Garmonika Generatsiyasi (YuTG): Al nishoni yuzasida ishlab chiqarilgan lazer plazmasida yuqori tartibli garmonika hosil bo'lishini namoyish qilish bizning tadqiqotimiz maqsadlaridan biri edi. Muayyan sharoitlarda vakuumdagi metallarning ablyatsiyasi NZ larni o'z ichiga olgan lazer yordamida hosil qilingan plazma (LHQP) hosil bo'lishiga olib kelishi mumkin [Phys. Rev. B 71, 174405 (2005)]. Isitish nurlanishining impuls davomiyligi, lazer impulslarining ravonligi va "optimal plazma" shakllanishi kabi turli xil talablar NZ hosil bo'lganda saqlanishi kerak, bu esa ultra qisqa impulslar bilan o'zaro ta'sir qilishi mumkin, ular bilan solishtirganda kuchli yuqori tartibli garmonikalar hosil bo'ladi. lazer-atomlarning o'zaro ta'siri. "Optimal plazma" atamasi ultraqisqa impulslarning samarali YuTG shartlarini anglatadi, bu esa harakatlantiruvchi va garmonik to'lqinlar o'rtasidagi faza nomuvofiqligiga olib keladigan to'sqinlik qiluvchi jarayonlarni bostirish uchun plazmadagi oz miqdordagi erkin elektronlarni saqlashni talab qiladi, bu esa garmonik konversiya samaradorligini pasayishiga olib keladi. Op. Commun. 135, 251 (1997), Phys. Rev. A 83, 023832 (2012)].

Ushbu tadqiqotlar davomida muhim parametr isitish (nanosekund, pikosekund yoki femtosekund) impulslar orqali ablyatsiyaning boshlanishi va oldindan hosil bo'lgan plazma orqali haydash (femtosekund) impulslarining tarqalishi o'rtasidagi kechikish edi. Optimal kechikish faol turlarning maksimal kontsentratsiyasi (bizning holatlarimizda NZ) tarqaladigan lazer zarbasi bilan uchrashadigan sharoitlarni

belgilaydi. Garmonik rentabellikni bevosita tajriba kuzatishdan tashqari optimal kechikishni aniqlash usuli vaqtga bog'liq bo'lgan emissiya spektrini tahlil qilish edi, 56-rasm (h), bu bizni YuTG tajribalaridan oldin ushbu tadqiqotlarni amalga oshirishga undadi. Ushbu tadqiqotlar shuni ko'rsatdiki, ablyatsiya boshlanishidan boshlab 100-150 ns oralig'ida kechikish bilan plazma harakatlantiruvchi femtosekund nurlarining tarqalish maydoniga etib boradi va shu bilan eng yuqori garmonik hosil uchun sharoit yaratadi. Ilgari shunga o'xshash yondashuv oltin plazma holatida ko'rsatilgan edi [J. Appl. Phys. 102, 073105 (2007)]. Plazma emissiyasi bo'yicha vaqtni o'rganishning qo'shimcha motivatsiyasi nishonning ablyatsiya shartlarini aniqlash bilan bog'liq edi, bunda faqat neytral (Al I) va yakka ionlangan (Al II) zarralar yaqin UB diapazonida chiqariladi, Fig.5(h).

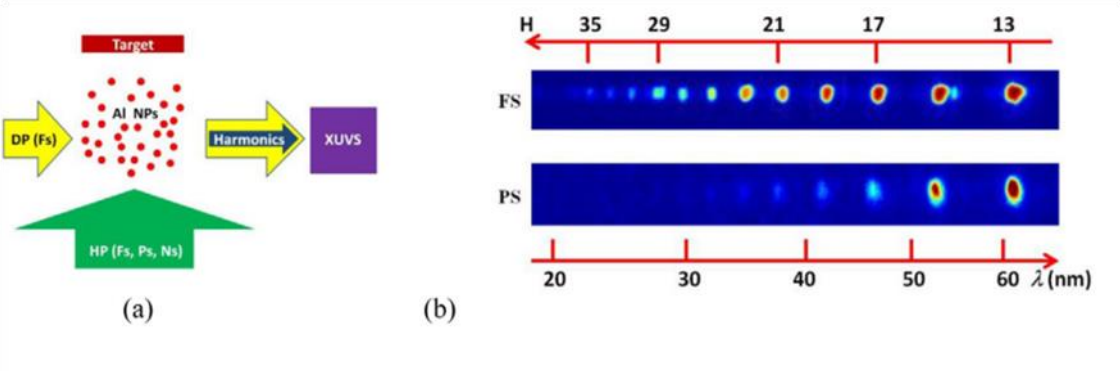

7-rasm (a) Al LHQPda YuTG uchun sxema. DP (Fs): haydash femtosekund puls, HP (Fs, Ps): isitish (yoki nanosekund, yoki pikosoniya yoki femtosekund) puls, Nishon: alyuminiy ommaviy nishon; Al NZ: alyuminiy nanozarrachalarini o'z ichiga olgan plazma, Garmonika: harakatlantiruvchi imulsdan yuqori tartibli garmonika, EUB: ekstremal ultrabinafsha spektrometri. (b) Femtosekund (yuqori panel) va pikosekund (pastki panel) LHQP dan garmonik spektrlar [Appl. Surf. Sci. 527, 146702 (2020)].

YuTG tajribalarida biz femtosekundli lazerdan (800 nm, 40 fs) foydalandik. Lazer nurlanishi nishon yuzasidan ~200 mkm masofada Al NZlarni o'z ichiga olgan LHQP orqali tarqaladi, 7(a)-rasm. LHQP 5 mm uzunlikdagi plazma shu'lasini hosil qilish uchun 300 mm fokusli silindrsimon linzalar yordamida alyuminiy nishon yuzasiga xuddi shu lazerning siqilmagan nurlanishining 200 ps, 800 nm impulslarini yo'naltirish orqali hosil qilingan. Garmonik emissiya vertikal yoriqdan, oltin bilan qoplangan silindrsimon oynadan, 1200 chiziq/mm diffraksion panjarasidan, mikrokanal plastinkasidan va CCD kameradan tashkil topgan EUB spektrometri yordamida tahlil qilindi. 7(b)-rasmda ko'rsatilgan garmonika spektri femtosekund bilan induktsiyalangan LHQP (H35) holatida kesish pikosekunddan kelib chiqqan LHQP (H25) holatidan kattaroq ekanligini ko'rsatadi. Oldingi holatda yuqori tartibli garmonikalarning rentabelligi pikosekundli impulslar bilan hosil qilingan LHQPdagi YuTG holatiga qaraganda ham kattaroq edi.

Biz YuTGning Levenshteyn modelidan foydalandik [Phys. Rev. A 49, 2117 (1994)] neytral atomlar va ionlarning garmonik hosildorlikka ta'sirini tahlil qilish. Al NZ plazmasining garmoniklari odatda neytral zarrachalardan kelib chiqishi mumkin. E'tibor bering, 3 × 1010 Vt sm-2 dan yuqori bo'lgan pikosekundlik isitish impulsi intensivligining oshishi katta miqdordagi erkin elektronlarning paydo bo'lishi tufayli garmonik rentabellikning sezilarli darajada pasayishiga olib keldi. Biz, shuningdek, alyuminiy plazmasining ikki rangli nasosi (TCP, 800 nm+400 nm) yordamida NZ LPPda YuTGni amalga oshirdik. Tajribalarimiz davomida ikkinchi garmonika impulslarning almashtirish samaradorligi (λ=400 nm) nisbatan past edi (mos ravishda 0,2 va 0,4 mm qalinlikdagi BBO kristallari uchun ~ 2% va ~ 4%). Sobiq BBO kristalida kichik guruh tezligi dispersiyasi tufayli plazma sohasidagi ikkita harakatlantiruvchi impulsning vaqtinchalik bir-biriga mos kelishi EUB ning uzunroq to'lqin uzunligi diapazonida YuTG uchun yetarli edi. Shu bilan birga, biz hatto garmonikalarning butun guruhi yo'qligini kuzatdik, ayniqsa H=4(n+1) ga mos keladi. Xususan, H12, H16 va H20 ning diskriminatsiyasi 0,4 mm qalinlikdagi BBO dan foydalanilgan TCP holatida o'ziga xos xususiyat edi, 0,2 mm qalinlikdagi BBO qo'llanganda esa, bu garmonikalarning barchasi boshqa garmonikalarga deyarli o'xshash edi, garmonikalar, shuningdek, g'alati garmonikalar bilan solishtirish mumkin.

Ushbu tadqiqot orqali biz vakuumda Al NZ ning in-situ hosil bo'lishi va sintez qilingan nanozarrachalar buluti orqali harakatlantiruvchi impulslarning tarqalishi alyuminiy atomlari va ionlarini qo'llash bilan solishtirganda yaxshilangan garmonik rentabellikka olib kelishini ko'rsatdik. Al NZlar alyuminiy nishoniga yaqin joyda tarqaladigan 40 fs impulslar yordamida 37-tartibga qadar yuqori tartibli garmonikalarni hosil qilishga imkon berdi.

Namlanish: Materiallar sirtlarining namlash xususiyatlari turli amaliy va fundamental ilovalarda muhim rol o'ynaydi va ularning namlanish burchagi (NB) bilan tavsiflanadi, bu suyuqlik yuzasi va kontakt yuzasi konturlari orasidagi burchakdir. Qisqacha aytganda, ideal tekis sirtning namlanish burchagi qattiq, suyuqlik va bug 'interfeyslarining sirt erkin energiyasiga qarab, Young tenglamasi bilan tavsiflanadi:

$$cos\,(\theta) = \frac{\gamma_{SV} - \gamma_{SL}}{\gamma_{LV}} \qquad (9)$$

bu yerda θ - qattiq (S), suyuqlik (L) va bug'(V) bilan interfeysdagi suv bilan namlanish burchagi, γ_{SV}, γ_{SL} va γ_{LV} esa mos ravishda fazalararo sirt tarangliklari.
Tenglamadan xulosa chiqarish mumkin. (9) kontakt burchagi qattiq, suyuqlik va bug' interfeysidagi erkin energiyaning termodinamik muvozanatining natijasidir. Biroq, bu tenglama g ‘adur-budurlik yoki kimyoviy xilma-xillikni ko'rsatadigan haqiqiy yuzalar uchun foydali emas. Umuman olganda, sirt namligini baholashda sirtlarning g’adur-budurlik koeffitsientini hisobga olish kerak. Notekis Notekis yuzalar uchun Young tenglamasi quyidagicha o'qiladi [Ind. Eng. Chem. 28, 988–994 (1936)],

$$cos\theta_w = \frac{r(\gamma_{SV}-\gamma_{SL})}{\gamma_{LV}} = rcos\theta \quad (10)$$

bu yerda r - namlanish reaktsiyasini sezilarli darajada yaxshilaydigan sirt g'adur-budurlik omili. Shu munosabatga ko'ra, gidrofobik materialning g'adur-budurligining oshishi uning gidrofobikligining o'sishiga olib keladi va aksincha. 9 va 10 tenglamalar odatda sirt g'adur-budurlik qattiq sirtdagi suyuqlik tomchisining yopishish burchagi bilan bog'lash uchun ishlatiladi. Suv bilan namlanish burchaklari (SNB) <90^o gidrofilik, SNB>90^o bo'lgan sirtlar esa gidrofobik hisoblanadi. Kontakt burchagi 150^o dan kattaroq bo'lganda sirtlar supergidrofobik deb ataladi. Turli holatlarga ega bo'lgan supergidrofobik sirtlarning rivojlanishi amaliy qo'llanmalarga keng ta'sir qiladi va fundamental tadqiqotlar uchun ham katta ahamiyatga ega bo'ladi [Adv. Mater. 19, 3423-3424 (2007)]. [Langmuir 26, 18621-18623 (2010)] ga ko'ra, supergidrofillik sirt g'adur-budurlik koeffitsienti (10) tenglamada aniqlanganidek) kattaroq bo'lgan teksturali va / yoki tuzilgan (r>1) birdan ortiq materiallarga (notekis va/yoki g'ovakli) tegishli bo'lishi mumkin. Notekis sirt uchun namlanish burchagi tenglama bilan berilgan:

$$cos\,\theta_c = f \times cos\theta_\gamma + f - 1 \quad (11)$$

bu yerda f - suv tomchisining qattiq suyuqlik bilan namlanish maydonining nisbati. Bu tenglamadan f ning qiymatini kamaytirish orqali SNB sirtlarning g'adur-budurlik tufayli ortadi, deb xulosa qilish mumkin (8-rasm). Metall qotishmasining o'zgartirilgan yuzasida to'yinganlik jarayoni metall sirtining oksidlanishining shakllanishi tufayli ablyatsiyadan keyin namlanish burchagini o'zgartirish uchun muhim rol o'ynashi mumkin.

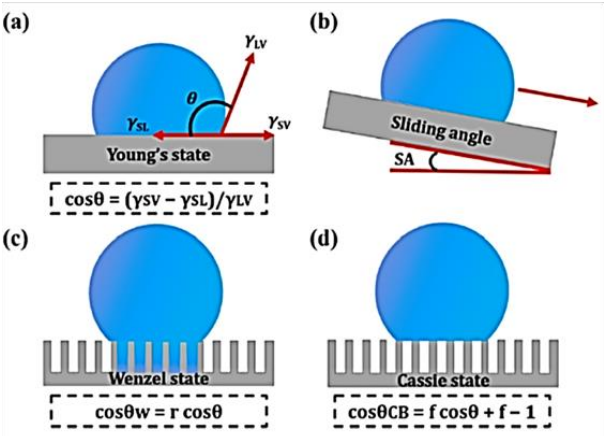

8-rasm. Kontakt burchagi tahlili uchun suvning turli namlanish holatlari sxemasi. a) tekis yuzadagi suv tomchisining yosh holati; (b) toymasin burchak (SA) yoki aylanma burchakni aniqlash; (c) Venzel holati, bu erda suv tomchilari sirt tuzilmalariga kirib boradi; (d) Kessi-Baxter holati, bu erda suv mikro tuzilmalar tepasida joylashgan va havo uning ostida qolib, kirishni cheklaydi. Bu erda "r" va "f" sirt pürüzlülüğünü va mos ravishda Venzel va Kessi-Bakster shtatlari uchun aloqada bo'lgan samarali maydon fraktsiyasini ifodalaydi [Ind. Eng. Chem.28, 988–994 (1936), Trans. Faraday Soc. 40, 546 – 551 (1944)].

Bizning ishimizda [Appl. Surf. Sci. 527, 146702 (2020)] biz shisha yuzalarga yotqizilgan NZ qatlamlarini o'z-o'zidan yig'ish orqali tayyorlangan Al asosidagi NZ plyonkalarining namlash xususiyatlarini o'rgandik. Filmni tayyorlash uchun suvda nanosoniya va femtosekund impulslari natijasida hosil bo'lgan Al bazli NZ suspenziyalari quyma materialning ablatsiyasidan foydalanilgan. NZ suspenziyasining

qatlam qatlami tomchilab quyish usuli bilan tozalangan shisha slaydga yotqizildi. Yangi qatlamni tayyorlashdan oldin, avvalgi qatlam havoda to'liq quritilgan. Qatlamlarning o'zgaruvchan soni shisha slaydlari rangining o'zgarishini ko'rsatdi va shuningdek, shisha substratning namlash xususiyatlarining o'zgarishini tasvirladi. Biz, shuningdek, vakuumda alyuminiyni ablatsiya qilish paytida to'plangan Al asosidagi NZ qatlamlarining namlanishini tahlil qildik. Tomchi shakli analizatori (DSA 100-E, Kruss) qoplangan va qoplanmagan shisha yuzalarning namlanish burchagi o'lchovlari

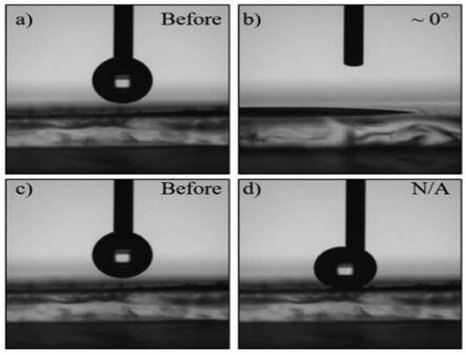

9-rasm. (a, b) Al asosidagi NZ suspenziyasining namlanish burchagi o'lchovi, suvda ablyatsiya paytida hosil bo'lgan va 0° ga yaqin namlanish burchagi bilan supergidrofil xususiyatlarni ko'rsatadigan shisha slaydlarga yotqizilgan. (c, d) Vakuumda lazerli ablyatsiya yordamida shisha slaydga yotqizilgan Al NZlar juda supergidrofobik sirtni ko'rsatadi. Ushbu o'lchovlar davomida biz suv tomchisini sirtga joylashtira olmadik [Appl. Surf. Sci. 527, 146702 (2020)].

uchun ishlatilgan. NZlarning vakuumda cho'kishi paytida juda notekis nanostrukturali plyonka hosil bo'lishi Al NZlar qoplamalarining supergidrofobik xususiyatlariga sabab bo'ldi va shuning uchun bu nanostrukturalar suv bilan namlanganda past yopishqoqlikni keltirib chiqardi. NZ bilan qoplangan sirt topografiyasini tahlil qilish uchun atom kuchi mikroskopi (hpAFM, Nanomagnitika) ishlatilgan. Vakuumda yotqizilgan bu qoplamalarning qalinligi ~150-200 nm edi. Ushbu tadqiqotlar vakuumda to'plangan Al NZ lar qoplama qalinligidan qat'i nazar, supergidrofobik xususiyatlarga ega ekanligini ko'rsatdi. Biz deyarli shaffof bo'lgan yotqizilgan yuzalardagi namlanish burchagini o'lchadik va ularning supergidrofobik reaktsiyasini ko'rsatdik. Qoplama bir xil emas edi. Biroq, yotqizilgan oynaning turli joylarida namlanish burchagi bir xil bo'lib qoldi. Quyida keltirilgan namlanish burchagi o'lchovlari (9-rasm) shishaning turli qoplamali hududlarida namlanish burchagi o'lchovlarining o'rtacha qiymatlari hisoblanadi. Yana bir muhim jihat - sintezlangan NZ muhitining roli. Suv muhitida $Al(OH)_3$, $AlO(OH)$ va Al_2O_3 hosil bo'ladi. Ma'lumki, oksidlanish Al ni suvda yoki havoda lazer bilan olib tashlashda sodir bo'ladi va nanozarrachalarning oksidlanishini minimallashtirish uchun maxsus harakatlar qilish kerak. Oksidlanish ns vaqt shkalasi bo'yicha nanopartikullarning shakllanishiga, ularning tuzilishiga (masalan, kattaroq yadro-qobiq zarralari yoki to'liq oksidlangan kichikroq klasterlar) va o'lcham taqsimotiga katta ta'sir ko'rsatadi. Bundan tashqari, bu jarayon sintez qilingan NZlarning namlanish xususiyatlariga ham ta'sir qiladi. Shunday qilib, Al bazli NZ bilan qoplangan sirtlarning namlanishining farqining ikkinchi mumkin bo'lgan izohi cho'kma yuzasida gidroksidlarning mavjudligi yoki yo'qligi bilan bog'liq bo'lishi mumkin. Yuqorida aytib o'tilganidek, suyuqlikdagi lazerli ablyatsiya paytida yangi hosil bo'lgan sirt suv bilan reaksiyaga kirishadi va tabiatda

gidrofil bo'lgan alyuminiy gidroksidi ($Al(OH)_3$) hosil qiladi. Shu bilan birga, vakuum sharoitida Al sirtining ablatsiyasi birinchi navbatda Al NZlarning cho'kishiga olib keladi, chunki kislorod va suv komponentlari ablatsiya yuzasi bilan o'zaro ta'sir qilmaydi. Ikkinchisida substratlarning namlanishining o'zgarishidagi asosiy rol sirt erkin energiyasining o'zgarishi bilan bog'liq. E'tibor bering, qattiq substratlarning namlanishi ularning sirt erkin energiyasi va sirt geometrik tuzilishi bilan boshqariladi.

Boshqa bir maqolada [Appl. Surf. Sci. 542, 148560 (2021)] biz ultra tez tolali lazerlar (femtosekund va pikosekundlik impuls davomiyligi) tomonidan olib tashlangan uch xil metalning (alyuminiy, mis va galvanizli po'lat) namlash xususiyatlarining o'zgarishini o'rganib chiqdik. Lazer-sirt strukturasida ishlatiladigan puls davomiyligi va skanerlash tezligining roli tahlil qilindi. Skanerli elektron mikroskopiya, atom kuch mikroskopiyasi va zaiflashtirilgan to'liq aks ettirish Furye transform infraqizil spektroskopiyasi (ATR-FTIR) lazer bilan tuzilgan sirtlarning pürüzlülüğü va kimyosini tavsiflash uchun ishlatilgan. Lazerli tuzilishga ega uchta metallning gidrofobiklik darajasi va o'z-o'zini tozalash xususiyatlari turli xil ablyatsiyadan keyingi muhitlarda qariganda solishtirildi. Alyuminiy, mis va galvanizli po'latdan yangi lazer bilan ishlangan namunalar lazer ablyatsiyasindan so'ng ularning kontakt burchaklari o'lchanganda, supergidrofil namlanish reaktsiyasini ko'rsatdi. Ushbu yangi lazer tuzilmali sirtlarning supergidrofil xususiyatlari atrof-muhit atmosferasida 30 kunlik qarishdan so'ng gidrofobik holatga o'tishi aniqlandi, past bosimli muhitda qariganda supergidrofobik holatga o'tish uchun atigi 6 soat vaqt kerak bo'ldi. Ultrafast lazerli sirt nano-strukturalash vakuumli qarish bilan birgalikda turli metallarda ekstremal supergidrofobik holatlarga erishishda samarali va tezkor yondashuv bo'lib chiqdi, bu esa uni o'z-o'zini tozalashning keng doirasi uchun mos qiladi.

Sirt tuzilishi lazer tizimi (AFS-UFFL-300-2000-1030-300; Active Fiber Systems GmbH) yordamida $\lambda = 1030$ nm va takrorlash chastotasi 50 kHz da amalga oshirildi. F=160 mm bo'lgan F-Theta linzalari bilan jihozlangan galvanometrik skaner (FARO tech. Xtreme-20) orqali namunalar ustida lazer nurlari skanerdan o'tkazildi. 40 femtosekund (fs) va 1,0 pikosoniya (ps) lazer impulslari lazer nurini fokuslash orqali alyuminiy, mis va galvanizli po'latning sirtini turli skanerlash tezligida (200 mm/s bosqichlarida 50-1250 mm/s) tuzilishi uchun ishlatilgan. nishon yuzasida. Lazer nurlari namunani gorizontal yo'nalishda (0^o) va keyin vertikal yo'nalish bo'ylab (90^o) nurlantirish orqali to'rtburchaklar shaklida namuna ustida skanerdan o'tkazildi, bu panjara naqshlarini yaratish uchun amalga oshirildi. Ikki qo'shni chiziq orasidagi masofa 100 mkm edi. Sirtdagi fokuslangan nuqtaning diametri ~100 mkm edi. Alyuminiy, mis va galvanizli po'latning ablyatsiya chegaralaridan yuqori bo'lgan

ablyatsiya uchun 5 J/sm^2 lik qattiq lazer oqimi ishlatilgan. Lazerli ablyatsiyadan oldin alyuminiy va mis plitalarning sirtlari qum qog'oz sonini (300#, 800#, 1000# va 1200#) ketma-ket oshirish orqali tekislandi va keyin 1 mikron olmos pastasini qo'llash orqali sayqallandi. Mahalliy yetkazib beruvchidan olingan galvanizli po'latdan foydalanilgan.

Lazer ablyatsiyasi sirt pürüzlülüğünü oshiradi va skanerlash tezligi va puls davomiyligiga qarab turli sirt tuzilmalarini yaratadi.

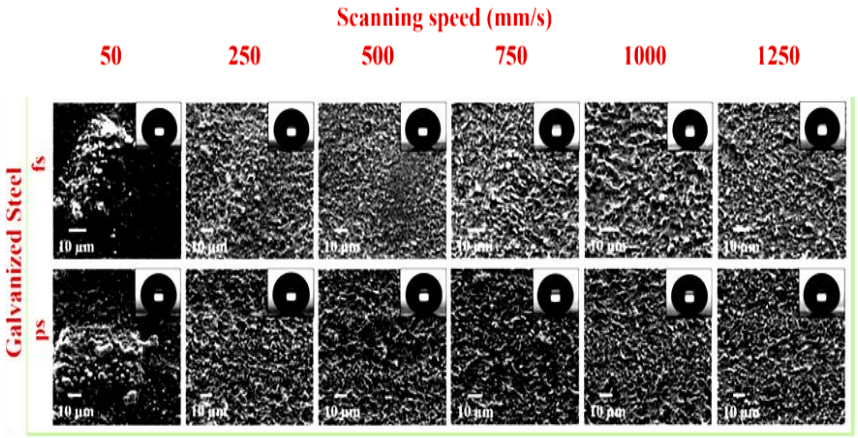

10-rasm. Turli skanerlash tezligida fs va ps lazer bilan nurlantirilgandan so'ng vakuumda saqlanadigan galvanizli po'latning ablyatsiyalangan yuzalarining SEMlari. Qo'shimchalar turli skanerlash tezligida tuzilgan namunalardagi suv tomchilari shakllarini ko'rsatadi [Appl. Surf. Sci.542, 148560 (2021)].

10-rasmda 50 dan 1250 mm/s gacha bo'lgan turli skanerlash tezligida o'rganilayotgan metallar yuzalarida 40 fs va 1,0 ps lazer impulslari bilan hosil qilingan tuzilmalarning taqqoslanishi ko'rsatilgan. Alyuminiy bo'lsa, fs va ps lazerlari yordamida sirt pürüzlülüğünü sezilarli darajada oshiradigan juda tasodifiy sirt tuzilmalari yaratilgan. Mis va galvanizli po'lat uchun lazer nurlari yo'li bo'ylab LIPSSlar va ierarxik mikro va nano o'lchovli tuzilmalar kuzatildi. LIPSS 250 va 500 mm/s skanerlash tezligida ustunlik qildi, yuqoriroq skanerlash tezligida esa sezilarli darajada kamroq LIPSS va yuqori marjon rifiga o'xshash tuzilmalar bilan bir xil keng miqyosli pürüzlülük hosil bo'ldi (qarang. SEM tasvirlari 750 mm/s va skanerlash tezligida. yuqori). Fs lazer impulslari holatida ko'tarilgan mikro/nanostrukturalarning shakllanishi, ps impulslari bilan solishtirganda, metall yuzasi bilan qisqaroq o'zaro ta'sir qilish vaqti bilan bog'liq. Notekis tuzilmalar barcha metallarning ps va fs lazerli strukturasida hosil bo'lgan. Sirtning pürüzlülüğü materialning o'ziga xos namlanish xususiyatini yaxshiladi. Kuzatilgan o'tkir sirt tuzilmalari suv o'tkazmaydigan xususiyatini yaxshilaydigan sirt bilan pastroq yopishishni osonlashtirishi mumkin. Vakuumda qarishdan so'ng lazer bilan tuzilgan sirtlarning supergidrofilikdan supergidrofobik holatga o'zgarishini ko'rsatish uchun biz qarishdan oldin va keyin namlanish burchagini o'lchadik. 11(a,b)-rasmda vakuumda ~6 soat davomida qarigandan so'ng (a) fs va (b) ps lazerlari bilan o'chirilgan alyuminiy, mis va galvanizli po'lat namunalarining suv bilan namlanish burchaklarini ko'rsatadi. Ushbu grafiklarda ko'rsatilgandek, ps yoki fs lazerlari bilan tuzilgan plitalar skanerlash tezligining chet el diapazonida namlanish burchagining yuqori qiymati bilan namoyon bo'ladigan supergidrofobik xususiyatlarni ko'rsatdi. Shu bilan birga, 11-rasm (c, d) ablyatsiyadan so'ng darhol (c) fs va (d) ps lazer impulslari bilan o'lchangan alyuminiy, mis va

galvanizli po'lat namunalarining namlanish burchaklarini ko'rsatadi. Turli skanerlash tezligida tuzilgan barcha metallar sirtlari odatda lazer ablyatsiyasidan so'ng fs va ps

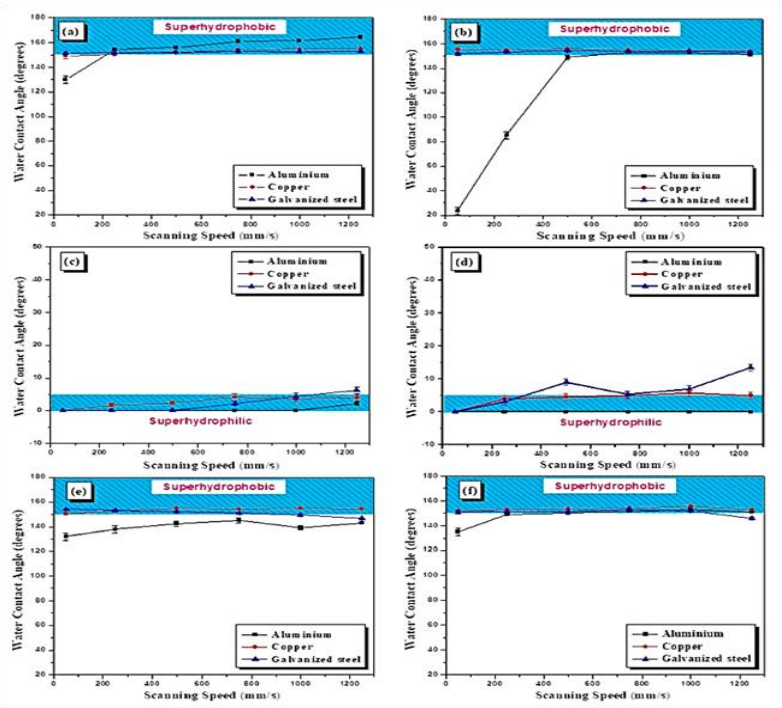

11-rasm. Aluminiy, mis va galvanizli po'lat namunalarining suv bilan namlanish burchaklari fs lazerli ablyatsiya (a) vakuumda 6 soat saqlashdan keyin va (c) havoda tuzilgandan so'ng darhol o'lchanadi. Xuddi shunday, ps lazerli ablyatsiya bilan ablatsiya qilingan namunalar (b) vakuumda va (d) havoda saqlanadi. (e) fs va (f) ps lazerli ablyatsiya bilan ishlov berilgan va 30 kun davomida havoda qarigan namunalar supergidrofobik javobni ko'rsatdi. Namlanish burchagi lazer bilan tuzilgan sirtdagi turli nuqtalarda bajarilgan o'lchovlarning o'rtacha qiymati [Appl. Surf. Sci.542, 148560 (2021)].

uchun supergidrofil javobni ko'rsatdi, o'lchangan namlanish burchagi alyuminiy va mis uchun 5o dan past va galvanizli po'lat uchun 15◦ dan kam. Shuni ta'kidlash kerakki, alyuminiy, mis va galvanizli po'latning tuzilmagan sayqallangan sirtlari mos ravishda 85,2◦, 78.8◦ va 86.0◦ suv bilan namlanish qilish burchaklarini ko'rsatdi.

Bizning ishimizda taqdim etilgan uchta metallar orasida, bizning ma'lumotlarga ko'ra, galvanizli po'lat vakuum yoki havo qarishi bilan ultra tez lazer tuzilishi yordamida namlanishni qo'llash uchun ilgari o'rganilmagan. Galvanizli po'lat boshqa po'lat variantlarga nisbatan nisbatan arzonligi va yuqori korroziyaga chidamliligi tufayli tom yopish, relslar, ustunlar va boshqalarda eng ko'p ishlatiladigan qurilish materiallaridan biridir. Shunday qilib, galvanizli po'latga berilgan suv o'tkazmaydigan xususiyat o'z-o'zini tozalashda keng ko'lamli dasturlarni taqdim etishi mumkin.

11 (a, b)-rasmda ko'rsatilganidek, galvanizli po'lat fs va ps lazerli ablyatsiyadan keyin vakuumda qarishdan keyin ham yuqori namlanish burchagini ko'rsatdi. Vakuumda saqlashdan so'ng kontakt burchagi mos ravishda 500 mm/s va 750 mm/s skanerlash tezligida fs va ps lazer ablyatsiyasi uchun 153º va 154º eng yuqori qiymatga yetdi. Biroq, havoda qarigan namuna uchun 151º namlanish burchagi olingan. Ushbu tadqiqot shuni ko'rsatdiki, vakuumli tizimli sirt galvanizli po'latdan, ayniqsa lazer bilan ishlov berishning yuqori skanerlash tezligida havo bilan ishlaydiganlarga qaraganda yaxshiroq ishlashga ega. Vakuumda saqlanadigan lazerli tuzilmali sirtlarning suvni qaytaruvchi xususiyatlaridan tashqari, biz ushbu sirtlarning sirpanish burchagini o'lchash orqali ularning o'z-o'zini tozalash harakatlarini ham tekshirdik.

12-rasmda fs va ps impulslari bilan tuzilgan alyuminiy, mis va galvanizli po'lat plitalar uchun vakuumda 6 soat davomida qaritilgandan keyin sirpanish burchagi ko'rsatilgan. Alyuminiy holatida, skanerlash tezligining oshishi bilan fs va ps lazerli tuzilmali sirtlarning sirpanish burchagi kamaydi.

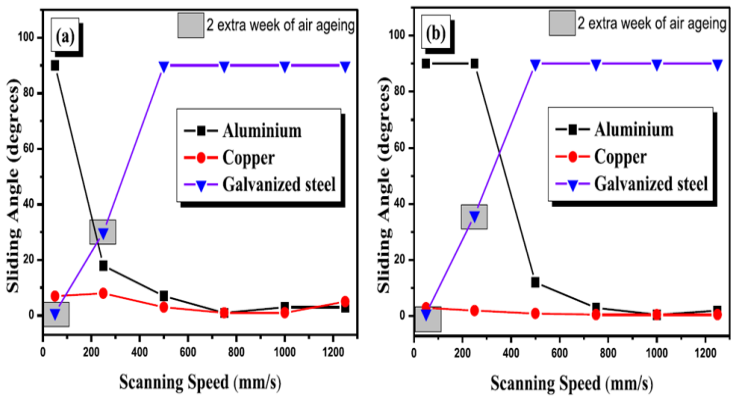

12-rasm. (a) fs va (b) ps impulslari bilan ishlov berilgan alyuminiy, mis va ruxlangan po'latning sirpanish burchagi o'lchovlari, so'ngra vakuumda saqlash. 90° burilish burchagi alyuminiy va galvanizli po'lat uchun ma'lum tezliklarda toymasin burchakni aniqlash mumkin emasligini ko'rsatdi. Shunga mos ravishda, 90° eng yuqori qiymat sifatida ishlatiladi, bu suv tomchisining sirtga yuqori yopishishini ko'rsatadi [Appl. Surf. Sci.542, 148560 (2021)].

Pastroq skanerlash tezligida suv tomchisi sirtga yopishgan holda qoldi va aylanmadi. Boshqa tomondan, mis har xil skanerlash tezligida 3° dan ~0,5° gacha bo'lgan kichik o'zgarishlar bilan barcha skanerlash tezligi uchun o'z-o'zini tozalaydigan suv o'tkazmaydigan harakatini ko'rsatdi. Vakuumda 6 soat davomida qarigandan so'ng, mis va alyuminiy namunalari Kassi-Baksterning yuqori skanerlash tezligida namlanish holatini ko'rsatdi, chunki ular yuqori namlanish burchagi va past aylanish burchagini ko'rsatdi. Shu bilan birga, lazerli tuzilmali galvanizli po'lat, hatto vakuumda 6 soat qariganidan keyin ham, 90° yuqori burilish burchagini ko'rsatdi va barcha skanerlash uchun lazer bilan tuzilgan joylar bilan suv tomchisining kuchli yopishishi tufayli tomchi tushmadi. tezliklar.

Biroq, strukturali galvanizli po'lat namunasini havoda qo'shimcha ikki hafta davomida saqlagandan so'ng, sirpanish burchagi o'lchanganida, biz uning namlanish burchagi 150° ga oshganini va aylanma burchagi sezilarli darajada kamayganini aniqladik, ayniqsa 50 past skanerlash tezligida. va fs va ps impulslarini davolash uchun 250 mm/s. Ushbu skanerlash tezligi uchun fs impulslari yordamida mos ravishda ~0,5° va ~30° qiymatlarining aylanish burchagiga erishildi. Ps impulslari uchun esa 50 va 250 mm/s past skanerlash tezligida ~1° va ~36° burilish burchaklari olingan. Davomiyliklari fs va ps lazerli ablyatsiya bilan yuqori skanerlash tezligi uchun vakuumli qarish va qo'shimcha 2 hafta qarigandan keyin aylanish burchagi o'zgarishsiz qoldi va suv tomchilarining kuchli yopishishi kuzatildi. Shunday qilib, biz galvanizli po'latdan supergidrofobik namlanish holatiga o'tish va o'z-o'zini tozalash qobiliyatini namoyish qilish uchun alyuminiy va misga nisbatan ko'proq qarish vaqtini talab qiladi degan xulosaga keldik va bu faqat past skanerlash tezligida sodir bo'ladi. Past skanerlash tezligi galvanizli po'latdan chuqurroq po'lat qatlamiga etib boradigan chuqurroq tuzilmalarga olib keladi, yuqori skanerlash tezligida tuzilmalar asosan

yuqori sink qatlamida hosil bo'ladi. Po'latning uglerod birikmalarini adsorbsiyalash qobiliyati sink qatlamidan yuqori bo'lib, bu asosan past skanerlash tezligida supergidrofobik va o'z-o'zini tozalash xususiyatlarini kuzatish bilan mos keladi.

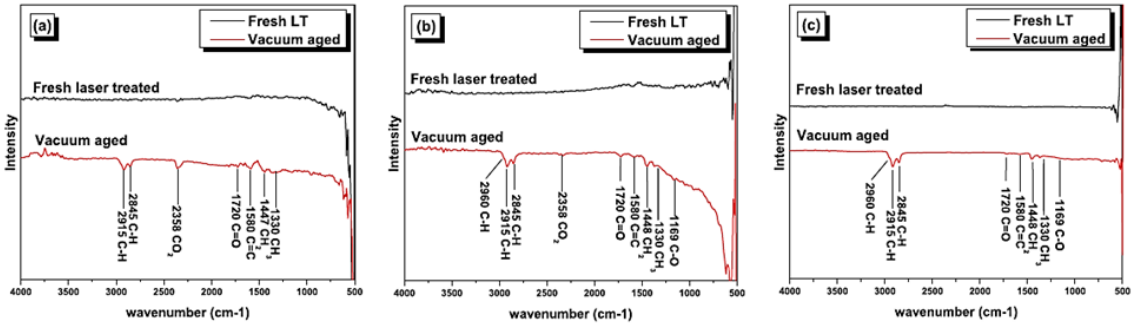

13-rasm. Fs lazerli strukturali (a) alyuminiy, (b) mis va (c) vakuumli qarishdan oldin va keyin galvanizli po'latning ATR-FTIR tahlili. Vakuumli eskirgan namunalar uglevodorodning adsorbsiyasini ko'rsatdi [Appl. Surf. Sci.542, 148560 (2021)].

13-rasmda lazer bilan ishlov berilgan alyuminiy (13(a)-rasm), mis (13(b)-rasm) va galvanizli po‘lat (13(v)-rasm) vakuumda saqlashdan oldin va keyin ATR-FTIR spektrlari ko‘rsatilgan. Ushbu namunalar 50 mm/s skanerlash tezligida tuzilgan. Ko'rinib turibdiki, lazer bilan ishlov berilgan namunalar 2800–3000 va 1100–1750 sm-1 hududlarida asosiy IR rejimlari yo'q. Bu hududlar sirtga biriktirilgan organik birikmalar bilan bog'liq. Yangi tuzilgan metall yuzalar gidroksillangan qatlam hosil bo'lishi tufayli CA <5° bilan kuchli gidrofil bo'lganligi taxmin qilingan edi. Sirtdagi gidroksil guruhlari va suvda adsorbsiyalangan belgilar o'zlarining tabiatida zaif va ularni aniqlash qiyin. Bundan farqli o'laroq, ifloslangan vakuum kamerasida eskirgan lazerli strukturali metall yuzalarning ATR-FTIR spektrlari qayta ishlangan yuzalarda organik guruhlarning adsorbsiyasi bilan bog'liq bo'lgan IR rejimlarini ko'rsatdi. 2960, 2923 va 2858 sm^{-1} da paydo bo'lgan chiziqlar alifatik -CH_3 va -CH_2-qismlari uchun simmetrik va assimetrik C-H cho'zish rejimlari uchun tayinlangan. Ushbu bantlar, shuningdek, vakuumli metallarda 1370 sm^{-1} da paydo bo'ladigan υ_{CH3} bukilish modasi bilan bog'liq. $\upsilon_{C=C}$ bo‘ylama modalariga tayinlangan qo'shimcha imzolar 1460 sm^{-1} da paydo bo'ladi. Bundan tashqari, vakuum bilan ishlov berilgan namunalar mos ravishda C=O va C-O-C cho'zish rejimlari uchun tayinlangan 1720 va 1169 sm^{-1} da qo'shimcha bandlarni ko'rsatdi. Xulosa qilib aytganda, ho'llanishni o'zgartirish uchun juda oz miqdordagi uglevodorodlar kerakligi va faqat lazerli tuzilish va vakuum sharoitlarining mukammal kombinatsiyasi maksimal suv o'tkazmaydigan va o'z-o'zini tozalash xususiyatlariga olib kelishi kuzatildi.

2-Bo’lim. Turli materiallarda ko'p funktsiyali yuzalarni o'ta tez femtosekundli lazer yordamida ishlab chiqarish va ularning yangi ilovalari.

Ushbu bo'limda biz o'z ishimizni taqdim etamiz [Front. Chem. 8, 768 (2020), J. Phys. D: Appl. Phys. 54, 185109 (2021), Appl. Sci.10, 6207 (2020)] turli xil

materiallarda ko'p funktsiyali yuzalarni ultra tez femtosekundli lazer ishlab chiqarish va ularning yangi ilovalari. Metall yuzalarda yaxshi boshqariladigan nano/mikrometr o'lchamdagi tuzilmalarning shakllanishi ularning optik va namlash xususiyatlarini o'zgartirish imkonini beradi. Bunday tuzilmalarni biomoslashuvchan materiallar yuzasida shakllantirish, xususan, ularning fan va texnikaning turli sohalarida qo'llanilishini kengaytirishi mumkin. Bu erda [J. Phys. D: Appl. Phys. 54, 185109 (2021)] biz biomoslashuvchan material tantal (Ta) ni metall namunani hurmat bilan aylantirish orqali azimutal va radial yo‘naltirilgan lazer yordamida induktsiyalangan davriy sirt tuzilmalarini (LIPSS) o‘z ichiga olgan murakkab nano o‘lchamli tuzilmalar bilan qoplash natijalarini taqdim etamiz. nurlantiruvchi lazer impulslarining polarizatsiya yo'nalishiga.

Materialning ultraqisqa lazer impulslari bilan o'zaro ta'siri lazer pulslarining energiyasini nishon material yuzasining juda kichik mikro/nano o'lchovli joyida cheklash orqali davriy sirt tuzilmalarini keltirib chiqaradi. Bu yangi sirt topologiyasini tashkil etuvchi reaktsiyalar zanjirini boshlaydi. Sipe samaradorligi nazariyasi bilan Drude modeli tushuntiradiki, past fazoviy chastotali LIPSS (LSFL) hosil bo'lish jarayoni sirtda zich erkin elektron-plazma hosil qiluvchi kritik tashuvchi zichlik darajasidan oshib ketganidan keyin notekis sirtning sirt plazmon polaritonlari (SPP) uyg’otilishi natijasida boshlanadi. materialdan [Appl. Surf. Sci. 257, 5420 (2011), IEEE J. Sel. Top. Quantum Electron. 23, 109–23 (2017)]. Keyingi termal diffuziya jarayoni va elektron-fononning tarqalishi elektronning vaqtinchalik evolyutsiyasi va g bog'lanish parametri orqali panjara harorati tufayli sodir bo'ladi. Shakllangan LIPSS tuzilma davri LLIPSS ning tushayotgan nur to'lqin uzunligi l, burchak th va sirt plazmon to'lqin uzunligi lSP bilan bog'liqligi bir pulsli lazer tajribasidan [Opt. Express 19, 9035–43 (2011)]:

$$\Lambda_{LIPSS} = \frac{\lambda\, \lambda_{SP}}{\lambda \pm \lambda_{SP} \sin(\theta)} \tag{12}$$

$$\lambda_{SP} = \chi R \left[\frac{(\varepsilon_d + \tilde{\varepsilon_m})^{1/2}}{\epsilon_d \tilde{\varepsilon_m}}\right] \tag{13}$$

Bu yerda $\tilde{\varepsilon_m}$, ϵ_d metall va uning atrofidagi dielektrik muhitning o‘tkazuvchanlik ko‘rsatkichlari. λ_{SP} muhit va metall plazmon to'lqin vektorining chegara shartlaridan kelib chiqadi. Shakllanish jarayoni bir nechta lazer impulslari bilan ham amalga oshirilishi mumkin, ular mahalliy darajada ko'proq energiya to'playdi, to'lqinlarning cho'qqisidan cho'qqigacha chuqurligini oshiradi va to'lqinlar davrini qisqartiradi. To'plangan oqimning oshishi to'qnashuvlar chastotasiga kvadratik ta'sir ko'rsatadi, bu metallning dielektrik o'tkazuvchanligining haqiqiy qismining oshishiga olib keladi va natijada to'lqinlar yuqori darajada butunlay yo'qolib ketish xavfi bilan qisqaradi. oqim to'planishi [Front. Phys. 10, 861098 (2022)]. Biroq, impuls soni ortib borishi bilan to'plangan oqim kuchayadi va plazmatik qo'zg'alishning qo'shilishi tufayli yuqori fazoviy chastotali LIPSS (HSFL) strukturalar paydo bo'la boshlaydi, bu issiqlik

to'planishi ablyatsiya chegarasiga etgunga qadar o'z ta'sirini davom ettiradi, bu erda issiqlik to'planishi to'xtatiladi. Ta sirtini radial va azimutal yo'naltirilgan LIPSS bilan qoplash uchun biz tolaga asoslangan yuqori takroriy chastotali femtosekundli lazerdan foydalandik. Lazer tizimi 14-rasmda ko'rsatilganidek, 150 kHz takrorlash tezligida 30mJ energiyali va davomiyligi 37 fs impulslarni generasiyalaydi. Bunda namuna yuzasida diameter d=70 mkmgacha fokuslangan nur dastasining energiya zichligi $F_P \approx$ 0.8 J sm^{-2} ga teng bo'lgan laser nuridan foydalanildi. F_P lazer nurining energiya zichligining maximal qiymati quyidagi nisbat yordamida hisoblanadi:

$$F_P = 4E/\pi d^2, \quad (14)$$

bu yerda E - lazer impulsining energiyasi. Fokuslangan lazer nur dastasining energiya zichligi bu material sirtlarini femtosekund lazer impulslari bilan o'zgartirishning asosiy parametrlaridan biri hisoblanadi. Ushbu tadqiqot davomida biz ablatsiya nurining o'rtacha oqimidan foydalandik. Yonayotgan nurning yuqori oqimi nano-to'lqinli tuzilmalarni yo'q qilishi yoki bir xil nishon materialning kichik o'lchamdagi nanozarrachalarini to'lqinlarga joylashtirishi mumkin. 0,8 J sm^{-2} ablatsiyali impulslarni qo'llash orqali biz namunaning markaziy maydonidan uzoqda joylashgan nurlangan

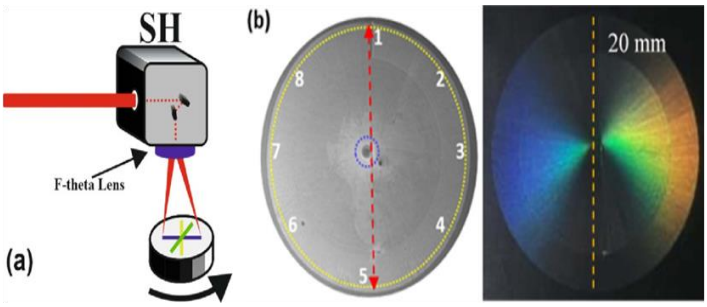

14-rasm. (a) 150 kHz takrorlash tezligi va 37 fs impulslar yordamida Ta yuzasida radial va azimutal yo'naltirilgan LIPSSlarni yaratish uchun eksperimental o'rnatish. F-teta linzalaridan (FL = 160 mm) foydalanadigan Faro skanerlash boshi tizimi (SH), ish joyi bo'ylab bir xil oqimni ta'minlaydi, femtosekund lazer manbai bilan birlashtirildi. (b) Uzoq maydondagi SEM tasviri (chapda) va Ta namunasining nurlangan yuzasining rangli optik tasviri (o'ngda) [J. Phy. D: App. Phy. 54, 185109 (2021)].

sirtda nanozarrachalar cho'kmasdan Ta sirtlarida nanopartikullarni kuzatdik.

Chiziqli polarizatsiyalangan lazer nurlari namuna yuzasiga perpendikulyar ravishda yo'naltirilgan, sirtga normal esa tushayotgan yorug'lik tarqalishi bo'ylab joylashgan. Skanerlash chizig'ining kengligi 70 mkm ga teng edi, bu fokuslangan lazer nurining nuqta o'lchamiga mos keladi. Namunalarni tuzgandan so'ng, ularning sirt morfologiyasi skanerlash elektron mikroskopi (SEM, Tescan) yordamida tavsiflangan. Biz foydalangan namunalar 30×30×0,5 mm^3 o'lchamdagi Ta varaqlari edi. Namunalar sirtlari lazer ablyatsiyasidan oldin etanol bilan tozalangan. 15-rasmdagi yuqori panelda lazer nurlanishining polarizatsiyasi nurlanish impulslarining skanerlash yo'nalishiga parallel bo'lgan birinchi namunaning o'ziga xos sirt joylarida (raqamlar va sariq chiziqli chiziqlar bilan belgilangan) SEM tasvirlari va polarizatsiyasi ko'rsatilgan (qizil o'qlar)). Ablatsiya impulslarining qutblanish yo'nalishini skanerlash yo'nalishiga nisbatan paralleldan perpendikulyarga o'tkazish uchun biz SHdan oldin o'rnatilgan yarim to'lqinli plastinkadan foydalandik. 16-rasmning pastki paneli ikkinchi Ta

namunasining sirt joylarining SEM tasvirlarini aks ettiradi, bu erda ablyatsiya impulslarining polarizatsiyasi skanerlash yo'nalishiga perpendikulyar bo'lgan. Bunday holda, biz kesilgan maydonning markaziga nisbatan radial yo'naltirilgan to'lqinlarni kuzatdik. Yuzaki morfologiya o'lchovlari 14-rasm (b) da ko'rsatilgan belgilangan joylarda amalga oshirildi.

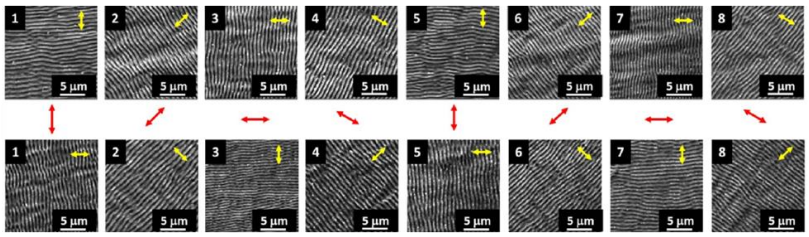

15-rasm. Lazer impulslarining turli polarizatsiya yo'nalishlari bilan nurlangan Ta diskining tashqi aylanasidagi 14(b)-rasmdagi 1-8 pozitsiyalariga mos keladigan belgilangan joylarning SEM tasvirlari. [J. Phy. D: App. Phy. 54, 185109 (2021)].

Biz Ta namunalarini birinchi marta azimutal va radial yo'naltirilgan LIPSS bilan qoplash bo'yicha natijalarni taqdim etdik. Biz yuqori takrorlash tezligi (150 kHz) nurlantiruvchi femtosekundli lazer yordamida metall yuzasida murakkab LIPSS hosil qilishda SH va aylanish bosqichini birlashtirishning afzalligini ko'rsatdik. Namunani aylantirish skanerlash yo'nalishiga nisbatan ablyatsiya impulslarining polarizatsiya yo'nalishini o'zgartirishga imkon berdi. Skanerlash jarayonida namunalarni aylantirish orqali 20 mm diametrli o'chirilgan metall yuzaning diski parallel va perpendikulyar yo'naltirilgan to'lqinlar bilan qoplangan. Yer yuzasida ikki xil LIPSS zonasi hosil bo'lgan. Birinchi zonada davriylik bilan HSFL ($\Lambda_{HSFL} \approx 0{,}4 \pm 0{,}2 \mu m$) va ikkinchi zonada davriylik bilan LSFL ($\Lambda_{LSFL} \approx 1{,}5 \pm 0{,}1 \mu m$) mavjud. Lazerli sirt nanostrukturasi asosida optik aks ettirishni sozlashdan tashqari, Ta yuzasida LIPSS kompleksining gidrofil harakati ko'rsatildi. Biz lazer bilan ishlov berilgan Ta sirtining namlash xususiyatlarini o'lchadik va uni $23^o \pm 5^o$ ga teng SNB bilan gidrofil ekanligini aniqladik. Lazer ta'sirida murakkab davriy tuzilmalarning shakllanishi Ta ning namlash xususiyatlarini nazorat qilish imkonini beradi va implant sifatida ishlatilganda hujayra yopishish va ko'payish tendentsiyasini yaxshilaydi. Bizning usulimiz boshqa metall va dielektrik materiallarga osonlik bilan kengaytirilishi mumkin, bu erda sirtda bunday murakkab tuzilmalarni shakllantirish ushbu materiallardan keng ko'lamli ilovalarda foydalanishni kengaytiradi.

Bizning ishimizda [Appl. Sci. 10, 6207 (2020)] biz ultra qisqa lazer impulslari tomonidan ishlab chiqarilgan nanostrukturalar (LIPSS) po'lat, mis va jez yuzalar alyuminiyda burchakka bog'liq ranglarning paydo bo'lishiga olib keladigan optik diffraktsiya effektlarini qanday o'zgartirishi mumkinligini ko'rsatdik. Qayta ishlangan namunalarning barqarorligi va qayta ishlatilishini isbotlash uchun alyuminiyni qayta bo'yashning oddiy jarayonini taqdim etdik. Biz bunday sirtlarning namlanish xususiyatlarini tahlil qildik va bu xususiyatlar bilan yuzalarning doimiy ranglanishi o'rtasidagi bog'liqlikni ko'rsatdik. Biz, shuningdek, lazer bilan ishlov berishdan keyin bir necha soat davomida vakuumda saqlanganida, femtosekund lazer bilan ishlov

berish orqali supergidrofobik alyuminiy sirtini qanday ishlab chiqish mumkinligini ko'rsatdik.

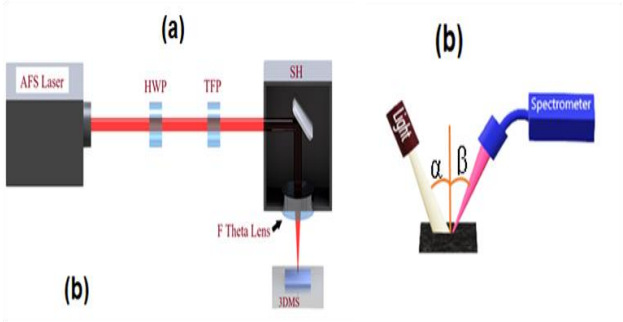

16-rasm. (a) 4,5 Vt quvvatda, impuls davomiyligi 40 fs, markaziy to'lqin uzunligi 1030 nm va takrorlash chastotasi 150 kHz, F-Teta linzali ob'ektivni o'z ichiga olgan skanerlash boshi (SH) bilan femtosekundli lazer yordamida metall yuzalarni qayta ishlash uchun eksperimental qurilma [App. Sci. 10, 6207 (2020)].

Zanglamaydigan po'lat, jez, alyuminiy va mis plitalar skanerlash boshining turli tezligida nurlangan. Jez namunasi 5 mm qalinlikda, boshqa qayta ishlangan namunalarning qalinligi ~ 2 mm edi. Namuna sirtlari nurlanishdan oldin izopropanol bilan tozalangan. Turli ishlov berilgan namunalarning sirtlarini tavsiflash uchun skanerlovchi elektron mikroskop (SEM) ishlatilgan. Yuzaki optik xarakteristikalar 16(b)-rasmda da ko'rsatilgan tajriba tartib yordamida tahlil qilindi. Gorizontal o'rnatilgan namuna ko'rinadigan spektral diapazonda doimiy spektrga ega bo'lmagan qutbsiz yorug'lik manbai bilan yoritilgan, u ikkita linza va diafragma orqali parallel nurga aylantirilgan. Bizning tadqiqotimizda hodisa holati burchagi (α) 20° da o'rnatildi. Qayta ishlangan hududning rang beruvchi ta'sirini tekshirish uchun turli burchaklardagi tarqalgan yorug'lik spektrlari (β) optik tolali spektrometr (Flame, Ocean Optics) bilan o'lchandi. Turli metallarning rangli palletlari 17-rasmda ko'rsatilgan. Paletalar (a-d) mos ravishda zanglamaydigan po'lat, mis, alyuminiy va jez namunalariga mos keladi. Turli ranglarni kuzatish uchun LIPSSni optimallashtirish uchun barcha namunalar turli skanerlash tezligida tayyorlangan. Zanglamaydigan po'lat, jez, alyuminiy va mis uchun optimal skanerlash tezligi mos ravishda 350, 400, 500 va 450 mm/s edi. Namunalarning suratlari quyosh nurida belgilangan hodisa holatida ($\alpha = 20^o$) olingan. Turli ranglar kuzatilganda namunani kuzatish burchagi 0^o dan 40^o ga o'zgartirildi. Diametri 20 mm bo'lgan zanglamaydigan po'latdan, jezdan, alyuminiydan va misdan yasalgan disklar uchun ishlov berish vaqtlari mos ravishda 15 s, 14 s, 11 s va 12 s edi. Sirtlardan burchakka bog'liq bo'lgan rang aks ettirish o'lchovlari 16-rasm (b) da ko'rsatilgan o'rnatish yordamida amalga oshirildi. Volfram lampasining keng tarmoqli kengligi namunaning lazer bilan ishlangan maydoniga yo'naltirildi va difraksiyalangan yorug'lik tolali spektrometr yordamida qayta ishlangan sirtning normaliga nisbatan turli burchaklarda o'lchandi. Diffraktsiya tenglamasi:

$$m\lambda = d\,(\sin\alpha + \sin\beta) \qquad (15)$$

LIPSS natijasida paydo bo'lgan turli ranglar ko'rish mumkin bo'lgan yo'nalishni aniqlash uchun ishlatilgan. Bu erda *m* - diffraktsiya tartibi, λ - to'lqin uzunligi, *d* - LIPSS oralig'i, α - tushayotgan yorug'lik burchagi, β - difraksiyalangan yorug'lik burchagi. Qayta ishlangan alyuminiy, mis va zanglamaydigan po'latdan yasalgan yuzalarning spektral tahlillari 18-rasm (a)-(c) da ko'rsatilgan. Ushbu grafiklar barcha metall namunalar uchun juda mos naqshni ko'rsatadi va shuning uchun turli metall yuzalarda bir xil LIPSS tufayli aks ettirish o'xshashligining dalili bo'lib xizmat qiladi. Shu bilan birga, ishlov berilmagan sirtlarda (18-rasm (d) - (f)), ishlov berilgan yuzalardan farqli o'laroq, ko'zgu spektrlari kuzatuvning turli burchaklarida bir xil bo'lib qoladi (18 (a)-rasm). (c)).

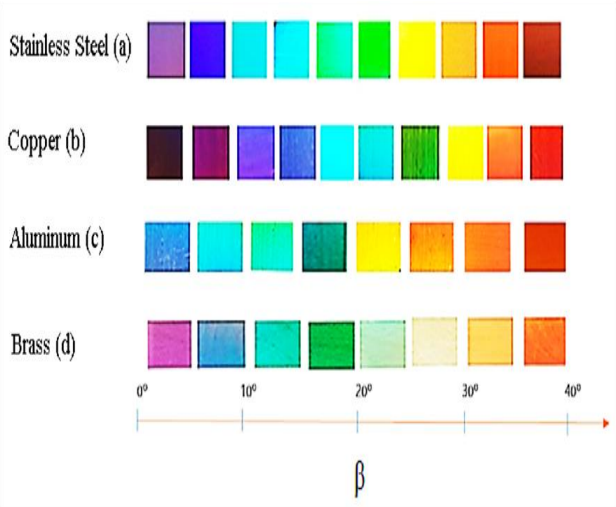

17-rasm. Rangli palitralar qayta ishlangan (a) zanglamaydigan po'latdan, (b) misdan, (c) alyuminiydan va (d) jezdan raqamli kamera orqali turli ko'rish burchaklarida olinadi. Zanglamaydigan po'lat, mis, alyuminiy va jez uchun skanerlash tezligi mos ravishda 350, 400, 500 va 450 mm/s edi. Lazer nurlarining energiya zichligi 1,0 J/sm^2 ni tashkil etdi. β oshgani sayin ranglar ko'rinadigan spektrning uzunroq to'lqin uzunligi hududiga siljidi. Voqea nurining burchagi 20^o daraja atrofida edi [App. Sci. 10, 6207 (2020)].

Toza namunalarda yangi ranglar ishlab chiqarish qobiliyatini ko'rsatishdan tashqari, quyida biz qayta ishlangan metallar yuzasidagi rangni bir xil lazer nurlanishidan foydalanib o'chirish va qayta rang berish mumkinligini ko'rsatamiz.

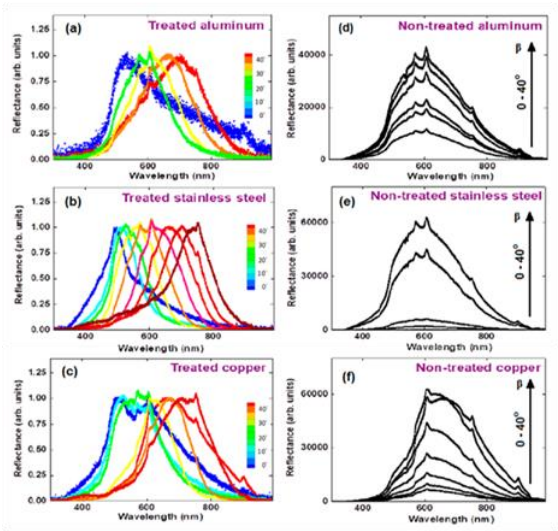

18-rasm. Qayta ishlangan yuzalardan [(a) alyuminiy, (b) zanglamaydigan po'lat, (c) mis] va ishlov berilmagan yuzalardan [(d) alyuminiy, (e) zanglamaydigan po'lat, (f) mis] aks ettirish spektrlari. Har bir grafikdagi turli egri chiziqlar kuzatishning turli burchaklariga mos keladi. Ko'rinib turibdiki, ishlov berilmagan yuzalarda, qayta ishlangan yuzalardan farqli o'laroq, aks ettirish spektrlari kuzatuvning turli burchaklarida bir xil bo'lib qoladi. (a–c) dagi ranglar mos keladigan burchaklarda ko'z bilan ko'rish mumkin bo'lgan ranglarga mos keladi. Burchak (β) 0° dan 40° gacha bo‘lgan, bunda 0° spektrometrning namunaga perpendikulyar bo‘lgan holatiga to‘g‘ri keladi. β oshgani sayin uzunroq to'lqin uzunliklari aniqlandi [App. Sci. 10, 6207 (2020)].

19-rasmda ko'rsatilganidek, alyuminiy namunasi to'q oltin rangga (A) aylantirildi va keyin uni deyarli asl rangiga qaytarish uchun o'chirildi. Keyin xuddi shu namuna oq rangga (B) bo'yalgan, uning bir qismi yana o'chirilgan va qora yarim doira (C) ga bo'yalgan. Biz lazer yordamida davriy sirt tuzilmalarini shakllantirish va davriy

bo'lmagan nano/mikro tuzilmalarni shakllantirish orqali alyuminiy, mis, po'lat va guruchning femtosekundli lazerli sirt tuzilishi yordamida doimiy va burchakka bog'liq ranglarning ko'rinishini namoyish etdik. Biz ushbu ikkala rangli turlar guruhini lazer bilan ishlov berishning qo'shimcha bosqichidan foydalanib o'chirish yoki qayta bo'yash mumkinligini ko'rsatdik. Materialning sirtini qayta qurish jarayoni SPP uyg'otilishi va uning lazer nurlanishiga aralashuvi bilan bog'liq. Ushbu shovqin sirt bo'ylab lazer intensivligining qayta taqsimlanishiga va uning davriy naqshiga olib keldi. Skanerlash tezligi yaratilgan tuzilmalarning natijaviy optik xususiyatlarini aniqlashda asosiy omil ekanligi aniqlandi. Oldindan o'zgartirilgan sirt strukturasi har bir keyingi impuls uchun teskari aloqa sifatida xizmat qilishi mumkin bo'lgan optimal skanerlash tezligi mavjud, bu ko'p impulsli rejimda ishlab chiqarilgan LIPSSning aniqligini oshiradi.

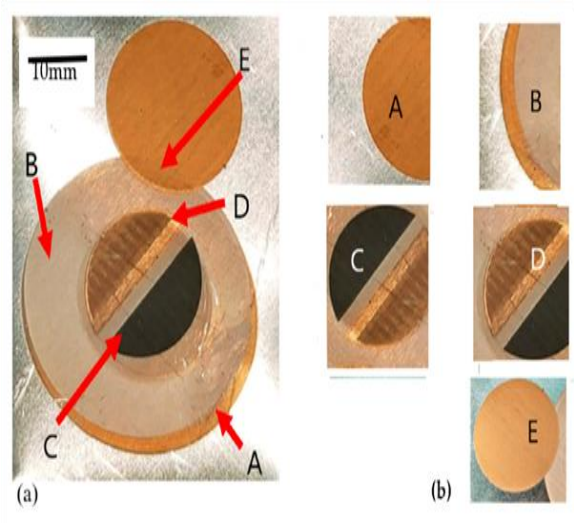

19-rasm. Ishlov berilgan namunadagi rangni o'chirish va alyuminiyning o'chirilgan yuzasida hosil bo'lgan yangi ranglarning shakllanishini namoyish qilish. Panel (a): original namuna; panel (b): panelni tushuntirish (a): A, dastlab quyuq oltin disk yaratilgan. B, to‘q oltin rang o‘chirilgandan keyin oqartirilgan rang, C, oqartirilgandan keyin qora yarim doira, D, oqish rang o‘chirilgandan keyin och oltin rangli chiziq va E, oq rangga bo‘yalgan quyuq oltin rang. To‘q oltin, oq, qora va och oltin ranglami skanerlash tezligi mos ravishda 70 mm/s, 1500 mm/s, 10 mm/s, 200 mm/s (ikki marta) edi. Lazer nurlarining ravonligi 0,5-1,0 J/sm^2 oralig'ida edi. 5b-rasmda mos ravishda A, B, C, D va E qismlarining tasvirlari berilgan [App. Sci. 10, 6207 (2020)].

Turli rangdagi metallarning spektral aks ettiruvchi xossalari va qayta ishlangan metall yuzalarning namlanishi o'rtasidagi bog'liqlik ham o'rganildi. Biz qayta ishlashda qo'llaniladigan lazer parametrlari to'plamini optimallashtirish orqali bir vaqtning o'zida rang berish va metallaming namlanish xususiyatlarini moslashtirish imkoniyatini ko'rsatdik. Bundan tashqari, lazer bilan ishlov berilgan namunalarni vakuumda saqlash ularning namlanishga bo'lgan javobini gidrofildan supergidrofobikka o'zgartirdi, hatto vakuumda saqlangan namunani atrof-muhit atmosferasida qoldirgandan keyin ham doimiy davom etadi. Vakuumli qarish namunaning sirt energiyasini oksid qatlamining desorbsiyasi, so'ngra atrof-muhitdan uglerod turlarining adsorbsiyasi orqali o'zgartirishga imkon beradi. Neft-suvni ajratish uchun membranalarni o'ta namlash va tanlab o'tkazuvchanligi yordamida yog'ni suvni ajratish katta ekologik va iqtisodiy ahamiyatga ega. Biz [Front. Chem. 8, 768, (2020)] da ultraqisqa femtosekundli impulslar yordamida zanglamaydigan po'lat va mis to'rlarni nanostrukturalash orqali suv ostidagi supergidrofil-superoleofobik holatga namlanish reaktsiyasining

supergidrofobik-superoleofob holatiga o'tishi haqida xabar beramiz. Bizning yondashuvimiz ekologik toza, kimyoviy moddalarsiz va samaralidir, chunki u yuqori vakuumli muhitda qayta ishlangan namunalarni qarish afzalliklaridan foydalanadi. Yog'-suv aralashmasi uchun 98% ajoyib ajratish samaradorligini ko'rsatadigan membranalarni ishlab chiqarish uchun lazerni skanerlash parametrlarini, to'r bo'shliklarining hajmini va qarish sharoitlarini optimallashtirdik.

Lazerli skanerlash tezligining funksiyasi sifatida turli tarmoqlar uchun suv va moy bilan namlanish burchaklarining o'zgarishi ko'rsatilgan. 150 mkm kovakchalar o'lchamli zanglamaydigan po'latdan yasalgan to'rlar va 100 mikron gözenek o'lchamli mis to'rlar neft va suv fazalari uchun ajoyib namlanish reaktsiyasini namoyish etdi.

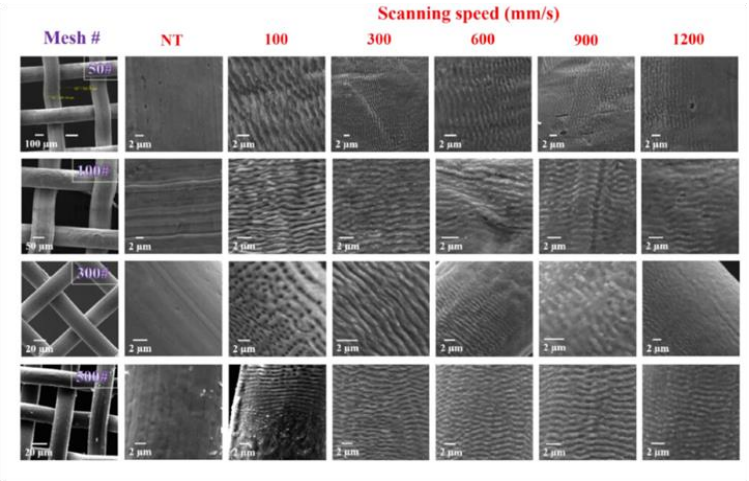

20-rasm. Turli skanerlash tezligida (100-1200 mm/s) tuzilgan SS meshlarining SEM. Lazer bilan induktsiyalangan davriy sirt tuzilmalari (LIPSS) turli xil skanerlash tezligida ~1 mkm bo'lgan turli xil to'r o'lchamlari uchun kuzatilgan [Front. Chem. 8, 768 (2020)].

Vakuumli qarish suv molekulalari yo'qligida lazer tuzilmali yuzalarda uglevodorodlarning tez kimyosorbsiyasini keltirib chiqaradi, bu esa namlanish holatini tezda supergidrofildan supergidrofobikka o'zgartiradi. Lazer ta'siri ostida yuza tuzilmalari 100 dan 1200 mm / s gacha bo'lgan o'zgaruvchan skanerlash tezligida turli xil o'lchamdagi SS to'rlarida yaratilgan. Lazer yordamida tuzilish uchun turli xil qalinlikdagi va g'ovak o'lchamdagi SS to‘rlari (50 #, 100 #, 300 # va 500 #) tanlangan (20-rasmning chap ustuni). Ushbu panellarning barchasida LIPSS yo'nalishi har doim lazer polarizatsiyasiga perpendikulyar edi. Ikkita eng yuqori skanerlash tezligida 900 va 1200 mm/s bo'lgan tarmoqlarda ishlov berilmagan hududlar keng tarqaldi va davriy tuzilmalarning chuqurligi sezilarli darajada pasaydi. E'tibor bering, NT ishlov berilmagan to'rlarni anglatadi. 50# to‘r sim diametri 200 mkm va g‘ovak o'lchamlari 400 mkm. 100# to‘r sim diametri 100 mkm va g‘ovak o'lchamlari 150 mkm. 300# to‘r sim diametri 30 mkm va g‘ovaklar o'lchamlari 50 mkm. Nihoyat, 500# to‘r sim qalinligi 25 mkm va g‘ovak o'lchamlari 30 mkm. Lazer nurlanishining parametrlariga qarab, ishlov berilgan sirt spallatsiya yoki fazali portlash mexanizmlari tomonidan boshqariladigan ablyatsiya jarayonidan o'tishi mumkin [Appl. Surf. Sci. 255, 9724 (2009)]. Spallasyon lazer ta'siridan kelib chiqadigan stresslarni yumshatish orqali katta suyuqlik yoki qattiq zarrachalarni chiqarib yuborish sifatida aniqlanadi. Holbuki, portlovchi qaynash deb ham ataladigan fazali portlash nishon yuzasining o'ta qizib

ketgan qismlarining portlovchi parchalanishi natijasida materiallarni olib tashlashni o'z ichiga oladi [J. Phys. Chem. C 113, 11892 (2009)] SS to‘rlari 300# va 500# uchun 100 mm/s sekin skanerlash tezligida LIPPS bo'ylab mikro-g‘ovak hosil bo‘lishi va mikro-zarrachalaming qayta joylashishi kuzatildi. 300 va 600 mm/s skanerlash tezligi uchun barcha tarmoq turlari uchun ~1 mkm davriy yagona LIPSS hosil bo'ldi. Ishlov berilmagan to'r yuzasi bilan taqqoslaganda, lazer bilan ishlov berilgan yuzalar LIPSS bilan qoplangan, bu ularning sirt g‘adur-budurligi keskin oshiradi.

Biz ablyatsiyadan so'ng darhol lazer bilan tuzilgan sirtlarning namlanish burchagini o'lchadik. Dayriy strukturaviy shakllar 21-rasmda ko'rsatilganidek, ablyatsiyadan so'ng darhol supergidrofil reaktsiyasini ko'rsatdi.

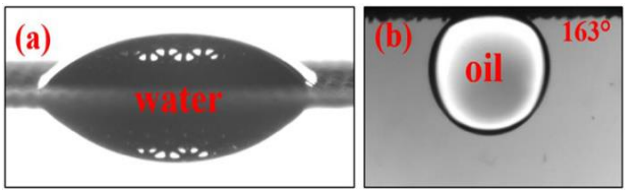

21-rasm. (a) havodagi supergidrofil hodisani va (b) suv osti-superoleofob xususiyatlarini ko'rsatadigan femtosekundli lazerli strukturali tarmoqning namlanishi [Front. Chem. 8, 768 (2020)].

Bu hodisa lazer tuzilishi paytida metall oksidi qatlamining shakllanishi bilan bog'liq. Yangi o'chirilgan metall to'rlar uchun suv bilan namlanish burchagi ~0º va suv tomchisi to'r orqali ~0,1ms tezlikda o'tib, supergidrofil xususiyatlarni namoyon qildi. Ushbu supergidrofil to'rlar suv ostida superoleofobik javobni ko'rsatdi, moy bilan namlanish burchagi (YNB) barcha skanerlash tezligi va metall to'r turlari bo'yicha 155º dan 163º gacha. Atrof muhitda 60 kun davomida uzoq muddatli ta'sir qilishdan so'ng yoki vakuumda 4 soat qarigandan so'ng, lazer bilan tuzilgan to'rlarda supergidrofobik xususiyat ustun bo'ldi. 22-rasmda lazerli tuzilmali SS to'rlarining turli xil o'lchamlar uchun skanerlash tezligi 100 dan 1200 mm/s gacha bo'lgan kontakt burchagi o'lchovlari ko'rsatilgan. Suv bilan namlanish burchagi va moy bilan namlanish burchagi lazer bilan ishlov berilgan joylarga 5 mkl suv va moy (n-geksan) tomchilarini dozalash orqali aniqlandi. Biz yangi (ya'ni, ablyatsiyadan so'ng darhol) tuzilgan sirtlarga nisbatan vakuum yoki havoda eskirgan namunalarning namlanish reaktsiyasida sezilarli o'zgarishlarni kuzatdik. SS 50, 100 va 300# to‘rlar uchun yog‘ chiqib ketdi, SS 500# to‘r uchun esa yog‘ning namlanish burchagi 0° ga yaqin edi va moy bo’shliklardan oqib chiqmadi, balki kapillyar ta’sir tufayli bir tekis tarqaldi.

LIPSS ham vakuumli, ham havodagi to'rlar uchun.Havoda yoki vakuum muhitida qarish natijasida lazer ablyatsiyasi lazer tuzilmali yuzalarni bir vaqtning o'zida ko'proq gidrofobik va oleofil holga keltirdi. Lazerni skanerlash tezligining oshishi bilan yog'ning o'tkazuvchanligi biroz pasaydi, shu bilan birga oleofil xususiyatlar saqlanib qoldi. 50, 250 va 400 mkm sim diametrlari bilan mos ravishda 100, 500 va 800 mkm g‘ovak o'lchamdagi mis to'rlari femtosekundli lazer bilan o'chirildi va keyin havo va

vakuum muhitida saqlangan. Mis to'rlarda lazer ta'siri ostida tuzilmalarning shakllanishi ularning sirt rangini kulrang qora rangga o'zgartirdi. 100 mm/s skanerlash tezligida to'rlarning tuzilgan yuzasida mikro va nanozarrachalar bilan qoplangan LIPSS hosil bo'ldi; to'lqinlar orasidagi o'rtacha davr ~1 mkm edi. 300 mm/s skanerlash tezligida tuzilgan 500 va 800 mkm mis to'rlar uchun biz toza mis to'rga o'xshash teksturasiz joylarni topdik. Bundan tashqari, 300 mm/s skanerlash tezligida lazer nurlari yo'li bo'ylab chiqib ketishlari bo'lgan tasodifiy nanostrukturalar kuzatildi. Ikki xil skanerlash tezligida o'zgartirilgan lazerli tuzilmali mis to‘rlarning suv va moy bilan namlanish burchagi uchun o'lchovlar o'tkazildi, so'ngra 4 soat davomida vakuumda qarish va 60 kun davomida havo qarishi amalga oshirildi. Strukturaviy 100 mkm mis to‘r suv bilan namlanish burchagi 153,2° bo'lgan vakuumda saqlashdan keyin 300 mm/s skanerlash tezligida kuchli supergidrofobik javobni ko'rsatdi.

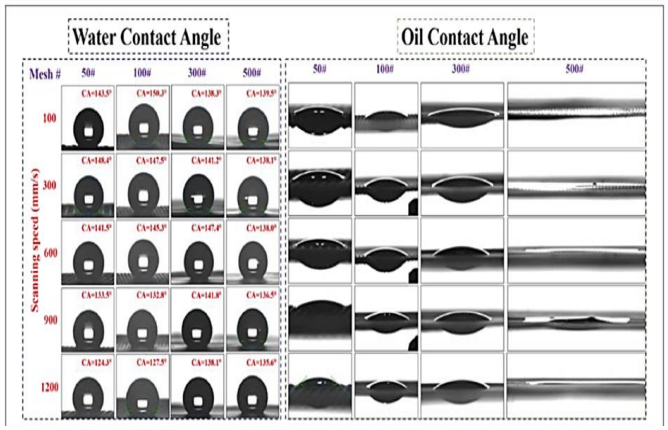

22-rasm. SS to‘rlarining suv bilan namlanish burchagi va moy bilan namlanish burchagi o‘lchovlari (50#, 100#, 300# va 500#) keyin 4 soat davomida vakuumda saqlanadi. 100-1200 mm/s skanerlash tezligida femtosekundli lazer bilan tuzilish [Front. Chem. 8, 768 (2020)].

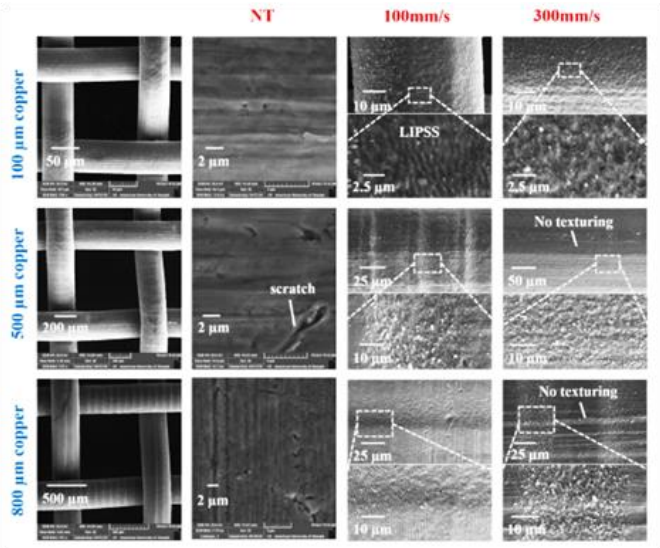

23-rasm. 100 va 300 mm/s skanerlash tezligida femtosoniyali lazer yordamida tuzilgan uchta mis to'rning (100, 500 va 800 mikron gözenek o'lchamlari) SEM tasvirlari. Lazer bilan ishlov berish LIPSS va qo'pol sirt tuzilmalarini shakllantirishga imkon berdi. Ba'zi hududlar 300 mm/s skanerlash tezligida 500 va 800 mikron gözenek o'lchamli to'rlar uchun teksturasiz bo'lib qoldi. Eslatma: NT ishlov berilmagan to'rni anglatadi [Front. Chem. 8, 768 (2020)].

E'tibor bering, shunga o'xshash sharoitlarda havo yoshidagi namunalar uchun 135,7° suv bilan namlanish burchagi olingan. Vakuumli saqlashdan keyin yuqori suv bilan namlanish burchagiga erishish tendentsiyasi har bir mis to‘r uchun va turli skanerlash tezligida kuzatildi. Shu bilan birga, yog' tomchilari to'r orqali o'tib, super oleofil javobni ko'rsatadi. Lazer bilan ishlangan 500 va 800 mkm mis to'rlari vakuum va havo qarishidan keyin ham gidrofobik xususiyatlarni ko'rsatdi. 100 va 300 mm/s skanerlash

tezligida lazer tuzilishidan so‘ng yuqori vakuumda saqlanadigan 500 mkm mis to‘r uchun 145,2° va 141,1° SNBlari olingan, havoda eskirgan namunalar esa kichikroq SNBlarini ko‘rsatdi (mos ravishda 134.2° va 141.2°). Xuddi shunday tendentsiya 100 mm/s skanerlash tezligida tuzilgan 800 mkm to'r uchun suv bilan namlanish burchagi 137,2° vakuumli va havo yoshidagi namunalar uchun 126,8° uchun kuzatildi. Shu bilan birga, namunalarning moy bilan namlanish burchagi superoleofil xususiyatlarga ega bo'lgan neft uchun yuqori o'tkazuvchanlikni ko'rsatdi. 24-rasmda 100 mm/s skanerlash tezligida tayyorlangan namunalar uchun vakuum qarishidan oldin va keyin lazerli strukturali zanglamaydigan po'lat va mis metall yuzalar uchun ATR-FTIR spektrlari ko'rsatilgan.

24-rasmda ko'rsatilganidek, lazer bilan ishlov berilgan namunalar 2,800-3,000 va 1,100-1,750 sm-1 hududlarida asosiy IR rejimlariga ega emas, ular sirtga uglevodorod birikmalari bilan bog'liq. Bu kutilmoqda, chunki lazer bilan ishlov berilgan namunalar tuzilishdan so'ng darhol kontakt o'lchanganida kuchli gidrofil edi. Biroq, sirt gidroksil va suvda adsorbsiyalangan belgilar tabiatda zaif va hozirgi ZnSe kristalli yordamida aniqlash qiyin. Bundan farqli o'laroq, vakuumda lazer bilan ishlov berilgan metall yuzalar uchun ATR spektrlari ishlov berilgan sirtlarda uglevodorodlarning adsorbsiyasi bilan bog'liq bo'lgan IR rejimlarini ko'rsatdi. Alifatik -CH_3 va -CH_2- qismlari uchun C-H cho'zish rejimlari uchun tayinlangan 2,960, 2,923 va 2,858 sm^{-1} da o'ziga xos chiziqlar paydo bo'ladi. Ushbu bantlar, shuningdek, vakuumli metallarning ikkalasida ham 1370 sm^{-1} da paydo bo'ladigan u_{CH3} bukilish modasi bilan bog'liq. Qo'shimcha imzolar $u_{C=C}$ bo‘ylama modalariga tayinlangan 1,460 sm^{-1} da paydo bo'ladi. Bundan tashqari, vakuum bilan ishlov berilgan mis namunasi mos ravishda C=O va C-O-C cho'zish rejimlari uchun tayinlangan 1,720 va 1,169 sm^{-1} da qo'shimcha bandlarni ko'rsatdi. Xulosa qilib aytganda, vakuum kamerasidagi lazer bilan ishlov berilgan metall yuzalar organik uglevodorodlarning sirtda adsorbsiyasini osonlashtiradi, bu esa yuqorida aytib o'tilgan vakuumli to'r yuzalarida kuzatilgan super gidrofobik harakatga olib keladi.

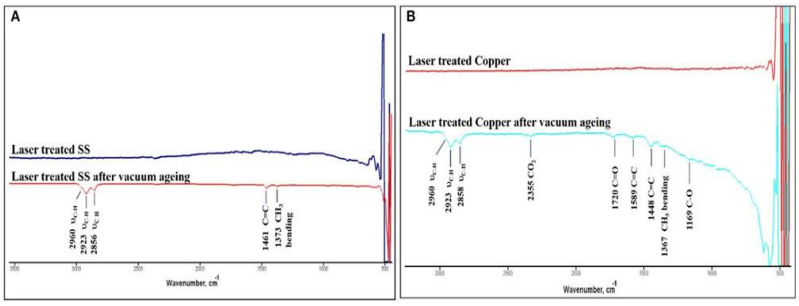

24-rasm. Vakuumli qarishdan oldin va keyin lazer bilan ishlov berilgan (A) SS va (B) misning ATR-FTIR spektrlari [Front. Chem. 8, 768 (2020)].

Biz lazer bilan qayta ishlangan to'rlarni yuqori vakuumli muhitda bir necha soat davomida saqlash neft va suvni ajratish ilovalari uchun qisqa vaqt ichida

superhidrofobik superoleofil to'rlarni ishlab chiqarish uchun samarali yondashuv ekanligini ko'rsatdik. Shuningdek, biz havo, vakuum yoki uglerodga boy atmosferalarni saqlash muhiti sifatida ishlatadigan pikosekundli impulslar yordamida ilgari xabar qilinganidan oshib ketadigan namlanish xususiyatlarining shakllanishini namoyish etdik [J. Laser. Appl. 27, S29107 (2015)].

Davomiyligi 10^{-12} s bo'lgan lazer impulslaridan foydalangan holda suv bilan maksimal namlanish burchagi 120° ekanligi xabar qilingan, bizda esa 36 fs impulslar bilan ishlab chiqarilgan mis to‘rlarning vakuumli qarishi holatlarida namlanish burchagi 153,5° gacha bo‘lgan qiymatlarga yetdi va shu bilan ajoyiblikni namoyish etdi. namunalarimiz super hidrofobiklik harakati.

Bizning tadqiqotimizdagi suv bilan namlanish burchagining kuchayishi femtosekund impulslari tomonidan yaratilgan nanoripllarning o'tkir qirralariga ega bo'lgan chuqurroq davriy tuzilmalarning shakllanishi bilan bog'liq bo'lishi mumkin. O'tkir qirrali nanoripellar yaqinida kuchliroq mahalliy maydonlarni ko'rsatadigan bunday tuzilmalar vakuum nasoslari yoki vakuum kamerasi devorlaridagi yog'li ifloslantiruvchi moddalardan ko'p miqdorda uglevodorodlarni uzoqroq (pikosekundli) impulslar natijasida hosil bo'lgan tuzilmalarga qaraganda yaxshiroq adsorbsiyalash tendentsiyasiga ega. Vakuum va havo qarishidan so'ng super hidrofobiklik va superoleofillikni ko'rsatgan ishlab chiqarilgan mis va SS to'rlari suvni to'sib qo'yish va neftning o'tishini ta'minlash orqali neft-suv aralashmalarini ikki xil komponentga ajratishda sinovdan o'tkazilishi mumkin.

25-rasmda yog'-suv aralashmasini ajratish uchun vakuumda eskirgan lazerli strukturali mis to'rning imkoniyatlari ko'rsatilgan. To'r lazer bilan ishlov berilgan sirt aralashmaga qaragan tarzda joylashtirilgan. Yog'-suv aralashmasi n-geksan (yog') uchun yuqori o'tkazuvchanlikka ega bo'lgan lazerli tizimli to'rga quyiladi. Identifikatsiya qilish uchun suv metilen ko'k rangga bo'yalgan. Yog'-suv aralashmasi

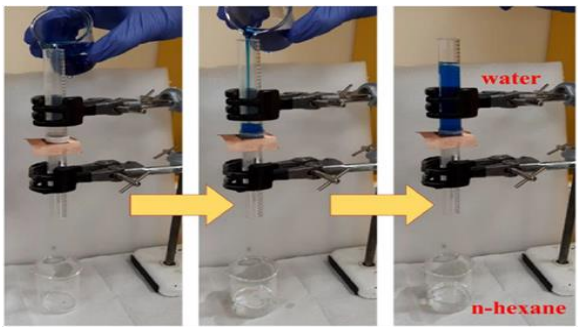

25-rasm. 300 mm/s skanerlash tezligida tayyorlangan lazerli strukturali va vakuumli mis to'r yordamida neft-suvni ajratishni ko'rsatish. Ikki suyuqlikni yaxshiroq aniqlash uchun suv metilen ko'k bilan bo'yalgan. Yog 'o'tadi, suv esa superhidrofobik-superoleofil xususiyatga ega bo'lgan to'r ustida qoladi [Front. Chem. 8, 768 (2020)].

mis to'rning lazer tuzilmali yuzasiga quyilganda, yog' to'rdan o'tib, trubka ostidagi stakanga yig'ildi, suv esa to'r ustidagi trubkada (o'ng panelda) to'silgan. Og'irlik kuchiga asoslangan ajralish 50 $Lm^{-2}h^{-1}$ bo'lgan o'tkazuvchanlik oqimi (F) bilan 15 soniyadan ko'p bo'lmagan tezlikda sodir bo'ldi va ajratilgan yog'da suv kam yoki umuman suvsiz 98% ajratish samaradorligini ta'minladi.

Mis va SS to'rlarining qalinligi va g'ovak o'lchamlari, lazerni skanerlash tezligi va qarish muhiti bo'yicha olib borilgan tizimli tadqiqotimiz 98% va undan yuqori samaradorlik bilan yog'-suv aralashmalarini ajratishda femtosekundli lazerli tuzilmali tarmoqlardan foydalanish bo'yicha ko'rsatmalar berdi. Femtosekundli lazerli strukturali metall to'rlarning namlanishining supergidrofilik suvosti-superoleofobikdan supergidrofobik-superoleofilga o'tishi tez, oson, ekologik toza, kimyoviy moddalarsiz va yangi vakuumli qarish texnikasi orqali erishildi, erishilgan namlanish burchagi 153,5^{o} ni tashkil etdi. Moy bilan namlanish burchagi 0^{o} ni tashkil etdi.

Mazkur ishda [Appl. Phys. A 126, 62 (2020)] biz havoda 5 ns lazer impulslari yordamida ablatsiya qilingan turli materiallarning tekisligi va egri sirtlarining hidrofobik va hidrofilik xususiyatlarini ko'rib chiqdik. Suyuqlik va modifikatsiyalangan grafit va AlNiCo qotishma novdalar yuzasi o'rtasidagi namlanish burchaklarining turli xil oqim pulslari yordamida ko'rsatilgan. Ablatsiyalangan grafit novdaning namlash burchagi 147°, ya'ni o'zgartirilgan kavisli yuzalar supergidrofobik xususiyatlami ko'rsatdi. Boshqa tomondan, 7° ho'llash bilan namlanish burchagi bo'lgan supergidrofil xususiyatlar ablyatsiyalangan alyuminiy qotishmasida namoyon bo'ldi. Yog'-suvni ajratish uchun membrana sifatida grafit tayoqchasini qo'llash uchun sxematik model taklif qilindi.

Keyingi ilmiy tadqiqotda [Front. Chem. 9, 792641 (2021)], biz $NaAlSi_2O_6$-H_2O zeolitini femtosekund lazerli nanostrukturali zanglamaydigan po'latdan yasalgan substratlarda o'stirdik. Qoplangan sirt XRD, SEM va EDX tomonidan tahlil qilindi va toza po'latdan yasalgan to'rlar, zeolit bilan qoplangan to'rlar va lazerli tuzilmali to'rlar bilan taqqoslandi. Batafsil kontakt burchagi o'lchovlari toza po'latdan yasalgan to'rlar, zeolit bilan qoplangan to'rlar, lazerli tuzilmalar va zeolit bilan qoplangan lazerli tuzilishli SS-100 to'rlari namunalarida amalga oshirildi. Qoplangan va tuzilgan namunalarda yaxshilangan supergidrofil xatti-harakatlar kuzatildi, zeolit bilan qoplangan lazerli tuzilmali SS-100 to'rlari o'rtacha 15° namlanish burchagini va uzoq vaqt davomida va takroriy foydalanishda yuqori chidamlilikni namoyish etdi. Bundan tashqari, zeolit bilan qoplangan lazerli tuzilmali SS-100 to'rlari neft-suv ajratish tajribalaridan o'tkazildi va neft-suvni ajratishning kengaytirilgan samaradorligini aniqladi. Jumladan, ajratish tortishish kuchi orqali 18 sekundda 12,738 $L \cdot m^{-2} \cdot h^{-1}$ suv oqimi bilan amalga oshirildi va 95% ni tashkil etgan sezilarli ajratish samaradorligini berdi. Seolit bilan qoplangan lazerli tuzilmali SS100 to'rlarining ishlashini tekshirish uchun yog'-suvni ajratish tajribasi 20 ml suv-n-geksan aralashmasi (hajm bo'yicha 1:1) bilan amalga oshirildi va SS to'rga quyildi. Ikki suyuqlik suvni metilen ko'k bo'yoq bilan bo'yash bilan ajralib turardi. To'r orqali umumiy suv oqimi va moyning kirib

borish bosimi mos ravishda (18) va (19) tenglamalar bo'yicha hisoblab chiqilgan [J. Memb. Sci. 608, 118201 (2020)].

$$F = \frac{V}{A \times t} \tag{16}$$

bu yerda F - suvning o'tkazuvchanlik oqimi, V - to'r maydonidan A (m^2) o'tgan suyuqlik hajmi va t - ajralishning umumiy vaqti.

$$P_{int} = 2\gamma_{l1/2}\frac{Cos\theta}{d} \tag{17}$$

P_{int} - kirish bosimi (kPa), $c_{\ell 1/2}$ - moy va suvning oraliq kuchlanishi (mN/m), θ - OCA (°), d - to'rning g'ovak o‘lchami (m). Ushbu tajribalarda to'r shunday joylashtirilganki, tuzilgan va qoplangan sirt pastga qarab oqadigan oqimga qaraydi. Supergidrofil sirt xususiyati tufayli suv to'r yuzasidan bir necha soniya ichida o'tib ketadi, neft esa to'r yuzasidan qaytariladi va u orqali o'tishni rad etadi. Xususan, neft-suv aralashmasidan suvni ajratish tortishish kuchi orqali 18 soniya ichida 12,738 $L \cdot m^{-2} \cdot h^{-1}$ suv oqimi bilan amalga oshirildi va neftning kirib borishi bosimi bilan 95% dan yuqori ajratish samaradorligini berdi. 1,2 kPa. 26-rasmda 15 sikl ishlagandan so'ng zeolit bilan qoplangan lazerli tuzilmali SS-100 to'rlari uchun suvni ajratish samaradorligi va oxirgi tsiklda o'rtacha 94,4% samaradorlikka erishilganligi ko'rsatilgan. Ushbu olingan natijalar lazer nurlanish bilan strukturalangan SS-100 to'rlarini zeolit moddalari bilam qoplashorqali ularning uzoq muddat foydalanishga chidamliligi va qo'llanilishini ko'rsatadi. Zeolit bilan qoplangan lazerli tuzilmali SS-100 to'rlarining kuzatilgan barqarorligi va qayta ishlatilishi ularni sanoat jarayonlarida neft va suvni ajratishda kuchli va mustahkam qiladi.

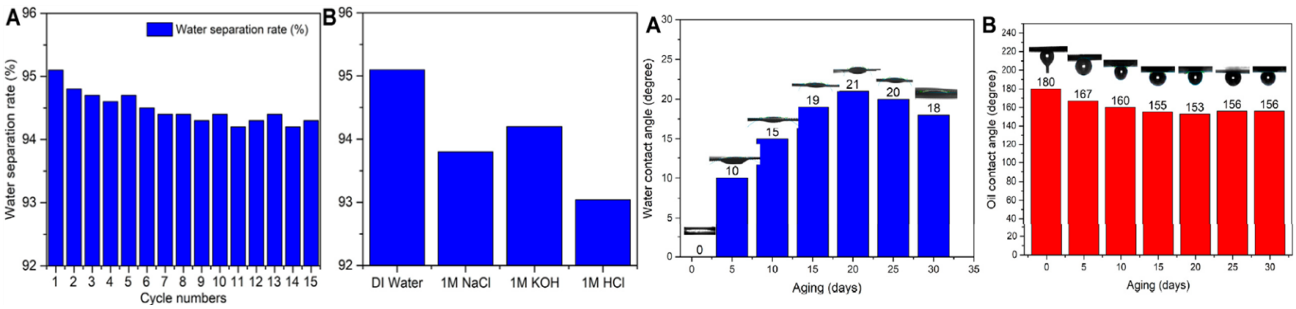

26-rasm. Yuqorida zeolit bilan qoplangan lazer tuzilmali SS-100 meshlarining suv bilan namlanish burchagi (SNB) (A) va OCT (B) ga qarish vaqtining ta'siri ko'rsatilgan. [Front. Chem. 9, 792641 (2021)].

Bizning keyingi ishimizda [Langmuir 39, 1815−1825 (2023)], mis ko'pik va to'rda ishlab chiqarilgan Yanus membranalarining assimetrik namlanishi yo'nalishli suv tashish va tumanni yig'ish nuqtai nazaridan o'rganildi. Namlanish farqini olish uchun membranalarning bir tomoni femtosekundli lazerli skanerlash jarayoni bilan ishlov berildi, bu esa uni supergidrofil (SHL) holatga aylantirdi va shu bilan birga ishlov berilmagan sirt gidrofobik (HB) ni saqlab qoldi. Janus tuzilmalari suvning gidrofobik yuzadan SHL tomoniga o'tishiga imkon berdi va uni teskari yo'nalishda tashishga

ruxsat bermadi. Ushbu anizotropik suv o'tkazuvchanlik xususiyatlari lazer nurlanishi bilan ko'piklar va to'rlarda hosil bo'lgan ko'ndalang kesimdagi namlanish gradientidan kelib chiqqan. Namlanish gradienti lazer bilan ishlov berish jarayonining skanerlash tezligiga bog'liq edi. Juda past skanerlash tezligida membrana butunlay hidrofil bo'lib qoldi (ko'pik holatida). Aksincha, nisbatan yuqori skanerlash tezligida ishlov berilgan maydonning qalinligi etarli emas edi, buning natijasida hidrofobik yuzaga adsorbsiyalangan bir tomchi suv membrananing hidrofilik qismiga etib bora olmadi.

Membranalar suv diodining xususiyatlarini ko'rsatadigan optimal skanerlash tezligi 50 mm/s edi. Gidrofob/gidrofil Janus to‘r-asosli tizimi tomonidan qurbaqadan suv yig'ish samaradorligi ko'pikli membrana (2,5 g/sm^2 soat) bilan solishtirganda yuqoriroq (3,9 g/sm^2 soat) edi. Tuman-suvni konversiyalash samaradorligi vaqt o'tishi bilan (2 hafta ichida 0,5 g/sm^2 soatgacha) tozalangan sirtning supergidrofilligini buzadigan organik ifloslantiruvchi moddalarning absorbsiyasi tufayli kamaydi. Namunalarni TiO_2 bilan qoplash ularni kamida 60 kun davomida degradatsiyadan himoya qildi va namunalarning supergidrofilligini tiklashga ularni shunchaki quyosh nuriga ta'sir qilish orqali erishildi. Bizning fikrimizcha, bu natijalar suv tanqisligi muammolarini bartaraf etish uchun tumanni yig'ish tizimini yanada rivojlantirishga yordam beradi, ayniqsa cho'llar, qirg'oqlar va tog' tizmalarida dolzarbdir.

XULOSA

Tadqiqotlarda olingan asosiy xulosalar quyidagilardan iborat:

1. Raqamli molekulyar dinamik simulyatsiyalar suyuq fazada nanozarrachalar hosil bo'lishining asosiy mexanizmlari va kerakli o'lchamdagi, shakldagi va morfologiyadagi alyuminiy nanozarrachalarini olish uchun optimal lazer nurlanish parametrlari mavjudligini tushunish imkonini berdi.
2. Suvli muhitda nanozarrachalarning vakuumdagiga nisbatan o’chamlari kichik va o’lchamlari bo’yicha tekis taqsimlanishiga olib keldi. Nanozarrachalarning o'lchamlari va shaklidagi sezilarli o'zgarishlar tayyorlangan kundan bir oy muddatdan keyin kuzatildi.
3. Davomiyligi nanosekund bo’lgan lazer impulslari, nistaban kichikroq o'lchamdagi bir xil nanozarrachalarni ishlab chiqarish nuqtai nazaridan samaraliroq va texnologik jihatdan dolzarbroq ekanligiga guvoh bo'ldik.
4. Suvda hosil bo'lgan alyuminiy nanozarrachalar bilan qoplangan shisha yuzasi supergidrofil xususiyatga ega va vacuum sharoitida hosil qilingan yupqa qatlamlar esa supergidrofobik xususiyatlarga ega ekanligi kuzatildi.
5. Nochiziqli yutilish koeffitsientlarining (β) va nochiziqli sindirish ko'rsatkichlarining (γ) to’lqin uzunligi 400 nm bo’lgan nurlanish soxalarida eng

yuqori qiymatlarga ega bo’lishi mumkinligi kuzatildi. Alyuminiy nanozarrachalarining nochiziqli yutilish koeffitsientlari (β) va nochiziqli sindirish ko'rsatkichlari (γ) qiymatlari mos ravishda ~ 10^{-7} sm W^{-1} va 10^{-9} sm^2 W^{-1} ga teng ekanligi hisoblandi.

6. Vakuum sharoitda alyuminiy nanozarrachalarini hosil bo'lishi, so'ngra hosil qilingan nanozarrachalar qatlami orqali tarqaluvchi lazer impulslarining alyuminiy nanozarrachalari tarkibidagi zich atomlari va ionlarini bialn o’zaro ta’sirlashuvi natijasida nochiziqli optik jaroyonlar ya’ni yuqori tartibli garmonikalar generasiyalari kuzatildi va ularning samaradorliklari ortishiga olib kelishitajribalarda ko’rsatildi. Bunda yuqori tartibli garmonikalarining tartib sonlari 37-tartibgacha generasiyalanishining imkonini berdi.
7. Femtosekund lazer yordamida metallar va metal qotishmalari yuzalarining doimiy va yorqin ranglarini o'chirish va qayta rangli tus berish mumkinligi ko'rsatildi.
8. Lazer nurlanishi parametrlarini optimallashtirish orqali bir vaqtning o'zida rang berish va metallarning namlanish xususiyatlarini boshqarish imkoniyatlari ko'rsatildi.
9. Lazer nurlanishi yordamida ishlov berilgan uglerod naychalaridan suv va moyni ajratishda foydalanish mumkinligi tajribalarda kuzatildi.
10. Lazer nurlanishi yordamida materiallar sirtida nanostrukturalarni hosil qilish va vacuum sharoitda ularning saqlashda kimyoviy tarkiblari o’zgarishlari natijasida turli metallarda superhidrofobik hususiyatlarga erishish mumkinligi va ulardan o'z-o'zini tozalovchi sirtlar sifatida foydalanish uchun keng imkoniyatlar yaratilishi mumkinligi ko’rsatildi.
11. Optimallashtirilgan lazer nurlanishi parameterlari ya’ni skanerlash parametrlari, to'r g'ovak o'lchami va saqlash sharoitlari orqali nanostrukturalangan zanglamaydigan po'lat va mis to'rlarida neft-suvni ajratishning 98% lik samaradorlikka erishish mumkinligi ko'rsatildi.
12. Tantal elementning sirtida lazer nurlanishi ta’siri davomida murakkab davriy azimutal va radial yo'naltirilgan davriy strukturalar olish imkoniyatlari ko’rsatildi. Olingan murrakab strukturalar namunani kelgusida implant sifatida foydalanish va ularga biologik hujayralarning birikishi va proliferatsiyasi uchun juda muhim ekanligi isbotlandi.
13. Femtosekund laser nurlanishi yordamida mis to’ri yoki uning pukka shaklidagi namunalarining qarama-qarshi tomonlarini turli xil xususiyatlariga ega holatda strukturalash mumkinligi ko’rsatildi va ulardan bit tomonga yo’nalgan suv oqimini yokiyuqori namlik sharoitlarida suv bug’larini yig'ishda qo’llash mumkinligi ko’rsatildi.

14. Lazerli tuzilmali zeolit bilan qoplangan po'lat to’rlar neft va suv aralashmasini turli neft va suv suyuqliklarini alohida ajratish mumkinligi ko’rsatildi, va ularning uzoq muddta davomida shu hususiyatlarining saqlanib qolinishi imkoniyatlarini namoyish etdi.

НАУЧНЫЙ СОВЕТ DSc.03/31.03.2022.T/FM.10.04 ПО ПРИСУЖДЕНИЮ УЧЕНЫХ СТЕПЕНЕЙ ПРИ ИНСТИТУТЕ ФУНДАМЕНТАЛЬНЫХ И ПРИКЛАДНЫХ ИССЛЕДОВАНИЙ, "ТИИИМСХ" НАЦИОНАЛЬНЫЙ ИССЛЕДОВАТЕЛЬСКИЙ УНИВЕРСИТЕТ

ИНСТИТУТ ФУНДАМЕНТАЛЬНЫХ И ПРИКЛАДНЫХ ИССЛЕДОВАНИЙ

Мазхар Икбал

ИССЛЕДОВАНИЯ МЕХАНИЗМОВ ФОРМИРОВАНИЯ И НОВЫХ ПРИМЕНЕНИЙ МИКРО/НАНОСТРУКТУРИРОВАННЫХ МАТЕРИАЛОВ С ИСПОЛЬЗОВАНИЕМ ИМПУЛЬСОВ ФЕМТОСЕКУНДНЫХ ЛАЗЕРОВ С ВЫСОКОЙ ЧАСТОТОЙ СЛЕДОВАНИЯ

01.04.02 – Теоретическая физика
(физико-математические науки)

ПРЕДСТАВЛЕНИЕ
по присуждению ученой степени доктора философии (PhD)
на основе научных публикаций без защиты диссертации

Ташкент – 2024

Тема диссертации доктора философии (PhD) по физико-математическим наукам зарегистрирована в Высшей аттестационной комиссии при Министерство высшего образования, науки и инноваций Республики Узбекистан под номером B2024.2.PhD/FM1043.

Результаты исследований выполнены выполнена в Институте фундаментальных и прикладных исследований Национального исследовательского университета «ТИИИМСХ».

Представление научного исследования на трех языках (узбекском, английском и русском (резуме)) размещен на сайтах Ученого совета (www.ifar.uz), Национального информационного агентства (www.uza.uz) и Информационно-образовательном портале «Ziyonet» (www.ziyonet.uz).

Научный консультанты:

Ганеев Рашид Аширович
доктор физико-математических наук, профессор,
ИФАР НИУ «ТИИИМСХ», Ташкент, Узбекистан

Али Сами Алнасер
Профессор физических наук, Американского
Университета в Шардже, Шарджа, ОАЭ

Защита представления состоится «___» _____ 2024 года в ___ часов на заседании Ученого совета № **DSc.03/31.03.2022.T/FM.10.04** при Институте фундаментальных и прикладных исследований, Национальной Исследовательский университет «ТИИИМСХ». Адрес: 100000, г.Ташкент, ул. Кори Ниязова 39, тел.: 71 237-09-61.; e-mail: info@ifar.uz.

Представление зерегистрированно в Информационно-ресурсном центре Института фундаментальных и прикладных исследований при Национальной Исследовательский университет «ТИИИМСХ» (регистрационный номер ____). С диссертацией можно ознакомиться в Библиотеке университета «ТИИИМСХ». Адрес: 100000, г.Ташкент, ул. Кори Ниязова 39, тел.: 71 237-09-62.

Представления разосланы «____» _____ 2024 г.

(протокол рассылки № ___ от __ _____2024 г.).

Б.Ж. Ахмедов
председатель Научного совета по присуждению
ученых степеней, д.ф.-м.н., профессор

Дж.Р. Рейимбаев
ученый секретарь Научного совета по присуждению
ученых степеней, д.ф.-м.н.

АБСТРАКТ

Явление лазерной абляции используется в различных областях науки и техники для лазерной обработки материалов и для аналитических методов. Использование лазерной абляции включают в себя получение наночастиц, микро-наноструктурирование, окраску поверхностей металлических изделий, контроль смачивающих свойств поверхностей, спектроскопию лазерного пробоя и импульсное лазерное осаждение. Исследования по синтезу и характеристике наночастиц металлов и оксидов с использованием метода импульсной лазерной абляции имеют решающее значение для понимания их свойств и потенциальных применений. Проведено исследование лазерной генерации наночастиц (НЧ) алюминия в жидкостях и в вакууме. Продемонстрирована способность НЧ изменять смачиваемость поверхностей и нелинейно-оптические свойства суспензий и плазмы. С помощью методов молекулярной динамики в сочетании с двухтемпературной моделью был проанализирован процесс образования НЧ алюминия во время абляции с поверхности мишеней. Численное моделирование позволило выявить основные механизмы формирования НЧ в жидких средах и существование оптимальных параметров лазерного излучения для получения НЧ алюминия желаемого размера и морфологии. Определены нелинейно-оптические свойства низшего порядка коллоидные растворы НЧ алюминия, полученных при абляции нано-, пико- и фемтосекундными импульсами. Коэффициенты нелинейного преломления и поглощения растворов НЧ алюминия при использовании импульсов длительностью 40 фс при $\lambda = 400$ нм составили ~ 10^{-9} см^2 Вт$^{-1}$ и 10^{-7} см Вт$^{-1}$ соответственно. Плазма содержающихся НЧ алюминия позволяет генерировать высшие гармоники вплоть до 37-го порядка с помощью зондирующих импульсов длительностью 40 фс, распространяющихся сквозь лазерный плазмы созданной на поверхности алюминиевой мишени. Формирование хорошо контролируемых структур нано/микронного размера на металлических поверхностях позволяет модифицировать их оптические и смачивающие свойства. Образование подобных структур на поверхности биосовместимых материалов, в частности, может расширить их применение в различных областях науки и техники. Для формирования сложных наноразмерных структур на металлических поверхностях использовался волоконный лазер с высокой частотой повторения (150 кГц) с импульсами длительностью 37 фс и центральной длиной волны 1030 нм. Обнаружена корреляция между оптическими свойствами обработанных лазером поверхностей и их смачиваемостью. Разделение нефти и воды с использованием сверхсмачивания и избирательной проницаемости мембран для

нефти или воды имеет большое экологическое и экономическое значение. Был разработан экологически чистый, не содержащий химикатов и эффективный подход с использованием мощного фемтосекундного лазера с высокой частотой повторений для наноструктурирования сеток из нержавеющей стали и меди для достижения желаемых смачивающих свойств. Параметры лазерного сканирования, размер пор сетки и условия старения были оптимизированы для создания мембран, демонстрирующих исключительную 98% эффективность разделения смеси нефти и воды.

ВВЕДЕНИЕ

Актуальность и значимость темы исследования. Лазерная абляция и лазерное структурирование широко изучались на протяжении многих десятилетий с момента изобретения лазеров в 60-х годах XX века. Однако интерес исследователей к данной тематике резко возрос с открытием метода усиления чирпированных лазерных импульсов и возможностью обработки материалов световыми импульсами с высокой плотностью энергии. Применение данного метода позволяет получить короткие лазерные импульсы длительностью до нескольких десятков фемтосекунд. Хотя эти импульсы имеют низкую энергию, пиковая мощность превышает тераватты и возможна интенсивность в диапазоне 10^{18} Вт/см^2 или выше. Это соответствует электрическому полю 10^{11} В/см. Механизмы взаимодействия лазерных излучения с веществом при такой высокой пиковой мощности и при столь коротких импульсах очень сложны и требуют понимания различных механизмов, поскольку длительности импульсов короче времени передачи энергии от электронной подсистемы к ионной решетке, также короче характерных времен теплопроводности решетки и гидродинамического временного параметра образца. Высокие пиковые интенсивности ультракоротких импульсов приводят к нелинейным процессам, имеют место ионизация сильным электрическим полем и ионизация электронным ударом. В зависимости от интенсивностей в фемтосекундном режиме происходят два механизма абляции: кулоновский взрыв и тепловое испарение. При низких интенсивностях, вблизи порога абляции, доминирует кулоновский взрыв (мягкая абляция), тогда как при высоких интенсивностях доминирует термическое испарение (жесткая абляция). В режиме кулоновского взрыва за импульс удаляется лишь несколько нанометров материала, а при термическом испарении за импульс удаляется на порядок больше материала. Понимание влияния температуры плазмы и плотности электронов имеет решающее значение для оптимизации продуктов лазерной абляции любой мишени.

Лазерная абляция используется для обработки материалов и для аналитических приложении. В качестве примеров можно привести получение наночастиц, микро-наноструктурирование, окраску металлов, контроль водоотталкивающих свойств поверхностей, спектроскопию лазерного пробоя и импульсное лазерное осаждение. Импульсная лазерная абляция широко используется при синтезе наночастиц (НЧ) различных металлов и оксидов. Однако на свойства НЧ влияют многие факторы, такие как длительность лазерного импульса, плотность энергии, тип окружающей среды, температура раствора и характеристики облучаемых мишеней. Наночастицы находят

применение в медицине для улучшения раннего выявления и лечения рака, для оптических датчиков, оптоэлектронике, создании тонких пленок и для создания источников энергии. Морфология и размер синтезированных наночастиц могут обуславливать вариации различных макроскопических свойств субстратов и суспензий, содержащих НЧ. Поэтому механизм образования НЧ необходимо исследовать при различных режимах объемной абляции мишени. С этой целью проведено численное моделирование процессов лазерной абляции алюминиевой мишени в жидких средах (воде) при различных параметрах облучения. Результаты моделирования могут быть использованы для их прямого сравнения с экспериментальными измерениями, с одной стороны, но также помогают получить более глубокое понимание фундаментальной физики процессов, связанных с лазерной генерацией НЧ, с другой стороны. Исследования нелинейно-оптических свойств НЧ низкого и высокого порядков обусловлены практическими и фундаментальными принципами применения малоразмерных агрегатов в различных областях нелинейной оптики. Эти агрегаты, образующиеся при лазерной абляции металлических поверхностей, служат эффективной средой для генерации гармоник высокого порядка в крайнем ультрафиолетовом диапазоне.

Обработка фемтосекундными лазерными импульсами позволяет точно контролировать локальные наноразмерные структуры на поверхности материалов, делая их высокоэффективными и многофункциональными, в частности, при окраске поверхностей. Лазерно-индуцированное окрашивание является экологически чистым, поскольку исключает использование каких-либо пигментов или химикатов, но при этом обеспечивает достаточную гибкость в достижении желаемых результатов за счет оптимизации параметров лазерного облучения. Уникальная способность мощных коротких лазерных импульсов модифицировать практически все виды материалов на наноуровне открывает большой потенциал для различных новых приложений в оптике, опто-электронике, микрофлюидике, цветовой маркировке и механике. Еще одним применением лазерной модификации поверхности является контроль смачиваемости металлических поверхностей, что в настоящее время является предметом растущего интереса к лазерной обработке материалов. Поверхности можно модифицировать с помощью интенсивных лазеров, чтобы они стали притягивающими воду (гидрофильными) или водоотталкивающими (гидрофобными). Такие модифицированные поверхности имеют множество применений, таких как самоочистка, предотвращение коррозии, уменьшение сопротивления, антибактериальные свойства, защита от запотевания, теплопередача, трибология, оптическое отражение и разделение масляных фракций и воды. Сепарация нефти и воды имеет большое экологическое и экономическое

значение. Традиционные методы разделения нефти, такие как сжигание, обезжиривание и химическое диспергирование, частично эффективны, но они производят вредные побочные продукты, которые ухудшают эффективность разделения. Контроль гидрофильных/фобных характеристик металлических сеток, структурированных фемтосекундным лазером, 2D-мембран или 3D-адсорбентных пен, является экологически чистым методом и имеет высокие характеристики эффективности разделения. Мембраны с избирательной проницаемостью по отношению к масляной и водной фазам могут быть получены путем индуцирования либо супергидрофобно-суперолеофильного, либо супергидрофильно-суперолеофоб-ного поведения при подводном смачивании.

Международный контекст исследования. Многие ведущие университеты и исследовательские центры по всему миру проводят исследования в физики сильных лазерных полей, в частности, ионизации, формирования наночастиц, наноструктурирования многофункциональных поверхностей, ГВГ и применения когерентного XUV для изучения сверхбыстрой динамики электронов в атомах, молекулах и материалах с аттосекундной шкалой времени. Среди них группа кафедры сверхбыстрой динамики Института многопрофильных наук Макса Планка (Геттинген, Германия), группа лаборатории лазерной энергетики (LLE) Рочестерского университета (США), группа наноструктур и сверхбыстрых рентгеновских технологий в ETH-Zurich (Цюрих, Швейцария), группа в МИФИ, Институт инженерной физики для биомедицины (PhysBio), 115409 Москва, Россия, группа в Институте физики и Центре междисциплинарных наноструктурных наук и технологий (CINSaT), Университет Касселя, 34125 Кассель, Германия, группа нелинейной оптики Чанчуньского института оптики, физики и точной механики (Чанчунь, Китай), группа Центр материаловедения и инженерных исследований Американского университета Шарджи (Шарджа, ОАЭ), группа Центра нанотехнологий в Университете Мюнстера (Мюнстер, Германия), группа нелинейной оптики Токийского университета (Токио, Япония), группа отдела лазерной плазмы Центра передовых технологий (ИНДОР, Индия), группа Национального института Science (Монреаль, Канада), спектроскопия HHG в Имперском колледже (Лондон, Англия),), научная группа генерации высших гармоник (ГВГ) и когерентного излучения в дальней ультрафиолетовой области (ДУФ) в Центре перспективных исследований нанолитографии (Амстердам, Нидерланды) и другие.

Текущее состояние исследований по теме. Импульсная лазерная абляция является постоянно развивающейся областью. Среди многих других приложений

большой интерес научного сообщества представляют формирование наночастиц, подготовка многофункциональных поверхностей, спектроскопия лазерного пробоя и ГВГ. Формирование наночастиц и микронаноструктур с помощью лазерной абляции превосходит традиционные методы, поскольку не требует химического воздействия, прямого контакта с исследователем и является экологически чистым методом.

Связь **темы исследования с исследовательской деятельностью других учреждений.** Экспериментальные результаты представленные в данном исследовании были получены в Центре материаловедения и исследований Американского университета Шарджи (ОАЭ), Латвийского университета (Латвия) и в сотрудничестве с группами моделирования различных университетов Германии, Японии и России.

Целью исследовательской работы является получение теоретических и экспериментальных знаний о механизмах формирования и новых применениях микро/наноструктурированных материалов, с использованием фемтосекундных лазеров с высокой частотой повторения.

Задачи исследования:

- Исследование лазерной генерации наночастиц (НЧ) на основе алюминия (Al) в жидкостях и в вакууме, а также их способности изменять смачиваемость и нелинейно-оптические свойства поверхностей, суспензий и плазмы.
- Исследование нелинейного поглащения и преломления в НЧ, а также их различных оптических свойств для потенциального применения в оптоэлектронике, оптических ограничителях и фотонике.
- Нахождение параметров лазерного излучения и условий для формирования лазерно-индуцированных периодических поверхностных структур (LIPSS) на поверхности металлических мишеней.
- Управление гидрофильными/фобными свойствами металлических сеток, плоских и изогнутых поверхностей различных материалов, обработанных фемтосекундными лазерными импульсами для разделения нефти и воды.
- Исследование применения лазерно-индуцированных факелов, обогащенных наночастицами для ГВГ.

Объектом исследования являются лазерно-индуцированные нано-микроструктуры на поверхности различных материалов, наночастицы Al, полученные на воздухе, в вакууме и в воде.

Предметом исследования являются смачивающие свойства и оптические характеристики нано/микроструктурированных поверхностей различных

материалов, нелинейно-оптические свойства НЧ аллюминия, а также спектральные характеристики генерируемых гармоник высокого порядка.

Методы исследования включают как теоретические, так и экспериментальные. Теоретические методы включают моделирование с использованием аналитической молекулярной динамики (MD) и двухтемпературной модели (TTM), полученных на основе дифференциальных уравнений диффузии. Экспериментальные методы формирования наночастиц в вакууме и в воде с использованием коротких лазерных импульсов большой мощности, и с высокой частотой повторения. Структурирование плоскостей, изогнутых поверхностей различных материалов и металлических сеток фемтосекундным волоконным лазером. Количественные измерения свойств смачиваемости поверхностей путем измерения угла контакта и угла отступа с помощью анализатора формы капли.

Научная новизна исследования.

- Численное моделирование в рамках модели MD-TTM использовалось для получения более глубоких знаний об оптимальных параметрах лазерного облучения для формирования наночастиц алюминия заданного размера и морфологии.
- Впервые наблюдались наибольшие значения коэффициентов нелинейного поглощения (β) и нелинейных показателей преломления (γ) в случае суспензии НЧ на основе Al, полученной путем абляции алюминия пикосекундными импульсами в спектральной области 400 нм. Значения коэффициентов нелинейного поглощения (β) и нелинейных показателей преломления (γ) алюминиевых НЧ равны ~ 10^{-7} см $Вт^{-1}$ и 10^{-9} $см^2$ $Вт^{-1}$ соответственно.
- Впервые установлено, что формирование НЧ аллюминия in-situ в вакууме с последующим распространением лазерных импульсов через облако синтезированных наночастиц дает повышенный коэфициент преоразования высоких гармоник по сравнению с атомами и ионами алюминия. Аллюминиевые НЧ позволили получить высшие гармоники до 37-го порядка с помощью импульсов длительностью 40 фс.
- Впервые показано, что пленки аллюминиевых НЧ, полученные абляцией в воде, проявляют супергидрофильные свойства, а НЧ, осажденные в вакууме, обладают супергидрофобными свойствами.
- Впервые продемонстрировано, что стойкие и переливающиеся цвета поверхностей металлов и металлических сплавов можно стирать и перекрашивать с помощью второй стадии фемтосекундной лазерной обработки.

- Впервые продемонстрирована корреляция между спектральными отражательными свойствами обработанных лазером поверхностей и их смачиваемостью.
- Впервые установлена возможность использования стержней из сплава AlNiCo, обработанных с использованием различных лазерных импульсов, для разделения нефти и воды.
- Найдены оптимальные параметры обработки медных и нержавеющих сеток, такие как скорость лазерного сканирования и условия старения, позволившие достигнуть эффективности 98% при разделении смесей нефти и воды.
- Продемонстрирован ускоренный метод изменения параметра смачиваемости металлических поверхностей, структурированных фемтосекундным лазером, путем выдержки в среде низкого давления для целей самоочистки.
- Впервые представлены сложные периодические азимутально и радиально направленные LIPSS, изготовленные лазером на большой площади на поверхности тантала. Данный метод может быть использован для улучшения адгезии и пролиферации клеток при использовании в качестве имплантата.
- Были продемонстрированы Янус-мембраны из медной сетки и губки, обработанные фемтосекундным лазером для эффективного направленного пропускания воды и сбора тумана. Стальные сетки с лазерным структурированием и покрытием из цеолита продемонстрировали улучшенные супергидрофильные свойства и превосходную долговечность в течение длительного периода при разделении нефти и воды.

Практические результаты работы. Результаты теоретического и экспериментального анализа были использованы при технологическом совершенствовании генерации наночастиц и обработки микро-наноструктурированных поверхностей различных материалов для новых применений в исследовательском центре материаловедения Американского университета Шарджи (ОАЭ). Различные программы для расчетов MD-TTM и обработки экспериментальных данных были разработаны и в настоящее время активно применяются в исследовательских группах Американского университета Шарджи (ОАЭ); лаборатории нелинейной оптики Латвийского университета (Латвия), Институте Физики и в Центре Междисциплинарных наноструктурных наук и технологий (CINSaT), Кассельский университет, Кассель, Германия; на физическом факультете Воронежского государственного университета, Воронеж, Россия; и в Ташкентском институте инженеров ирригации и механизации сельского хозяйства, Ташкент, Узбекистан.

Достоверность результатов исследований подтверждается тем, что они были получены с использованием современных методов расчетов,

моделирования и экспериментальных методик. Достоверность результатов также основана на совместимости полученных результатов с экспериментальными данными. Более того, чтобы еще раз подчеркнуть достоверность полученных результатов, все представленные статьи были рецензированы экспертами в области наук о поверхности, наноматериалов, нелинейной оптики и опубликованы в журналах с высоким рейтингом, отнесенных к квартилям Q1 и Q2.

Научная значимость результатов исследования. Теоретические и экспериментальные результаты исследований механизмов образования наночастиц и формирования микро/наноструктурированных поверхностей имеют множество применений. Наночастицы, полученные лазерным методом, являются зеленым, нетоксичным продуктом, поэтому подходят для раннего обнаружения и лечения рака, энергетики, тонких пленок, оптоэлектроники, рамановской спектроскопии с усилением сигнала и многих других приложений. Наноструктурированные поверхности имеют большое значение при создании многофункциональных поверхностей из различных материалов, таких как самоочищение, предотвращение коррозии, уменьшение сопротивления, антибактериальные свойства, защита от запотевания, теплопередача, трибология, оптическое отражение, разделение масла и воды.

Внедрение результатов исследования.

Полученные результаты исследований были опубликованы в многочисленных научных статьях. Среди них “Ultrafast fiber laser-induced fabrication of superhydrophobic and self-cleaning metal surfaces,” S.A. Khan, et.al., Appl. Surf. Sci. 542, 148560 (2021) (**75** ссылка), “Expedited transition in the wettability response of metal meshes structured by femtosecond laser pulses for oil-water separation,” S.A. Khan, et.al., Front. in Chem. 8, 768 (2020) (**20** ссылка), “The mechanism of laser-assisted generation of aluminum nanoparticles, their wettability and nonlinearity properties,” M. Iqbal, et.al., Appl. Surf. Sci. 527, 146702 (2020) (**17** ссылка), “Superhydrophobic and superhydrophilic properties of laser-ablated plane and curved surfaces,” G.S. Boltaev, et.al., Appl. Phys. A 126, 1-9 (2020) (**12** ссылка), “Near-field induced reaction yields from nanoparticle clusters,” P. Rosenberger, et.al., ACS Photonics 7, 1885-1892 (2020) (**20** ссылка), “Anomalous formation of trihydrogen cations from water on nanoparticles,” M.S. Alghabra, et.al., Nat. Commun. 12, 3839 (2021) (**15** ссылка), “Resonance enhancement of harmonics in the vicinity of 32 nm spectral range during propagation of femtosecond pulses through the molybdenum plasma,” V.V. Kim, et.al., J. Phys. B: At. Mol. Opt. Phys. 53, 195401 (2020) (**14** ссылка), “Giant third-order nonlinear response of mixed perovskite nanocrystals,”

A.M. Abu Baker, et.al Mater. 15, 389 (2022) (**12** ссылка), "Enhanced XUV harmonics generation from diatomic gases using two orthogonally polarized laser fields," G.S. Boltaev, et.al., Sci. Rep. 11, 5534 (2021) (**12** ссылка), "Application of 150 kHz laser for high-order harmonic generation in different plasmas," G.S. Boltaev, et.al., Photon. 7, 66 (2020) (**9** ссылка), "Simultaneous manipulation of the optical and wettability properties of metal surfaces using 150 kHz femtosecond fiber laser," M. Iqbal, et.al., Appl. Sci. 10, 6207 (2020) (**7** ссылка), и т.д.

Опубликованность результатов исследования.

Результаты исследований опубликованы в 30 научных статьях в международных журналах с высокими импакт-фактором и рекомендованных Высшей Аттестационной Комиссией Республики Узбекистан для публикации основных научных результатов докторских диссертаций и отображенных в научной базе данных Web of Science.

ЗАКЛЮЧЕНИЕ.

Основные выводы, сделанные в результате наших исследований, заключаются в следующем:

1. Численное моделирование в рамках модели MD-TTM позволило глубже понять основные механизмы образования НЧ в воде и получить оптимальные параметры лазерного излучения для получения НЧ на основе аллюминия желаемого размера, формы и морфологии.

2. Абляция в водной среде привела к более узкому и равномерному распределению наночастиц по размерам по сравнению с абляцией в вакууме. Значительные изменения размеров и формы наночастиц наблюдались через месяц после абляции.

3. Обнаружено что лазерные импульсы в пикосекундном диапозоне длительности более эффективны и технологически обоснованны с точки зрения производства однородных наночастиц, и возможно, меньшего размера.

4. Поверхность стекла, с осажденными НЧ на основе Al, полученными абляцией в воде, обладает супергидрофильными свойствами, а поверхности стекла с НЧ, осажденными в вакууме, - супергидрофобными.

5. Наибольшие значения коэффициентов нелинейного поглощения (β) и нелинейных показателей преломления (γ) в спектральной области 400 нм наблюдались в случае суспензии НЧ на основе Al, полученной путем абляции алюминия пикосекундными импульсами. Значения коэффициентов нелинейного поглощения (β) и нелинейных показателей преломления (γ) НЧ на основе Al составили ~ 10^{-7} см $Вт^{-1}$ и 10^{-9} $см^2$ $Вт^{-1}$ соответственно.

6. Продемонстрировано, что формирование НЧ аллюминия in-situ в вакууме с последующим распространением зондирующих импульсов через облако синтезированных наночастиц приводит к увеличению выхода гармоник по

сравнению с применением атомов и ионов алюминия. Аллюминиевые НЧ позволяют генерировать гармоники вплоть до 37-го порядка с использованием импульсов длительностью 40 фс.

7. Показано, что стойкие и переливающиеся цвета поверхностей металлов и металлических сплавов можно стирать и перекрашивать с помощью последующих стадии фемтосекундной лазерной обработки.

8. Продемонстрирована возможность одновременной настройки окраски и смачиваемости металлов за счет оптимизации лазерных параметров, используемых при обработке.

9. Отмечено, что углеродные мембраны, подвергнутые лазерной абляции, являются отличными кандидатами для разделения воды и масла.

10. Лазерное наноструктурирование поверхности в сочетании с передержкой в вакууме является эффективным и быстрым методом достижения экстремальных супергидрофобных состояний в различных металлах, что делает его пригодным для широкого спектра применений для самоочищающихся поверхностей.

11. Наноструктурированные сетки из нержавеющей стали и меди с оптимизированными параметрами лазерного сканирования, размером пор сетки и условиями старения продемонстрировали эффективность разделения нефти и воды на уровне 98%.

12. Представлены сложные периодические азимутально и радиально направленные LIPSS, изготовленные фемтосекундным лазером на большой площади поверхности тантала. Полученный материал имеет улучшенную адгезии и пролиферацию клеток при использовании в качестве имплантата.

13. Янус-мембраны из медной сетки и вспененного материала с противоположными характеристиками смачиваемости на каждой стороне поверхности были изготовлены с помощью фемтосекундного лазера и продемонстрироано их использование для эффективного направленного пропускания воды и сбора влаги из тумана.

14. Стальные сетки с лазерным структурированием и покрытием из цеолита продемонстрировали улучшенные супергидрофильные свойства и превосходную долговечность в течение длительного периода при разделении нефти и воды.

ACKNOWLEDGMENTS.

I would like to thank my supervisors Prof. Rashid Ganeev and Prof. Ali Alnaser for the their constant, invaluable support and guidance during more than five years of my research work and collaborations. Special thanks to Dr. G. S. Boltaev, Dr. V. V. Kim, Dr. S. A. Khan, and Dr. D. S. Ivanov for their contributions in carrying out the joint theoratical and experimental studies. I would also like to express my special gratitude to Prof. Bobomurat Ahmedov and his team at IFAR for allowing me to present the results of my Ph.D. research at IFAR.

MINNATDORCHILIK.

Ilmiy rahbarlarim professor Rashid Ganeev va professor Ali Alnaserga so'nggi 5 yil mobaynida ilmiy ishlarimdagi hamkorliklariga va bebaho qo'llab-quvvatlaganliklari va yo'l-yo'riqlari ko'rsatganliklari uchun minnatdorchilik bildiraman. Bundan tashqari, Dr. G.S. Boltayev, Dr. V.V. Kim, Dr. S.A. Khan va Dr. D.S. Ivanovga qo'shma tajribalarni birgalikda olib borishda qo'shgan hissalari uchun o'z minnatdorchiligimni bildiraman. Shuningdek, doktorlik dissertatsiyasining natijalarini taqdim etishimga amaliy yordam berganligi uchun Prof. Bobomurat Ahmedov va uning IFAR ilmiy jamoasiga alohida minnatdorchilik bildiraman.

БЛАГОДАРНОСТИ.

Я хотел бы поблагодарить моих научных руководителей профессора Рашида Ганеева и Али Алнасера за постоянную и неоценимую поддержку и руководство в течение более чем пяти лет сотрудничества. Особая благодарность д-ру Г.С. Болтаеву, д-ру В.В. Киму, , д-ру С.А. Хан и и д-ру Д.С. Иванову за их вклад в проведение совместных экспериментальных и теоретических исследований. Я также хотел бы выразить особую благодарность профессору Бобомурату Ахмедову и его команде ИФАР за то, что они позволили мне представить результаты моих PhD исследований в ИФАР.

E'LON QILINGAN ISHLAR RO'YHATI
СПИСОК ОПУБЛИКОВАННЫХ РАБОТ
LIST OF PUBLISHED PAPERS

I bo'lim (I часть, I part)

1. PA Piatkowski, A Ali, V Ialyshev, M Iqbal, AS Alnaser, Ytterbium femtosecond fiber laser ablation synthesis of silicon nanocrystals in water: Laser frequency and pulse energy dependence, Optical Materials 150, 115147 (2024). DOI: 10.1016/j.optmat.2024.115147
2. V. Sh. Yalishev, NA Abbasi, M Iqbal, AS Alnaser, Comparing water transport properties of Janus membranes fabricated from copper mesh and foam using a femtosecond laser, Langmuir 39 (5), 1815-1825 (2023). DOI: 10.1021/acs.langmuir.2c02697
3. Enhancing gas solubility in water via femtosecond laser-induced plasma, V. Ialyshev, G. Boltaev, M. Iqbal, M. Khamis, A.S. Alnaser, ACS Omega 7, 28182-28189 (2022). DOI: 10.1021/acsomega.2c02384
4. A.M. Abu Baker, G.S. Boltaev, M. Iqbal, M. Pylnev, N.M. Hamdan, A.S. Alnaser, Giant third-order nonlinear response of mixed perovskite nanocrystals, Materials 15, 389 (2022). DOI: 10.3390/ma15010389
5. M. Iqbal, G.S. Boltaev, N. Abbasi, R.A.Ganeev, A.S. Alnaser, Spatial and spectral variations of high-order harmonics generated in noble gases, Journal of Physics B: At. Mol. Opt. Phys. 55, 105601 (2022). DOI:10.1088/1361-6455/ac69c1
6. V.S. Yalishev, M. Iqbal, V.V. Kim, S.A. Khan, R.A. Ganeev, A.S. Alnaser, Reversible wettability transition of laser-textured metals after vacuum storing and low-temperature annealing, Applied Physics A 127, 1-7 (2022). DOI: 10.1007/s00339-021-04547-0
7. S. Ahmad, M. Egilmez, M. Iqbal, T. Ibrahim, M. Khamis, A.S. Alnaser, Pulsed laser deposited zeolite coatings on femtosecond laser-nanostructured steel meshes for durable superhydrophilic/oleophobic functionalities, Frontiers in Chemistry, 1027 (2021). DOI: 10.3389/fchem.2021.792641
8. V.V. Kim, V.S. Yalishev, S.A. Khan, M. Iqbal, G.S. Boltaev R.A. Ganeev, A.S. Alnaser, Influence of gas environment on the dynamics of wetting transition of laser-textured stainless steel meshes, AIP Advances 11, 075221 (2021). DOI: 10.1063/5.0047514
9. G.S. Boltaev, M. Iqbal, N.A. Abbasi, V.V. Kim, R.A. Ganeev, A.S. Alnaser, Enhanced XUV harmonics generation from diatomic gases using two orthogonally polarized laser fields, Scientific Reports 11, 1-10 (2021). DOI: 10.1038/s41598-021-85114-8
10. S.A. Khan, G.S. Boltaev, M. Iqbal, V.V. Kim, R.A. Ganeev, A.S. Alnaser, Ultrafast fiber laser-induced fabrication of superhydrophobic and self-cleaning metal surfaces, Applied Surface Science 542, 148560 (2021). DOI: 10.1016/j.apsusc.2020.148560

11. G.S. Boltaev, M.S. Alghabra, M. Iqbal, R.A. Ganeev, A.S. Alnaser, Creation of azimuthally and radially directed laser-induced periodic structures on large tantalum surface, Journal of Physics D: Applied Physics 54, 185109 (2021). DOI: 10.1088/1361-6463/abe26e
12. V. Yalishev, M. Iqbal, V. Kim, A.S. Alnaser Effect of processing environment on the wettability behavior of laser-processed titanium, Journal of Physics D: Applied Physics 55, 045401 (2021). DOI: 10.1088/1361-6463/ac296c
13. R.A. Ganeev, G.S. Boltaev, V.V. Kim, M. Iqbal, H. Kuroda, A.S. Alnaser, Distinction in resonance properties of the atomic and molecular contained plasmas used for high-order harmonics generation of ultrafast laser pulses, Journal of Applied Physics 129, 043103 (2021). DOI: 10.1063/5.0034861
14. V.V. Kim, R.A. Ganeev, G.S. Boltaev, M. Iqbal, A.S. Alnaser, Carbon nanostructure containing plasma: Medium for efficient high-order harmonics of 1030 nm laser, Physics of Plasmas 28, 023111 (2021). DOI: 10.1063/5.0035758
15. M.S. Alghabra, R. Ali, V. Kim, M. Iqbal, P. Rosenberger, S. Mitra, R. Dagar, P. Rupp, B. Bergues, D. Mathur, M.F. Kling, A.S. Alnaser; Anomalous formation of trihydrogen cations from water on nanoparticles, Nature Communications 12, 3839 (2021). DOI: 10.1038/s41467-021-24175-9
16. G.S. Boltaev, S.A. Khan, R.A. Ganeev, V.V. Kim, M. Iqbal, A.S. Alnaser, Superhydrophobic and superhydrophilic properties of laser-ablated plane and curved surfaces, Applied Physics A 126, 1-9 (2020). DOI: 10.1007/s00339-019-3245-x
17. P. Rosenberger, P. Rupp, R. Ali, M.S. Alghabra, S. Sun, S. Mitra, S.A. Khan, R. Dagar, V. Kim, M. Iqbal, J. Schotz, Q. Liu, S.K. Sundaram, J. Kredel, M. Gallei, C. Costa-Vera, B. Bergues, A.S. Alnaser, M.F. Kling, Near-field induced reaction yields from nanoparticle clusters ACS Photonics 7, 1885-1892 (2020). DOI: 10.1021/acsphotonics.0c00823
18. S.A. Khan, V. lalyshev, V.V. Kim, M. Iqbal, H. Al Harmi, G.S. Boltaev, R.A. Ganeev, A.S. Alnaser, Expedited transition in the wettability response of metal meshes structured by femtosecond laser pulses for oil-water separation Frontiers in Chemistry 8, 768 (2020). DOI:10.3389/fchem.2020.00768
19. M. Iqbal, V. Ialyshev, V. Kim, G. Boltaev, D. Ivanov, B. Rethfeld, R. Ganeev, A.S. Alnaser, Simultaneous manipulation of the optical and wettability properties of metal surfaces using 150 kHz femtosecond fiber laser Applied Sciences 10, 6207 (2020). DOI:10.3390/app10186207
20. M. Iqbal, R.A. Ganeev, G.S. Boltaev, V.V. Kim, A.S. Alnaser, Incoherent and coherent extreme ultraviolet emission from boron plasma, The European Physical Journal D 74, 1-1 (2020). DOI: 10.1140/epjd/e2020-100545-4
21. V.V. Kim, G.S. Boltaev, M. Iqbal, N.A. Abbasi, H. Al-Harmi, I.S. Wahyutama, T. Sato, K.L. Ishikawa, R.A. Ganeev, A.S. Alnaser, Resonance enhancement of harmonics in the vicinity of 32 nm spectral range during propagation of femtosecond pulses through the molybdenum plasma, Journal of Physics B: Atomic, Molecular and Optical Physics 53, 195401 (2020). DOI: 10.1088/1361-6455/aba581

22. G.S. Boltaev, R.A. Ganeev, V.V. Kim, N.A. Abbasi, M. Iqbal, A.S. Alnaser, High-order harmonics generation in the plasmas produced on different rotating targets during ablation using 1 kHz and 100 kHz lasers, Optics Express 28, 18859-18875 (2020). DOI: 10.1364/OE.393054
23. G.S Boltaev, V.V. Kim, M. Iqbal, N.A. Abbasi, V.S. Yalishev, R.A. Ganeev, A.S. Alnaser, Application of 150 kHz laser for high-order harmonic generation in different plasmas Photonics 7, 66 (2020). DOI: 10.3390/photonics7030066
24. G.S. Boltaev, R.A. Ganeev, N.A. Abbasi, M. Iqbal, V.V. Kim, H. Al-Harmi, X.-M. Tong, A.S. Alnaser, Routes to control Cooper minimum in high order harmonics generated in argon gas, New Journal of Physics 22, 083031 (2020). DOI: 10.1088/1367-2630/aba1b1
25. G.S. Boltaev, N.A. Abbasi, V.V. Kim, M. Iqbal, S.A. Khan, A.I. Zvyagin, M.S. Smirnov, O.V. Ovchinnikov, R.A. Ganeev, A.S. Alnaser, Third and fifth harmonics generation in air and nanoparticle-containing plasmas using 150-kHz fiber laser, Applied Physics B 126, 1-12 (2020). DOI: 10.1007/s00340-020-07430-7
26. M. Iqbal, S.A. Khan, D.S. Ivanov, R.A. Ganeev, V.V. Kim, G.S. Boltaev, I. Sapaev, N.A. Abbasi, S. Shaju, M.E. Garcia, B. Rethfeld, A.S. Alnaser, The mechanism of laser-assisted generation of aluminum nanoparticles, their wettability and nonlinearity properties, Applied Surface Science 527, 146702 (2020). DOI: 10.1016/j.apsusc.2020.146702
27. V.V. Kim, R.A. Ganeev, G.S. Boltaev, M. Iqbal, A.S. Alnaser, Calculation of high-order harmonic generation in laser-produced lithium plasma, Optics Letters 44, 3693-3696 (2019). DOI: 10.1364/OL.44.003693
28. G.S. Boltaev, R.A. Ganeev, S. Reyimboyev, B.R. Sobirov, T.Y. Shermatov, B.R. Kutlimurotov, V.V. Kim, N.Y. Iskandarov, Z.T. Azamatov, N.S. Khalilova, M. Iqbal, S.A. Khan, A.S. Alnaser, Application of combustion flames for generation of third harmonic and super-hydrophobic coating of glasses by deposited carbon nanoparticle films, Journal of Physics D: Applied Physics 53, 075301 (2019). DOI:10.1088/1361-6463/ab58ec

II bo‘lim (II часть, II part)

29. M. Iqbal, R. Ganeev, G. Boltaev, A. Alnaser, Coloring of metals and metal alloys surfaces by using 150 KHz fiber femtosecond laser, DAMOP20 Meeting of The American Physical Society, Portland, USA E01.00032 (2020).
30. R. Ganeev, G. Boltaev, V. Kim, M. Iqbal, N. Abbasi, A. Alnaser, High-harmonic generation in lanthanides-containing plasmas, DAMOP20 Meeting of The American Physical Society Portland, USA Q01.00067 (2020).
31. N. Abbasi, G. Boltaev, R. Ganeev, V. Kim, M. Iqbal, A. Alnaser, Plasma dynamics characterization for improvement of high-order harmonics generation in laser-produced plasmas, DAMOP20 Meeting of The American Physical Society, Portland, USA Q01.00069 (2020).

32. G. Boltaev, R. Ganeev, N. Abbasi, V. Kim, M. Iqbal, S. Khan, A. Alnaser, Enhancement of extreme ultraviolet harmonics generated in gases using two orthogonally polarized laser fields, DAMOP20 Meeting of The American Physical Society Portland, USA Q01.00177 (2020).

“Fan va innovatsiyalar” xalqaro ilmiy jurnali (International scientific journal “Science and Innovation”) tahririyatida tahrirdan o‘tkazilib, o‘zbek, ingliz va rus tillaridagi matnlari o‘zaro muvofiqlashtirildi (12.07.2024).

_____

Bosishga ruxsat etildi 12.07.2024. Qog‘oz o‘lchami 60x84 – 1/16
Hajmi 6 b.t. 50 nusxa.
TIQXMMI bosmaxonasida chop etildi.
Toshkent 100000, Qori-Niyoziy ko‘chasi 39 uy